DIFFERENTIATION OF EVOLUTIONARY STAGES IN FOG LIFE CYCLES BASED ON MICROPHYSICAL PROPERTIES – IMPLICATIONS FOR THE OPERATION OF NOVEL CLOUD RADAR PROFILERS

kumulative Dissertation
zur
Erlangung des Doktorgrades
der Naturwissenschaften
(Dr. rer. nat.)

dem
Fachbereich Geographie
der Philipps-Universität Marburg
vorgelegt von

Frank Markus Maier
aus Alzenau in Unterfranken

Frankfurt am Main, Februar 2014

Vom Fachbereich Geographie
der Philipps-Universität Marburg als Dissertation
am 23. April 2014 angenommen.

Erstgutachter: Prof. Dr. Jörg Bendix
Zweitgutachter: Prof. Dr. Georg Miehe

Tag der mündlichen Prüfung: 09. Juli 2014

Preface

Fog is often associated with solitude and tristesse in arts and literature. In the course of my thesis, I have experienced admittedly those feelings on rare occasions. Thankfully, I could enjoy the challenging and diversified work most of the time. Rarely, I have been able to get to know so many new things and people in such a short time as during my thesis. The support and encouragement I received were manifold and I am grateful to various colleagues and friends for their attendance during the hike through fog.

Firstly, I would like to express my special gratitude to my supervisor Jörg Bendix. He was the one who enabled me to do my thesis. At all hours of the day and almost all hours of the night, he provided me with any sup-port I needed and had an open ear for all my questions.

I am greatly thankful to my advisor Boris Thies who played a tremendous part in contributing to my work. He supported me with various ideas, constructive criticism and incessant encouragement so that our collegial relationship turned into a real friendship.

I thank my colleagues at the Laboratory for Climatology and Remote Sensing (LCRS) for the kind working atmosphere and their assistance. Particularly, I have to thank Sebastian Achilles for his very creative ideas at solving problems with the balloon-borne measuring system and his grand willingness to spend several nights on the measuring field in any wind and weather. A master thesis by Sebastian Achilles was of great use for accomplishing my thesis. I thank the rest of our working group for comfortable coffee brakes, common activities and fascinating discussions about scientific issues and beyond.

Special thanks go to Felix Lindner (TU Kaiserslautern) for his indispensable assistance in finding solutions for mathematical problems.

The thesis was made possible by financial support from the German Research Foundation (DFG) within the ProFog-project (BE1789/14-1; TH1531/1-1). This is gratefully acknowledged. Besides, I thank the Philipps-University of Marburg for granting a PhD-scholarship for natural sciences.

I would like to express my deepest gratitude for the everlasting support and encouragement that I received from my parents and two brothers.

Finally, I want to thank my girlfriend Isabell for her enduring backing and for reminding me that there is a life besides work. I still cannot imagine what we will be able to do with all of our additional leisure time in future.

Frankfurt, February 2014 Frank Maier

Contents

1. Introduction

1.1 Motivation and main issue

Fog and low stratus (FLS) gain in importance for our modern society. Low stratus is a type of low-level clouds featuring horizontal layering with a uniform base while fog is defined as an atmospheric condition with horizontal visibility below 1 km at ground level (WMO 1992).

Both pose threats for traffic safety (Andre et al. 2004, Pagowski et al. 2004). According to Gultepe et al. (2007, 2009) the total economic loss that can be ascribed to fog is comparable to that of more spectacular natural disasters as tornadoes or even hurricanes in some situations. In this context, the limited visibility range has to be named, mainly affected by microphysical properties, such as the liquid water content (LWC) and the drop size distribution (DSD) (Gultepe et al. 2006). From the numerical point of view, accurate fog forecasting and nowcasting still remain a challenge, since they have difficulties in representing the microphysical processes involved (Gultepe et al. 2007). Particularly, the knowledge about vertical LWC-profiles in fog and their spatiotemporal dynamics are not well understood which are essential for modelling fog. In addition, the so-called life cycle of fog (formation, development and dissipation) that is directly related to the temporal progress of DSD is not represented precisely enough in models (Müller et al. 2010). For an improvement of fog forecasting and nowcasting models comprehensive measurements of microphysical properties are necessary which provide continuous information about their vertical distribution and a high temporal resolution over the whole fog event, respectively.

Moreover, fog occurrences result frequently in problematic atmospheric pollution, especially in industrialized agglomerations as Beijing (Cermak and Knutti 2009). Emitted air pollutants accumulate underneath inversion layers accompanying fog events. The harmful substances solve in fog droplets before they sediment on plants and buildings with high concentrations. Featuring a high albedo, the fog top delays the thermal dissipation of the temperature inversion. In this context, LWC as well as DSD determine on the one hand the albedo of the fog top and on the other hand the concentration of the solved pollutant (Fuzzi et al. 1984, Kraus and Ebel 1989, Jaeschke et al. 1998). Since the air pollutants affect the drop growth over the whole fog event, an enhanced understanding of fog life cycle could provide valuable information about the degree of smog occurrences.

Furthermore, it has to be noted that the International Panel on Climate Change (IPCC) attaches much importance to low stratus in its actual, preliminary Fifth Assessment Report (AR5) (IPCC 2013). They delineate a low level of confidence for the understanding of boundary stratus clouds and their interactions with aerosol in the atmosphere (Fig. 1.1), resulting in major uncertainties for climate predictions. Especially the influence of these

boundary clouds on the radiation budget of the earth system cannot be explained satisfactorily. In comparison to its fourth assessment report from 2007 (AR4), the cloud albedo effect is the only radiative forcing whose level of scientific understanding could not be improved appreciably over the last six years (Fig. 1.2). Regarding global climate change, the impact of fog and low stratus on the radiative transfer in the earth-atmosphere-system is one of the main sources of uncertainties for the simulation of increasing CO_2-concentrations based on global climate prediction models (Houghten et al. 2001, Stephens 2005, IPCC 2013). The main cause for these big uncertainties is the deficient characterization of cloud microphysical properties, which affect the interaction between boundary clouds and radiation. Most notably, LWC and DSD have to be named as well as their vertical distribution within the cloud. An improved assessment of these microphysical properties of fog and low stratus permits an enhanced parameterization of these boundary clouds in the currently utilized climate models (Dong and Mace 2003) and is a necessary condition for a more reliable estimation of the potential effects of a shift in CO_2-concentations on the global climate change (Turner et al. 2007).

Because of the delineated importance of fog and low stratus clouds and the still remaining uncertainties concerning their microphysical properties and dynamics there is an increased need for detailed information about

1. The spatiotemporal dynamics of fog / low stratus clouds (FLS).
2. Their microphysical properties, particularly DSD and LWC in space and time.

In view of this urgent information need, an operational detection of these parameters and its spatiotemporal dynamics depicts a valuable enhancement for the understanding of the interactions between cloud properties and radiative budget. In this context, remote sensing techniques offer the potential to provide reliable and accurate information on LWC and DSD dynamics on an operational basis with a high spatiotemporal resolution (Meyer et al. 1986, Fitzjarrald and Lala 1989, Fuzzi et al. 1998, Gultepe et al. 2007, Zhou and Ferrier 2008, Liu et al. 2011, Dupont et al. 2012).

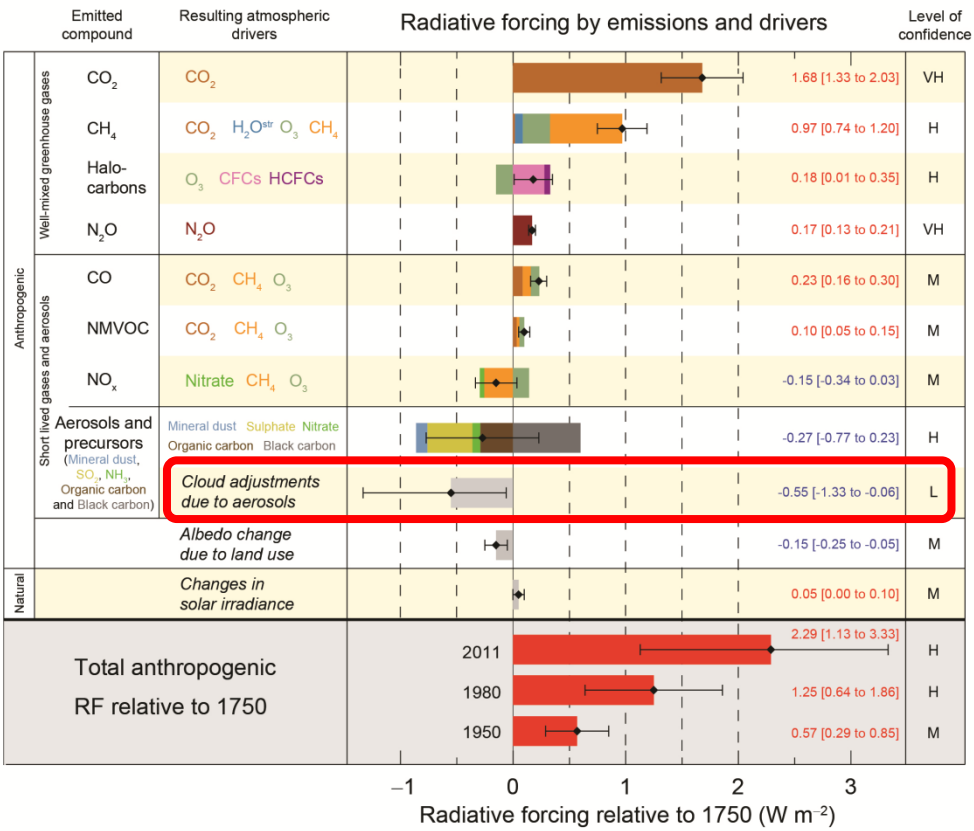

FIG. 1.1. Radiative forcing estimates in 2011 relative to 1750 and aggregated uncertainties for the main drivers of climate change. Values are global average radiative forcing (RF), partitioned according to the emitted compounds or processes that result in a combination of drivers. The best estimates of the net radiative forcing are shown as black diamonds with corresponding uncertainty intervals; the numerical values are provided on the right of the figure, together with the confidence level in the net forcing (VH – very high, H – high, M – medium, L – low, VL – very low). The cloud adjustments due to aerosol are highlighted in red as it remains the sole radiative forcing that still features a low confidence level (IPCC 2013a) since the fourth assessment report (see Fig. 1.2).

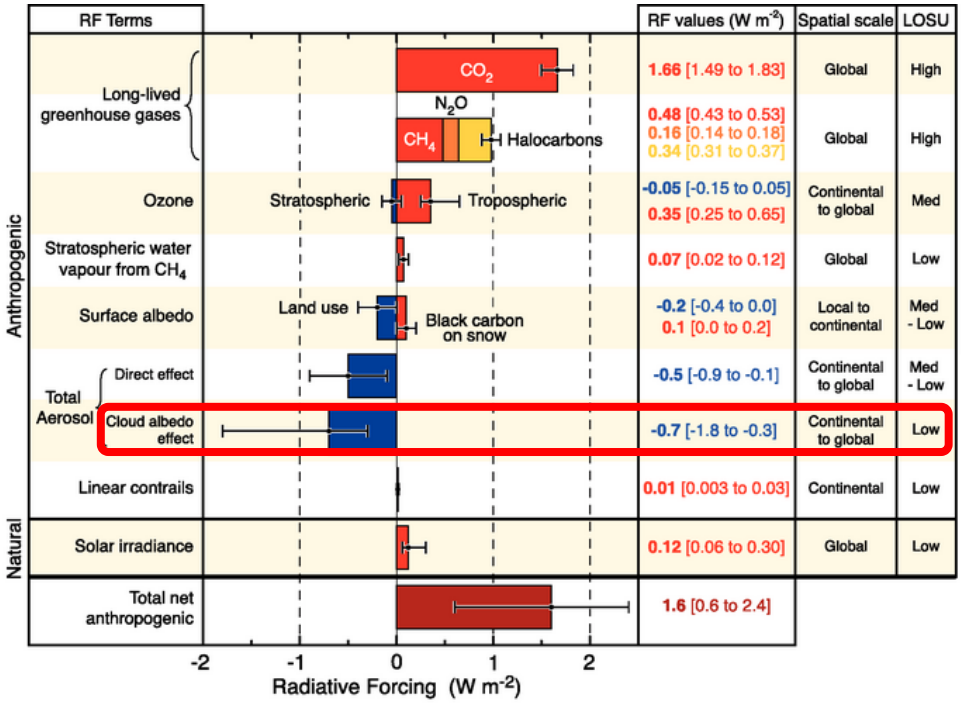

FIG. 1.2. Global mean radiative forcings (RF) and their 90% confidence intervals in 2005 for various agents and mechanisms. Columns on the right-hand side specify best estimates and confidence intervals (RF values); typical geographical extent of the forcing (Spatial scale); and level of scientific understanding (LOSU) indicating the scientific confidence level (IPCC 2007).

1.2 Existing remote sensing techniques for fog analyses and current limitations

The spatiotemporal observation of low stratus and fog with an operational system (human observer, scatterometer, radiometer etc.) is difficult because of the sparse density of field studies, notably in complex terrain regions as low mountain range in Germany (Bendix 2002). To overcome this problem, several satellite based techniques for the detection of FLS have been developed (e.g. Eyre et al. 1984, Ellrod 1995, Derrien et al. 1993, Lee et al. 1997, Gultepe et al. 2007, Cermak and Bendix 2011). These satellite-based techniques benefit from a high spatiotemporal resolution of operational weather satellites in the polar (LEO) and geostationary orbit (GEO).

On the one hand, there are passive measuring systems which permit an area-wide exploration FLS with a high temporal resolution over the whole cloud phenomena. Even though, some techniques, based on TERRA-MODIS and Meteosat Second Generation SEVIRI daytime data, permit a

differentiation between ground fog and low stratus (Bendix et al. 2005, Cermak and Bendix 2011), they lack of insights in the vertical profiles of FLS. Since information on the vertical structure of LWC is not directly available from optical satellite data, these approaches have to make assumptions on vertical LWC-profiles for the derivation of cloud geometrical thickness. Either adiabatic (e.g. Minnis et al. 1992, Brenguier et al. 2000a, Heidinger and Stephens 2000) or sub-adiabatic LWC-profiles have been implemented (Cermak 2006) which might not coincide with real conditions. This gap of knowledge arises from unavailable data on the vertical structure of fog varying with fog type and life cycle stages.

On the other hand, there are active remote sensing approaches that might be appropriate for the investigation FLS. Most used instruments are LIDARs, RADARs, SODARs or a combination of these instruments. An actual example for LIDARS is CALIOP (Cloud-Aerosol LIDAR with Orthogonal Polarization). The space-borne two-wavelength polarization LIDAR has been providing vertical profiles of aerosol and all cloud-types since 2006 (Kacenelenbogen et al. 2011). It is the primary instrument carried by the Earth Observation Satellite CALIPSO (Cloud-Aerosol LIDAR and Infrared Pathfinder Satellite Observations). Because of its construction for all kinds of clouds, it is not well suited for FLS featuring an insufficient sampling resolution of 30 to 60 m vertical and 333 m horizontal. In consequence of its 16 days repeat cycle the dynamics of the life cycle of fog cannot be detected in its full range (Winker et al. 2007). Besides, it is not possible to directly retrieve vertical LWC-profiles from the detected laser-beam.

The RADAR-based detection of clouds and their vertical profiles has a long tradition in weather observation with emphasis on azimuth-scanning rain-RADARs and the exploration of precipitation (e.g. Kitchen and Jackson 1993, Meischner et al. 1997, Kalinga and Gan 2007). In comparison, non-raining low stratus clouds have been disregarded widely in the past. Because of the low-frequency of rain-RADARs (2 GHz < f < 8 GHz, 5 cm < λ < 10 cm), they were only sensitive for bigger rain drops and not for much smaller cloud droplets (Clothiaux et al. 1995, Kollias et al. 2007). In contrast, novel cloud RADARs operating on high-frequency (75 GHz < f < 110 GHz, 2.7 mm < λ < 4.0 mm) are especially enabled to detect little cloud drops since the Rayleigh-approximation applies to the emitted microwaves (van de Hulst 1957). Millimeter-wave cloud RADARs again differ according to their mode of operation. There are pulse-RADARs which successively emit and receive single pulsed beams by turns and cloud RADAR profilers which are based on continuous-wave-techniques (CW). Pulse-RADARs measure the power backscattered by hydrometeors in cloud-layers as a function of distance from the RADAR, whereas cloud RADAR profilers provide information on multiple cloud layers from vertical RADAR reflectivity-profiles with a higher temporal resolution. The main instrument on the EOS CloudSat is the nadir-looking 94 GHz Cloud Profiling RADAR (CPR) with pulse-

Doppler signal processing. It performs ground sampling every 1.1 km and has a vertical resolution of 500 m, making it improper for fog exploration. Although, the attenuation by the atmospheric gaseous oxygen and water vapor is minimal due to its high frequency, it suffers nevertheless from saturation in boundary clouds, mainly caused by the long distance travelled (Stephens et al. 2002). Other, ground-based pulse cloud RADARs initially start measuring at about 500 m above the ground in order to exclude influences on the near-field (Löhnert et al. 2001). By this means, millimeter-wave pulse RADARs are not enabled to the detection of FLS in its entire extent (Cermak et al. 2006, Ruffieux et al. 2006).

Independently from the type of RADAR used for the detection of FLS, they all suffer from the fact that microphysical information such as LWC cannot be retrieved directly from RADAR reflectivity (Z). Thus, simple approaches for the derivation of vertical LWC-profiles are based on empirical regression coefficients which in turn rely on separately measured data of DSD. By means of the latter, the required parameters Z and LWC are computed (e.g. Sauvageot and Omar 1987, Liao and Sassen 1994, Fox and Illingworth 1997, Matrosov et al. 2004, Krasnov and Rauschenberg 2006). These equations benefit from their simple applicability. However, the regression equations suffer from their mutual dependency on the assumed DSD. Z is related to the latter by the third moment and LWC by the sixth moment. Thus, incorrect assumptions on DSD result in large errors for LWC and even larger ones for Z. Hence, computed LWC-values from measured Z-values vary extremely with presumed DSD leading to big uncertainties. Consequently, an improved knowledge about vertical LWC-profile is not only of general interest to understand the cloud adjustments effects (IPCC 2013) but also of most importance for the determination of the thickness of fog and low stratus cloud being the decisive criteria for the separation between both.

To minimize these uncertainties, more sophisticated methods use a combination of multiple sensors. Following the approach from Frisch et al. (1995, 1998) derived LWC-values from Z are initially integrated for the whole geometrical cloud depth resulting in the so-called liquid water path (LWP). The latter is measured directly and simultaneously by use of a microwave radiometer. Due to an iteration method, both LWP-values can be adjusted for emerging potential measurement errors of the LWP that is based on the microwave cloud RADAR. This approach has been conducted with minor modifications by several authors (e.g. Donovan and van Lammeren 2001, Dong and Mace 2003). Some other methods make use of additional data to those that are provided from RADAR and radiometer measurements in order to minimize errors in respect of derived vertical LWC-profiles. By using LIDAR data in addition to RADAR- and radiometer-measurements, McFarlane et al. (2002) developed an approach for deriving vertical LWC-profiles under the condition that prevailing DSDs are well-

known from airborne measurements. The Integrated Profiling Technique by Löhnert et al. (2001, 2004) combines a ground-based multichannel microwave radiometer, a cloud RADAR and also a LIDAR-ceilometer. The required regression coefficients for *Z*-LWC relationships are supplied by microphysical cloud models that are based on a priori knowledge of meteorological properties in the atmosphere.

In contrast, novel ground-based cloud RADAR profilers, which rely on the frequency modulated continuous wave technique (FMCW), are highly suitable for monitoring low stratus and fog (Cermak et al. 2006). Within the framework of COST action 722 (Short range forecasting methods of fog, visibility and low clouds) and COST action 720 (Integrated ground-based remote sensing stations for atmospheric profiling) ground- and satellite-based monitoring of FLS and their microphysical properties was given priority (Engelbart et al. 2008, Jacobs et al. 2008). In this context, the high potential of FMCW cloud RADAR profilers for the derivation of vertical profiles of microphysical properties was tested by means of a prototype operating at 78 GHz (Cermak et al. 2006). Their barely limited near-field enables the detection of low clouds as low as about 30 m (Huggard et al 2008). They deliver punctual vertical profiles of *Z* every 15 s in a vertical resolution of 4 m up to 2 km above the ground (Bennett et al. 2009). In combination with their high sensitivity to smaller drops, they are ideal for continuously monitoring the vertical distribution of low clouds and their microphysical properties such as DSD and therewith LWC. Since 94 GHz FMCW cloud profilers are new, there have been no suitable methods for the derivation of microphysical properties of fog and low stratus from RADAR reflectivity up to now.

As already mentioned further above, satellite-based remote sensing techniques for the detection of FLS suffer from a missing direct relationship between the recorded optical measurement parameter and the prevalent microphysical properties of the cloud phenomena. That is the reason why prevailing approaches have to rely on theoretical assumptions of vertical LWC-profiles. Thereby, an improved parameterization of LWC-profiles, relying on detailed measurements, is an essential requirement for a more precise satellite based derivation of cloud geometrical thickness and therewith for the distinction between ground fog and low stratus by means of satellite data. In order to get accurate information about the vertical structure of microphysical properties of low stratus a few cost-intensive in-situ airborne measurements were conducted. In this context, the Atlantic Stratocumulus Transition Experiment (ASTEX, Albrecht et al. 1995, Frisch et al. 1995), the Cloud LIDAR and RADAR Experiment (CLARE'98, ESA 1999), the second Aerosol Characterization Experiment (AGE-2, Brenguier et al. 2000b) and the Second Dynamics and Chemistry of the Marine Stratocumulus Field Study (DYCOMS-II, Stevens et al. 2003, Van Zenten et al. 2005) have to be named. These case studies provided more detailed information on

local microphysical properties and their vertical distribution, but they were very limited with respect to the spatiotemporal resolution. Furthermore, they did not supply a continuous detection of cloud microphysics for financial reasons. Besides, airborne measurements for the derivation of vertical microphysical properties are not permitted and not even possible during FLS situations because of low visibility and ceiling.

Since airborne measurements cannot provide vertical explorations of fog microphysical properties, some authors conducted balloon-borne field measurements with conventional sensors for temporally continuous profiles of fog properties and their vertical distribution (e.g. Okita 1962, Pinnick et al. 1978, Duda et al. 1991, Wetzel et al. 1996, Siebert et al. 2002). Previous field measurements confined themselves to effortful experimental single studies which were not suitable for operational applications. For this purpose, the used instruments had to be run on a tethered balloon-borne platform. Although only a few balloon-borne measurements have been performed so far, their good results proved their suitability for the detection of fog microphysical properties and their vertical distribution. Nevertheless, their application does not provide a spatiotemporal or even operational detection of fog properties for what reason they are primarily appropriate for validation purposes.

Another restriction of the existing approaches for the differentiation of FLS arises from the assumptions in consideration of DSD (e.g. lognormal or gamma-distribution). Besides, fixed values for drop number concentration regardless of height, as presumed by several authors, do not cope with the dynamics of low stratus clouds in any case. Particularly, FLS undergo processes of formation and dissipation, featuring diverse DSD and by association the relationship between Z and LWC (e.g. Pilié et al. 1972, 1975a, b, Wendisch et al. 1998). Meyer et al. (1986) and Welch and and Ravichandran (1986) identified five evolutionary stages during fog life cycle, whereas Pilié et al. (1972, 1975a, b) differentiated four consecutive ones, each having featured characteristic DSD (modified gamma distribution according to Deirmendjian 1964, 1969).The evolution of temperature and humidity near the ground were ascribed as crucial parameters for the formation and development of fog as well as turbulence (e.g. Gerber 1981, Wendisch et al. 1998, Terradellas and Bergot 2008, Zhou et al. 2008). In consequence of the variability of DSD as a function of evolutionary stages, the cloud dynamics serve as basis for a reliable derivation of vertical LWC-profiles (Guyot et al. 2000, Khain et al. 2008).

In summary it can be stated that the detection of numerous cloud-types as well as their microphysical properties has advanced in recent years, but there are still large research deficits concerning FLS:

1) There is an increased need of knowledge concerning the microphysics of FLS – especially relating to vertical LWC-profiles – with a

high temporal and spatial resolution. FMCW cloud RADAR profilers could fill this gap. However, it is not possible to derive microphysical properties as LWC directly from Z because both variables depend on the prevailing DSD.

2) Since FLS do not feature a constant DSD near the ground during their evolution and dissipation, their DSD evolves accordingly. Up to the present, there have been no systematic investigations on the evolution of DSD near the ground available for the entire fog life cycle.
3) As a result of the sophisticated exploration of fog events and their microphysics with regard to their entire vertical extensions, the variance of DSD with time and height is still undeclared.
4) By virtue of the dynamics of FLS in respect of their DSD, a temporal as well as spatial investigation of the latter is needed with a high resolution for a reliable derivation of LWC from Z of FMCW cloud RADAR profilers.

1.3 Aims of the thesis and outline

In view of the big relevance of FLS for the understanding of climate change and their meaning for air pollution control as well as traffic safety the application of a novel ground-based 94 GHz FMCW cloud RADAR profiler delineates big potential for a more precise exploration of these boundary cloud-types. However, there are no appropriate retrievals for the derivation of microphysical properties of FLS from RADAR reflectivity available.

The major aim of this thesis is therefore:

> The investigation of the temporal dynamics of fog microphysics with emphasis on DSD over its whole life cycle.

The major hypothesis of the presented thesis is stated as follows:

> A temporal separation of consecutive evolutionary stages within fog life cycle is possible by means of measurements of fog microphysics such as DSD at the ground as well as in vertical profiles.

In order to test the hypothesis the following working packages (WP) were required:

WP1: Theoretical analysis of the impact factors and their effects on the *Z*-LWC-relationship with consideration of the temporal dynamics of the evolutionary stages (Chapter 2).

WP2: Investigation of the temporal dynamics of fog microphysics at the ground-based on field measurements and a feasible classification of the evolutionary stages of fog (Chapter 3).

WP3: Exploration of vertical profiles of fog microphysics with respect to time within the life cycle (Chapter 4).

The structure of this work is presented in Fig. 1.3. After the introduction, a sensitivity study (WP1) reveals the influencing factors on the *Z*-LWC-relationship with regards to fog-types and evolutionary life cycle of fog events. Since it is not possible to derive microphysical properties as LWC from RADAR reflectivity directly, the DSD, which is the mathematical link between both variables by the third and sixth moment respectively, had to be investigated initially. Therefore, published values of DSD from field measurements were aggregated and elaborated in order to anticipate potential values of RADAR reflectivity. Contradictory assumptions on DSD would result in large errors in a new retrieval for deriving LWC from *Z* due to their high dependency on the latter. Thus, influencing factors on the *Z*-LWC-relationship had to be found out at first for the development of a novel method that enables the derivation of vertical fog properties from *Z*. Chapter 3 presents the development of a statistical approach for the separation of fog evolutionary stages being a major impact factor on the predominant DSD. Thereby, microphysical properties (LWC, total droplet number and mean radius) were measured by an Optical Particle Counter (OPC) during three radiation fog events accompanied by measurements of common meteorological parameters and horizontal visibility by a present weather sensor. On the basis of the recorded data a three-step statistical analysis was designed that enables an objective classification of three evolutionary stages in fog life cycles. In chapter 4, a novel balloon-borne measuring system is introduced, by which the vertical distributions of fog microphysics were investigated as a function of the prevailing evolutionary stage during fog life cycle. The allocation of evolutionary stage was conducted on the basis of the statistical approach from chapter 3. A blimp has been chosen as platform for the measurement equipment with the OPC as core, since it permits a continuous detection of fog properties in different vertical layers within fog. That way, the postulated thesis could be tested. Finally, in chapter 5 a summary of the previous chapters and a short outlook upon the possible applications of the findings in respect of the presented gaps of knowledge are given.

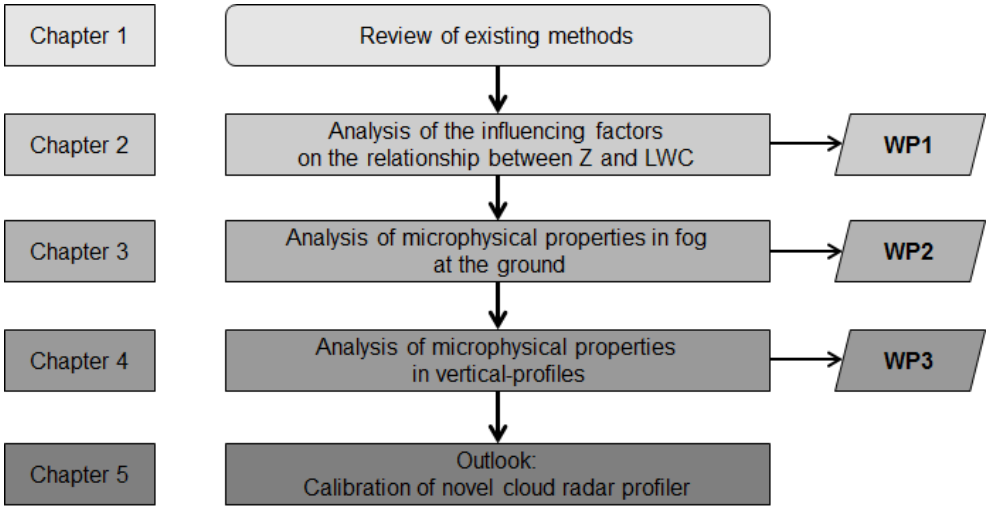

FIG. 1.3. Structure of the work.

1.4 Study area

The study area is located on the Ground Truth and Profiling Station (50.533048N/ 8.685358E, 172 m a.s.l) in the flood plain of the Lückebach-creek in the midst of small hills extending up to 250 m a.s.l (Fig. 1.4).

FIG. 1.4. Location of Marburg Ground Truth and Profiling Station highlighted by red arrow.

Because of the topographic position and a warm-moderate rain climate of mid-latitudes the measuring site is known for its high frequency of radiation fog in autumn (Bendix 2002). Based on the recommendation of COST action 722 and the good experiences of a predecessor-model operating at 78 GHz during COST action 720, the working group LCRS has been equipped with a novel 94 GHz FMCW cloud RADAR profiler from Rutherford Appleton Laboratory, UK, since 2008 (Fig. 1.5).

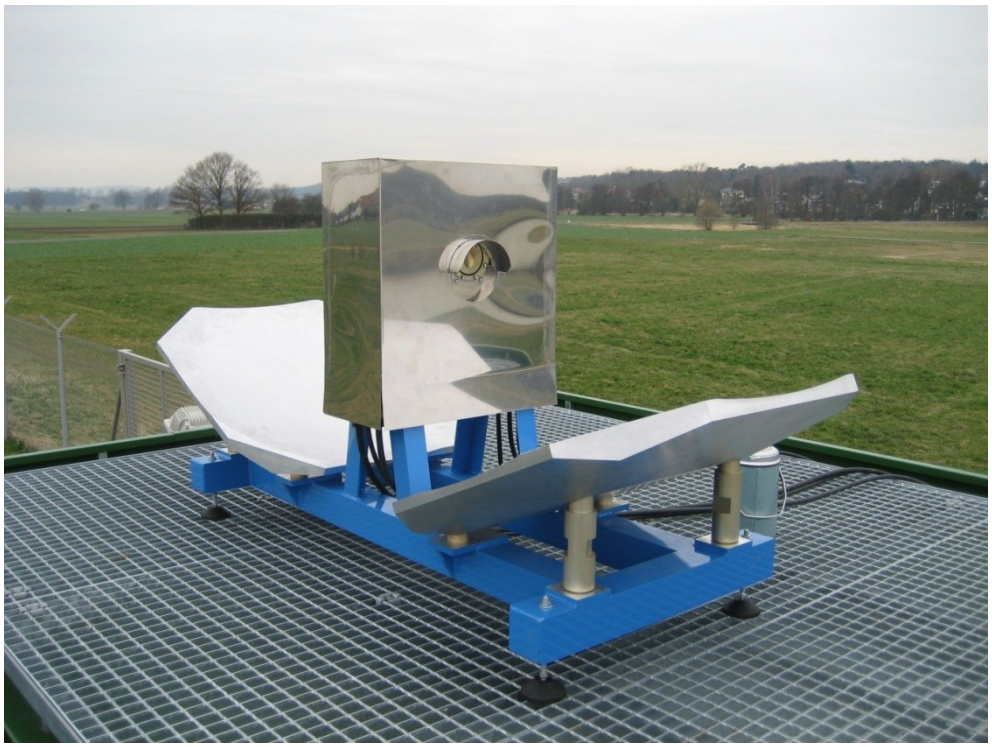

FIG. 1.5. 94 GHz FMCW cloud RADAR profiler situated on the Marburg Ground Truth and Profiling Station.

The balloon-borne measurements of vertical fog profiles were conducted by an Optical Particle Counter (OPC) accompanied by measurements of common meteorological parameters with the aid of a SmartTether-sonde (Fig. 1.6).

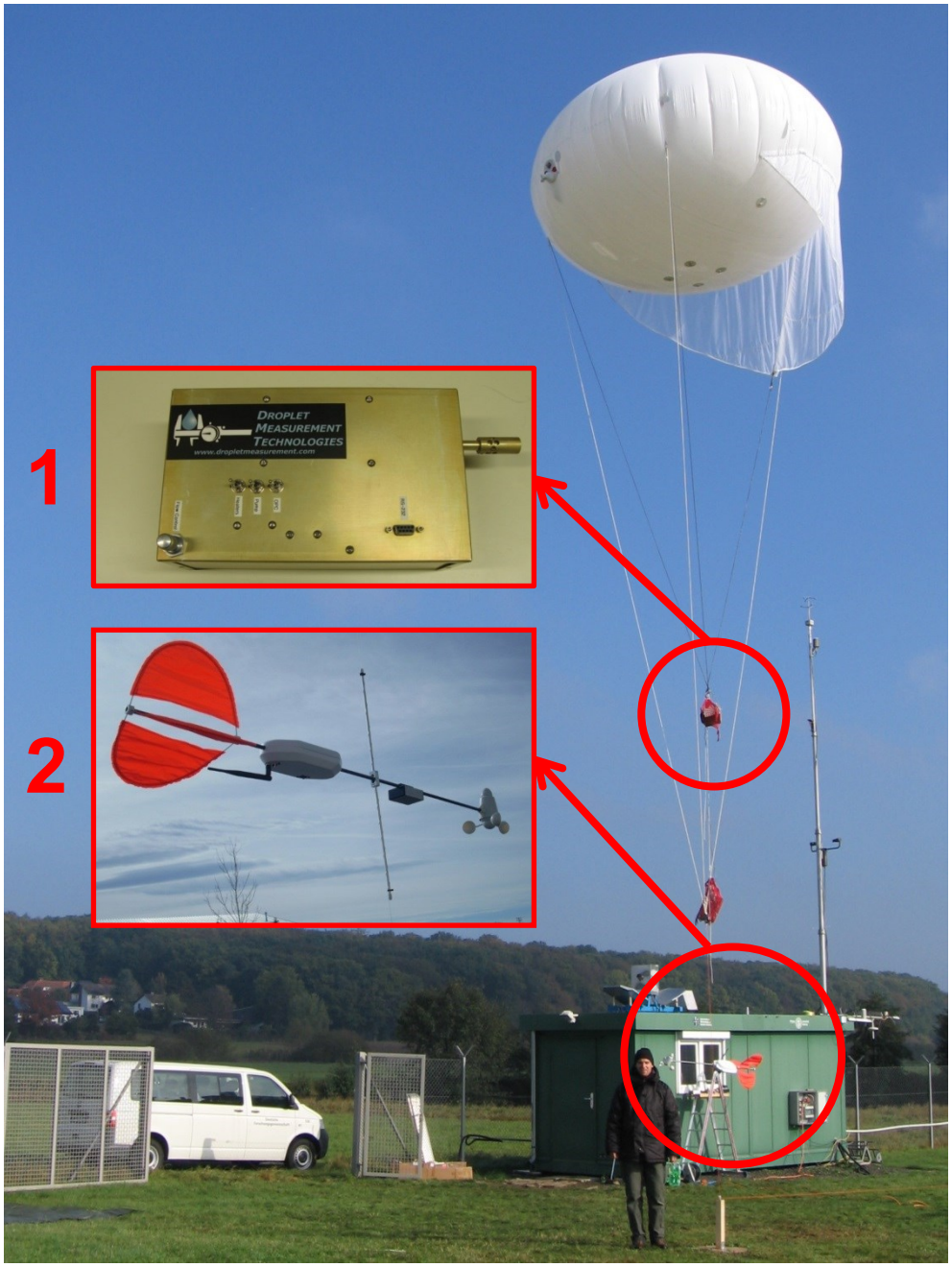

FIG. 1.6. Balloon-borne measuring system composed of Optical Particle Counter (1) and SmartTether-sonde (2).

Due to the location of Marburg Ground Truth and Profiling Station it is well-suited for a detailed and representative exploration of fog dynamics and microphysical properties on the basis of the available instruments.

1.5 References

Albrecht, B.A., Bretherton, C.S., Johnson, D., Scubert, W. and Frisch, A.S. 1995. The atlantic stratocumulus transition experiment. ASTEX. *Bulletin of the American Meteorological Society* **76**, 889–904.

Andre, P., Silva, C.A., Balocco, E., Boreux, J., Cavallo, V., Colomb, M., Dore, J., Dufour, J., Hannay, J., Hirech, K., Kelly, N., Lacote, P. and Mealares, L. 2004. The main results of a European research project: "Improvement of transport safety by control of fog production in a chamber (FOG). In: *Proceedings of the third International Conference on Fog, Fog Collection and Dew*, 11-15. October, Cape Town.

Bendix, J. 2002. A satellite-based climatology of fog and low-level stratus in Germany and adjacent areas. *Atmospheric Research* **64**, 3-18.

Bendix, J., Thies, B., Cermak, J., and Nauss, T. 2005. Ground fog detection from space based on MODIS daytime data – a feasibility study. *Weather and Forecasting* **20**, 989-1005.

Bennett, A. J., Gaffard, C., Oakley, T. and Moyna, B. 2009. Cloud radar – initial measurements from the 94 GHz FMCW cloud radar. *Proceedings of the 8th International Symposium on Tropospheric Profiling 19–23 October*, Delft, pp. 1-8.

Brenguier, J.L., Pawlowska, H., Schüller, L., Preusker, R., Fischer, J. (2000a). Radiative properties of boundary layer clouds. Droplet effective radius versus number concentration. *Journal of the Atmospheric Sciences* **57**, 803-821.

Brenguier, J.L., Chuang, P.Y., Fouquart, Y., Johnson, D.W., Parol, F., Pawlowska, H., Pelon, J., Schüller, L., Schröder, F. and Snider, J. (2000b). An overview of the AGE-2 CLOUDY COLUMN closure experiment. *Tellus B* **52**, 814–826.

Cermak, J. 2006. *SOFOS - A new satellite-based operational fog observation scheme. Dissertation*. Philipps-University of Marburg, Marburg, pp. 1-147.

Cermak, J., Schneebeli, M., Nowak, D., Vuilleumier, L., and Bendix, J. 2006. Characterization of low clouds with satellite and ground-based remote sensing systems. *Meteorologische Zeitschrift* **15**, 65-72.

Cermak J. and Knutti R. 2009. Beijing Olympics as an aerosol field experiment. *Geophysical Research Letters* **36**, L10806.

Cermak, J. and Bendix, J., 2011. Detecting ground fog from space – a micro-physics-based approach. *International Journal of Remote Sensing* **32**, 3345–3371.

Clothiaux, E.E., Miller, M.A., Albrecht, B.A., Ackermann, T.P., Verlinde, J., Babb, D.M., Peters, R.M., and Syrett, W.J. 1995. An evaluation of a 94 GHz radar for remote sensing of cloud properties. J*ournal of Atmospheric and Oceanic Technology* **12**, 201–229.

Deirmendjian, D. 1964. Scattering + polarization properties of water clouds + hazes in the visible + infrared. *Applied Optics* **3**, 187-196.

Deirmendjian, D. 1969. *Electromagnetic scattering on spherical polydispersions*. Elsevier Scientific Publishing, New York, pp. 1-290.

Derrien, M., Farki, B., Harang, L., Legleau, H., Noyalet, A., Pochic, D. and Sairouni, A. 1993. Automatic cloud detection applied to NOAA-11 /AVHRR imagery. *Remote Sensing of Environment* **46**, 246–267.

Dong, X. and Mace, G.G. 2003. Profiles of low-level stratus cloud microphysics deduced from ground-based measurements. *Journal of Atmospheric and Oceanic Technology* **20**, 42-53.

Donovan, D.P. and van Lammeren, A. 2001. Cloud effective particle size and water content profile retrievals using combined lidar and radar observations 1. Theory and examples. *Journal of Geophysical Research* **106**, 27425–27448.

Duda, D.P., Steffens, G.L. and Cox, S.K. 1991. Microphysical and radiative properties of marine stratocumulus from tethered balloon measurements. *Journal of* Applied Meteorology **30**, 170–186.

Dupont, J.C., Haefflin, M., Protat, A. Bouniol, D., Boyouk, N. and Morille, Y. 2012. Stratus-fog formation and dissipation. A 6-day case study. *Boundary-Layer Meteoro*l. **143**, 207-225.

Ellrod, G.P. 1995. Advances in the detection and analysis of fog at night using GOES multispectral infrared imagery. *Weather and Forecasting* **10**, 606–619.

Engelbart, D.A.M., Monna, W.A., Nash, J., and Mätzler, C. (eds). 2008. *Integrated ground-based redmote sensing stations for atmospheric profiling*. COST Action 720 final report, Final Report. COST office, Luxembourg, pp. 1-422.

ESA. 1999. CLARE'98. Cloud lidar and radar experiment. In: *Proceedings of the ESTEC International Workshop.* Noordwijk, Netherlands, European Space Research and Technology Center, pp. 1-239.

Eyre, J.R., Brownscombe, J.L., and Allam, R.J. 1984. Detection of fog at night using advanced very high resolution radiometer (AVHRR) imagery. Meteorological Magazine **113**, 266–271.

Fitzjarrald, D. R. and Lala, G. G. 1989. Hudson Valley Fog Environments. *J. Appl. Meteorol.* **28**, 1303-1328.

Fox, N.I. and Illingworth, A.J. 1997. The retrieval of stratocumulus cloud properties by ground-based cloud radar. *Journal of Applied Meteorology* **36**, 485-492.

Frisch, A.S., Fairall, C.W. and Snider, C.W. 1995. Measurement of stratus clouds and drizzle parameters in ASTEX with a K_a-band doppler radar and a microwave radiometer. *Journal of the Atmospheric Sciences* **52**, 2788–2799.

Frisch, A.S., Fairall, C.W., Feingold, G. Uttal, T. and Snider, J.B. 1998. On cloud radar microwave radiometer measurements of stratus cloud liquid water profiles. *Journal of Geophysical Research* **103**, 23195–23197.

Fuzzi, S., Castillo, R.A., Jiutso, J.E. and Lala, G.G. 1984. Chemical-composition of radiation fog water at Albany, New-York, and its relation-ship to fog microphysics. *Journal of Geophysical Research* **89**, 7159-7164.

Fuzzi, S., Laj, P., Ricci, L., Orsi, G., Heintzenberg, J., Wendisch, M., Yuskiewicz, B., Mertes, S., Orsini, D., Schwanz, M., Wiedensohler, A., Stratmann, F., Berg, O. H., Swietlcki, E., Frank, G., Martinsson, B. G., Gün-ther, A., Dierssen, J. P., Schell, D., Jaenschke, W. Berner, A., Dusek, U., Galambos, Z., Kruisz, C., Mesfin, N. S., Wobrock, W., Arends, B. and Tenb, H. 1998. Overview of the Po Valley fog experiment 1994 (CHEMDROP). *Contr. Atmos. Phys.***71**, 3–19.

Gerber, H.E. 1981. Microstructure of a radiation fog. *Journal of the Atmos-pheric Sciences* **38**, 454-458.

Gultepe, I., Muller, M.D. and Boybeyi, Z. 2006. A new visibility parameter-ization for warm-fog applications in numerical weather prediction models. *Journal of Applied Meteorology and Climatology* **45**, 1469–1480.

Gultepe, I., Tardif, R., Michaelides, S. C., Cermak, J., Bott, A., Bendix, J., Mueller, M. D., Pagowski, M., Hansen, B., Ellrod, G., Jacobs, W., Toth, G. and Cober, S. G. 2007. Fog research. A review of past achievements and future perspectives. *Pure Appl. Geophys.* **164**, 1121–1159.

Gultepe, I., Pearson, G., Milbrandt, J.A., Hansen, B., Platnick, S., Taylor, P., Gordon, M., Oakley, J.P. and Cober, S.G. 2009. The fog remote sensing and modeling field project. *Bulletin of the American Meteorological Society* **90**, 341-359.

Guyot, A., Testud, J. and Ackerman, T.P. 2000. Determination of the radia-tive properties of stratiform clouds from a nadir-looking 95-GHz radar. *Journal of Atmospheric and Oceanic Technology* **17**, 38-50.

Heidinger, A.K. and Stephens, G.L. 2000. Molecular line absorption in a scattering atmosphere. Part II. Application to remote sensing in the O_2 A band. *Journal of the Atmospheric Sciences* **57**, 1615-1634.

Houghten, J.T., Ding, Y., Griggs, D.J., Noguer, M., Linden, P.J.V.D., Dai, X., Maskel, K. and Johnsen, C.A. (eds). 2001. *Climate Change 2001: The scientific basis.* Cambridge University Press Cambridge, pp. 1-881.

Huggard, P.G., Oldfield, M.L., Moyna, B.P., Ellison, B.N., Matheson, D.N., Bennett, A.J., Gaffard, C., Oakley, T., and Nash, J. 2008. 94 GHz FMCW cloud radar. In: *Proceedings of the SPIE symposium on millimetre wave and terahertz sensors and technology*, 15-18 September 2008, Cardfiff, pp. 1-6.

IPCC. 2007. *Climate Change 2007. The physical science basis. Contribution of Working Group I to the Fourth Assessment Report of the Intergovernmental Panel on Climate Change.* [Solomon, S., D. Qin, M. Manning, Z. Chen, M. Marquis, K.B. Averty, M. Tignor and H.L. Miller (eds.)] Cambridge University Press, Cambridge, U.K. and New York, USA, pp. 1-996.

IPCC. 2013. Working Group I. Contribution to the IPCC 5th Assessment Report (AR5), Climate Change 2013: The Physical Science Basis. Online at: http://www.climatechange2013.org/images/uploads/WGIAR5_WGI-12Doc2b_FinalDraft_All.pdf. Last page view: 02/15/2014.

IPCC. 2013a. *Climate Change 2013. The Physical Science Basis. Summary for Policymakers.* Online at: http://www.climatechange2013.org/ images/uploads/WGI_AR5_SPM_brochure.pdf. Last page view: 02/15/2014.

Jacobs, W., Nietosvaara, V., Bott, A. Bendix, J., Cermak, J., Michaelides, S., and Gultepe, I. (eds). 2008. *Short range forecasting methods of fog, visibility and low clouds*, COST Action 722 final report, Brussels, Office for official publications of the European Communities, pp. 1-489.

Jaeschke, W., Dierssen, J.P., Günther, A., Schickedanz, W., Wolf, A., Ricci, L. and Arends, B.G. 1998. Mass fluxes and chemical pathways during a fog event. *Beiträge zur Physik der Atmosphäre* **71**, 145-157.

Kacenelenbogen, M., Vaughan, M.A., Redemann, J., Hoff, R.M., Rogers, R.R., Ferrare, R.A., Russell, P.B., Hostetler, C.A., Hair, J.W. and Holben, N.N. 2011. An accuracy assessment of the CALIOP/CALIPSO version 2/ version 3 daytime aerosol extinction product based on a detailed multi-sensor, multi-platform case study. *Atmos. Chem. Phys*. **11**, 2981-4000.

Kalinga, O.A. and Gan, T.Y. 2007. Small storm precipitation estimation using merged radar and gauging data. In*ternational Journal of Remote Sensing* **28**, 1101-1112.

Khain, A., Pinsky, M., Magaritz, L., Krasnov, O., and Russchenberg, H.W.J. 2008. Combined observational and model investigations of the Z–LWC relationship in stratocumulus clouds. *Journal of Applied Meteorology and Climatology* **47**, 591-606.

Kitchen, M. and Jackson, P.M. 1993. Weather radar performance at long-range. Simulated and observed. *Journal of Applied Meteorology* **32**, 975-985.

Kollias, P., Clothiaux, E.E., Miller, M.A., Albrecht, B.A., Stephens, G.L., and Ackerman, T.P. 2007. Millimeter-wavelength radars. New frontier in atmospheric cloud and precipitation research. *Bulletin of the American Meteorological Society* **88**, 1608-1624.

Krasnov, O.A. and Russchenberg, H.W.J. 2006. A synergetic radar-lidar technique for the LWC retrieval in water clouds. In: *Preprints, Seventh International Symposium on Tropospheric Profiling. Needs and Techniques*, Boulder, CO, pp. 1-13.

Kraus, H. and Ebel, U. 1989. Atmospheric boundary layer characteristics in severe smog episodes. *Meteorological and Atmospheric Physics* **40**, 211-224.

Lee, T.E., Turk, F.J. and Richardson 1997. Stratus and fog products using GOES-8-9 3.9-μm data. *Weather and Forecasting* **12**, 664–677.

Liao, L. and Sassen, K. 1994. Investigation of relationships between Ka-band radar reflectivity and ice and liquid water contents. *Atmospheric Research* **34**, 231–248.

Liu, D., Yang, J., Niu, S. and Li, Z. 2011. On the evolution and structure of a radiation fog event in Nanjing. *Adv. Atmos. Sci.* **28**, 223-237.

Löhnert, U., Crewell, S., Simmer, C. and Macke, A. 2001. Profiling cloud liquid water by combining active and passive microwave measurements with cloud model statistics. *Journal of Atmospheric and Oceanic Technology* **18**, 1354–1366.

Löhnert, U., Crewell, S. and Simmer, C. 2004. An integrated approach toward retrieving physically consistent profiles of temperature, humidity, and cloud liquid water. *Journal of Applied Meteorology* **43**, 1295-1307.

Matrosov, S.Y., Uttal. T. and Hazen, D.A. 2004. Evaluation of radar reflectivity-based estimates of water content in stratiform marine clouds. *Journal of Applied Meteorology* **43**, 405-419.

McFarlane, S.A., Evans, K.F. and Ackermann, A.S. 2002. A Bayesian algorithm for the retrieval of liquid water cloud properties from microwave radiometer and millimeter radar data. *Journal of Geophysical Research-Atmospheres* **107**, 4317-4338.

Meischner, P., Collier, C., Illingworth, A., Joss, J. and Randeu, W.L. 1997. Advanced weather radar systems in Europe. The CLOST 75 action. *Bull. Amer. Meteor. Soc.* **78**, 1411-1430.

Meyer, M.B., Lala, G.G., and Jiusto, J.E. 1986. FOG-82 - A cooperative field study of radiation fog. *Bulletin of the American Meteorological* Society **67**, 825-832.

Minnis, P., Young, D.F., Kratz, D.P., Coakley, J.A., King, M.D., Garber, D.P., Heck, P.W., Mayor, S., Arduini, R.F. 1997. Cloud optical property retrieval (subsystem 4.3). Clouds and the earth's radiant energy sSystem (CERES) *Algorithm Theoretical Basis Document*, pp. 1–60.

Müller, M.D., Masbou, M. and Bott, A. 2010. Three-dimensional fog forecasting in complex terrain. *Quarterly Journal of the Royal Meteorological Society* **136**, 2189-2202.

Okita, T. 1962. Observations of the vertical structure of a stratus cloud and radiation fogs in relation to the mechanism of drizzle formation. *Tellus* **14**, 310–322.

Pagowski, M., Gultepe, I. and King, P. 2004. Analysis and modeling of an extremely dense fog event in southern Ontario. *Journal of Applied Meteorology* **43**, 3-16.

Pilié, R.J., Eadie, W., Mack, E.J., Rogers, C., and Kocmond, W.C. 1972. Project Fog Drops. Part 1: Investigations of warm fog properties. Washington D.C., *NASA Contractor Report*. Buffalo, New York: Cornell Aeronautical Laboratory, Inc., pp. 1-149.

Pilié, R. J., Mack, E. J., Kocmond, W. C., Rogers, C. W., and Eadie, W.J. 1975a. The life-cycle of valley fog. 1. Micrometeorological characteristics. *Journal of Applied Meteorology* **14**, 347-363.

Pilié, R. J., Mack, E. J., Kocmond, W. C., Eadie, W. J., and Rogers, C. W. 1975b. The life-cycle of valley fog. 2. Fog microphysics. *Journal of Applied Meteorology* **14**, 364-374.

Pinnick, R.G., Hoihjelle, D.L., Fernandez, G., Stenmark, E.B., Lindberg, J.D., Hoidale, G.B. and Jennings, S.G. 1978. Vertical structure in atmospheric fog and haze and its effects on visible and infrared extinction. *Journal of the Atmospheric Sciences* **35**, 2020–2032.

Ruffieux, D. Nash, J., Jeannet, P., and Agnew, J.L. 2006. The COST 720. temperature, humidity, and cloud profiling campaign: TUC. *Meteorologische Zeitschrift* **15**, 5-10.

Sauvageot, H., and Omar, J. 1987. Radar reflectivity of cumulus clouds. *Journal of Atmospheric and Oceanic Technology* **4**, 264–272.Siebert, H., Wendisch, M. Conrath, T., Teichmann, U., Heintzenberg, J. 2003. A new tethered balloon-borne payload for fine-scale observations in the cloudy boundary layer. *Boundary Layer Meteorology* **106**, 461-482.

Siebert, J., Bott, A. and Zdunkowski, W. 1992. Influence of a vegetation-soil model on the simulation of radiation fog. *Contributions to Atmospheric Physics* **65**, 93-106.

Stephens, G.L., Vane, D.G., Boain, R.J., Mace, G.G., Sassen, K., Wang, Z., Illingworth, A.J., O'Connor, E.J., Rossow, W.B., Durden, S.L., Miller, S.D., Austin, R.T., Benedetti, A. and Mitrescu, C. 2002. The CloudSat mission and the A-Train. A new dimension of space-based observations of clouds and precipitation. *Bull. Amer. Meteor. Soc.*, **83**, 1771–1790.

Stephens, G.L. 2005. Cloud feedbacks in the climate system: A critical review. *Journal of Climate* **18**, 237-273.

Stevens, B., Lenschow, D.H., Vali, G., Gerber, H., Bandy, A., Blomquist, B., Brenguier, J.L., Bretherton, C.S., Burnet, F., Campos, T., Chai, S., Faloona, I., Freisen, D., Haimov, S., Laursen, K., Lilly, D.K., Loehrer, S.M., Malinowski, S.P., Morley, B., Petters, M.D., Rogers, D.C., Russell, L., Savicjovac, V., Snider, J.R., Straub, D., Szumowski, M.J., Takagi, H., Thornten, D.C., Tschudi, M., Twohy, C., Wetzel, M. and van Zanten, M.C. 2003. Dynamics and chemistry of maritime stratocumulus. DYCOMS-II. *Bulletin of the American Meteorological Society* **84**, 579–593.

Terradellas, E., and Bergot, T. 2008. Comparison between two single-column models designed for short-term fog and low-clouds forecasting. *Física de la Tierra* **19**, 189-203.

Turner, D.D., Vogelmann, A.M., Austin, R.T., Barnard, J.C., Cady-Pereira, K., Chiu, J.C., Clough, S.A., Flynn, C., Khaiyer, M.M., Liljegren, J., Johnsen, K.P., Lin, B., Long, C., Marshak, A., Matrosov, S.Y., McFarlance, S.A., Miller, M., Min, Q., Minnis, F., O'Hirok, W., Wang, Z. and Wiscombe, W. 2007. Thin liquid water clouds. Their importance and our challenge. *Bulletin of the American Meteorological Society* **88**, 177-190.

van de Hulst, H.C. 1957. *Light scattering by small particles*. Courier Dover Publications, Mineola N.Y, pp. 1-470.

Van Zanten, M.C., and Stevens, B. 2005. Observations of the structure of heavily precipitating maritime stratocumulus. Jo*urnal of the Atmospheric Sciences* **62**, 4327–4342.

Welch, R.M., and Ravichandran, M.G. 1986. Prediction of quasi-periodic oscillations in radiation fogs. 1. Comparison of simple similarity approaches. *Journal of the Atmospheric Sciences* **43**, 633-651.

Wendisch, M., Mertes, S., Heintzenberg, J., Wiedensohler, A., Schell, D., Wobrock, W., Frank, G., Martinsson, B.G., Fuzzi, S., Orsi, G., Kos, G., and Berner, A. 1998. Drop size distribution and LWC in Po Valley fog. *Contributions to Atmospheric Physics/Beiträge zur Physik der Atmosphäre* **71**, 87-100.

Welch, R.M. and Ravichandran, M.G. 1986. Prediction of quasi-periodic oscillations in radiation fogs. 1. Comparison of simple similarity approaches. *Journal of the Atmospheric Sciences* **43**, 633–651.

Wetzel, M.A., Randolph, D.B., Xu, L.E. 1996. Satellite microphysical retrievals for land-based fog with validation by balloon profiling. *Journal of Applied Meteorology* **35**, 810-829.

Winker, D.M., William, H.H. and McGill, M.J. 2007. Initial performance assessment of CALIOP. *Geophysical Research Letters* **34**, L19803.

WMO. 1992. International meteorological vocabulary. Vol. 182. (ed. WMO). Geneva, 1-276.

Zhou, B. B. and B. S. Ferrier. 2008. Asymptotic analysis of equilibrium in radiation fog. *J. Appl. Meteorol.* **47**, 1704-1722.

2. Simulating Z-LWC relations in natural fogs with radiative transfer calculations for future application to a cloud radar profiler

Frank Maier, Jörg Bendix and Boris Thies

Faculty of Geography, University of Marburg, Marburg, Germany

Printed in

PURE AND APPLIED GEOPHYSICS (2012)

Pure Appl. Geophys. **169**

Published online 19 May 2011

DOI 10.1007/s00024-011-0332-0

(Received 11/18 2010, Revised 3/7 2011, Accepted April 4/9 2011)

Abstract

The vertical distribution of liquid water content (LWC) in natural fog and low stratus is a crucial variable in many applications, e.g. the development of satellite based retrievals of ground fog. Unfortunately, there is very little data concerning fog LWC-profiles, mainly due to the lack of suitable operational instrumentation. A novel ground-based 94 GHz FMCW cloud radar could fill this gap if radar reflectivity *Z* could be converted to LWC by using appropriate *Z*-LWC relations.

However, this relation strongly depends on drop size distribution (DSD) and is hardly known for natural fog types. In this sensitivity study, the influence of the DSD on the *Z*-LWC relation in different types and life cycle stages of natural fogs is analyzed using a radiative transfer code (RTC) and published fog drop size distributions.

It could be shown that there is a direct but nonlinear relationship between LWC and radar reflectivity. The proportionality factor of the *Z*-LWC equation in particular reveals specific ranges for the different life cycle stages. If a proper classification of fog life cycle in the field is possible, the results could be used to properly convert *Z* to LWC.

2.1 Introduction

Fog defined as horizontal visibility < 1 km (WMO 1992) is a major obstruction for air, land and sea traffic, but can also have severe impacts on air quality (smog) if air pollutants are present. Unfortunately, the spatio-temporal observation with an operational (human observer, transmissiometer, scatterometer) network is difficult due to the sparse density of observations, particularly in complex terrain such as the lower mountain ranges in Germany (e.g. Schulze-Neuhoff 1976). To overcome this problem, different methods for operational fog forecasting and nowcasting have been developed over the last decades (for an overview, see Gultepe et al. 2007, Jacobs et al. 2008).

From the numerical modeling point of view, accurate fog forecasting still remains a challenge. One reason for the problem in accurately forecasting fog is the difficulty in representing the microphysical processes involved, which are still not completely understood (Gultepe et al. 2007). Several studies suggest that a better understanding of fog microphysics is needed to develop more accurate forecasting models (Tardif 2007, Gultepe and Milbrandt 2007, Pagowski et al. 2004). The life cycle of fog (formation, development and dissipation) is directly related to microphysical processes that are not represented accurately enough in models. Siebert et al. (1992a, b) and von Glasow and Bott (1999) developed models that explicitly resolve the evolution of the droplet size distribution and cloud condensation nuclei. In a comparative study, Terradellas et al. (2007) showed that 1-D models

can simulate the major features of the fog cycle. Their results also indicate a high sensibility to the model's physical parametrization and vertical resolution. However, such 1-D model approaches are computationally very intensive. Parametrized versions of the detailed 1-D fog microphysics models can be incorporated in 3-D models, resulting in more precise forecast results (Gultepe et al. 2006, Gultepe and Milbrandt 2007, Pagowski et al. 2004).

Another major challenge in nowcasting the spatio-temporal fog dynamics is their detection based on weather satellite data. Here, particularly the ability to distinguish low stratus and ground fog is not yet conclusively established. First approaches for ground fog detection using TERRA-MODIS and Meteosat Second Generation SEVIRI daytime data have been proposed by Bendix et al. (2005) and Cermak and Bendix (2011). However, these techniques require information on the vertical structure of liquid water content (LWC) within fog layers, which are not directly available from optical satellite data. For this reason, the approaches mentioned assume a sub-adiabatic LWC profile, which might not coincide with real conditions. This uncertainty is mainly due to a lack of data on the vertical structure of fog for different fog types and life cycle stages. In situ airborne measurements, as frequently conducted for higher clouds, are not permitted and not even possible during fog situations. Balloon-borne systems with suitable sensors for temporally continuous profile measurements are not available. Passive microwave profilers might bridge this gap, but their poor vertical resolution of > 500 m partly exceeds the vertical extent of fog layers (e.g. Cermak et al. 2006, Ruffieux et al. 2006). In this context, millimeter-wave cloud profiling radars operating at 35 or 94 GHz are well suited for continuous cloud observations, since the attenuation of the beam by oxygen and water vapor absorption is minimal near these frequencies. Furthermore, these radars are more sensitive for cloud particles with diameters of a few micrometers to precipitating drops. The sensitivity to small hydrometeors, the high spatial resolution and the ability to provide information on multiple cloud layers from millimeter-wavelength radars make them ideal for continuously monitoring the vertical distribution of clouds and their microphysical properties (e.g. Clothiaux et al. 1995, Kollias et al. 2007). Especially cloud radars that rely on the frequency modulated continuous wave technique (FMCW) are highly suitable for monitoring fog and low stratus layers because of their small near field. They enable the detection of clouds as low as about 30 m (Cermak et al. 2006, Nowak et al. 2008, Bennett et al. 2009), which contrasts starkly with existing pulse cloud radars with larger near fields reaching up to about 500 m (e.g. Löhnert et al. 2001).

Simple techniques use empirically derived relationships linking both parameters to retrieve LWC profiles from radar reflectivity Z (e.g. Sauvageot and Omar 1987, Lia and Sassen 1994, Fox and Illingworth,

Boers et al. 2000). The main advantage of these approaches lies in their simple application. However, the Rayleigh approximation applies since the radar wavelength is much longer compared to the size of the observed cloud droplets. Consequently, the radar reflectivity is proportional to the sixth moment of the droplet spectrum, whereas the LWC is proportional to the third moment of the droplet spectrum. A variation of the droplet spectrum thus strongly influences the relationship between *Z* and LWC. Using only one fixed relationship to retrieve the LWC from Z without considering the droplet spectrum leads to high uncertainties in the calculated LWC profile (e.g. Löhnert et al. 2001). Khain et al. (2008) emphasize the ambiguous character of *Z*–LWC relationships in low level water clouds, which is responsible for the low accuracy of retrieval algorithms. According to the authors, this is partially related to the fact that empirical *Z*-LWC relationships are often derived without a corresponding understanding of the microphysical processes within the cloud. The results of their numerical simulations indicate the significant importance of microphysical processes for the retrieval of LWC from radar reflectivity. Additional information about droplet size distributions and specific regimes of cloud formation has to be taken into account in order to derive proper *Z*-LWC relationships.

To minimize the uncertainties caused by the unknown droplet spectrum, more sophisticated techniques use different sensors in combination to incorporate additional information about the liquid water path and the backscatter coefficient measured by lidar ceilometers (e.g. Frisch et al. 1995 1998, Donovan and Van Lammeren 2001, McFarlane et al. 2002, Löhnert et al. 2001, 2004). However, these techniques also rely on assumptions about the droplet spectrum (e.g. lognormal or gamma) and/or the droplet concentration. Concerning the high temporal dynamic of low level stratiform clouds, such assumptions are not suitable for a proper retrieval of the LWC from radar reflectivity. Especially for fog and low stratus clouds, several authors have identified different evolutionary stages with strong influences on the drop size spectrum and thus the relationship between *Z* and LWC (e.g. Pilié et al. 1975a, Meyer et al. 1986, Welch et al. 1986, Wendisch et al. 1998).

The aim of the present study is to investigate the influence of the drop size spectrum on the relationship between *Z* and LWC by means of radiative transfer calculations. To this end, characteristic drop size distributions of natural fogs, as measured during various field studies, are taken from the literature. The results are used to test the sensitivity of the *Z*-LWC relation in natural fogs regarding variations in drop size distributions as reported for different fog situations and life cycle stages. In this context, the study aims to investigate three questions: (1) the influence of the drop size spectrum on the relationship between *Z* and LWC, (2) the different fog types with regard to their specific influence on the relationship between *Z* and LWC and (3) the relevance of the fog life cycle for the *Z*-LWC relation.

The results of the study provide valuable information for the development of a *Z*-LWC retrieval technique for a novel 94 GHz FMCW cloud radar profiler (Huggard et al. 2008, Bennett et al. 2009). In a next step, the retrieved LWC profiles from the radar reflectivity might be used to optimize satellite retrievals for ground fog. From the numerical modeling point of view, the investigation of the fog life cycle and its relevance for the droplet size distribution and the resulting *Z*-LWC relationship can contribute to a better understanding and parametrization of the microphysical processes shaping the microstructure of fog. The paper is structured as follows: the theoretical background of the study is described in Sect. 2.2. This concerns the radar characteristics, the relationship between the droplet spectrum, the liquid water content and the radar reflectivity, the adaptation of the radiative transfer code and the fog life cycles. The results of the sensitivity study are presented in Sect. 2.3 and discussed in Sect. 2.4. Finally, some conclusions and an outlook are given in Sect. 2.5.

2.2 Materials and methods

As mentioned in the introduction, the current study is focused on the development of an appropriate *Z*-LWC retrieval for a novel 94 GHz cloud radar profiler. The instrument is a 94 GHz frequency modulated continuous wave radar that is developed and crafted by Rutherford Appleton Laboratory, Great Britain. Because of its high frequency, it is highly sensitive to cloud droplets. It delivers vertical profiles of *Z* every 15 seconds in a vertical resolution of 4 m up to 2 km above ground. Because of the FMCW technique, continuous measurements can be provided from 30 m above the ground. For further details on the instrument see also Bennett et al. (2009) and Huggard et al. (2008).

Some theoretical considerations on the drop size spectra of natural fog and their statistical representation in a distribution function are needed to develop appropriate *Z*-LWC relations for different fog situations.

Generally, the drop size spectrum is defined such that $n(r)dr$ is the total number of particles within a given radius range of interest $r_1 \leq r \leq r_2$ per unit volume of air. Hence,

$$n(r) = \int_{r_1}^{r_2} n(r)dr \qquad (1)$$

is the total concentration of drops per unit volume of air with radii less than r_2 (Flatau et al. 1989). In order to describe the drop size spectrum, a suitable probability density function $f(r)$ has to be selected, which is defined by the intervals r_1 and r_2 (Flatau et al. 1989).

The drop size spectrum can then be represented by

$$n(r) = N_t f(r) \tag{2}$$

where N_t is the total number of drops per unit volume of air [cm^{-3}].

n(r) is a continuous and integrable function within the radius range of the fog drops for a given volume of air. Thus, its unit is [$\mu m^{-1}\ cm^{-3}$].

The suitable probability density function for describing the drop size distribution of low stratus clouds and fog is commonly characterized in literature by the so-called modified gamma distribution (Deirmendjian 1964)

$$f(r) = ar^{\alpha}\exp(-br^{\gamma}) \tag{3}$$

which is the derivative of the ordinary gamma-distribution to which it reduces when $\gamma = 1$. Its probability density function is defined by the scale parameter b and the shape parameter p

$$f(x) = \frac{b^p}{\Gamma(p)}\, x^{p-1}\exp(-bx) \text{ , p, b} \geq 0 \text{ and } p, b \in \mathbb{R} \tag{4}$$

with the gamma-function

$$\Gamma(x) = \int_0^{\infty} t^{x-1}\exp(-t)\, dt \qquad \text{for } x > 0 \tag{5}$$

which is an extension for the faculty of real and complex numbers. It has the following features for positive integer numbers

$$\Gamma(x) = (x-1)! \tag{6}$$

and (Flatau et al. 1989)

$$\Gamma(x+1) = x\Gamma(x) \tag{7}$$

The four factors a, α, b and γ in Eq. 3 are positive and real numbers. Additionally, a is an integer and the intercept of Eq. 3. The latter three parameters completely determine the shape of the distribution. The constant α is called the shape parameter and b the slope or gradient. The function is normalized by a to obtain the total number of drops per unit volume N_t. This guarantees that the integral of the size distribution over all radii is N_t.

The four parameters are not independent of each other and are related to quantities of the frequency distribution. An integration over the range of radii $r_1 \leq r \leq r_2$ by the drop size spectrum shows that a is only related to N_t (Deirmendjian 1969).

$$N_t = \int_{r_1}^{r_2} ar^{\alpha}\exp(-br^{\gamma})\, dr \tag{8}$$

$$N_t = \frac{a}{\gamma} b^{-\left(\frac{\alpha+1}{\gamma}\right)} \Gamma\left(\frac{\alpha+1}{\gamma}\right) \quad (9)$$

The latter (N_t) is, therefore, determined by the zeroth moment of the drop size spectrum. The following general solution for the modified gamma distribution is used for fog by Tampieri and Tomasi (1976) to compute the integral of the product of the modified gamma distribution multiplied with the power r^k over the entire radii interval.

$$I_k = a \int_{r_1}^{r_2} r^{\alpha+k} \exp(-br^\gamma)\, dr \quad (10)$$

$$I_k = \frac{a}{\gamma} b^{-\left(\frac{\alpha+k+1}{\gamma}\right)} \Gamma\left(\frac{\alpha+k+1}{\gamma}\right) \quad (11)$$

These equations are based on the calculations of the integrals from Gradshteyn and Ryshik (1980).

$$\int_0^\infty r^\alpha \exp(-br)\, dr = a!\, b^{-\alpha-1} = b^{-(\alpha+1)}\Gamma(\alpha+1) \quad (12)$$

A differentiation of the drop size spectrum with respect to r leads to

$$\frac{d}{dr} n(r) = a r^{\alpha-1}(\alpha - \gamma b r^\gamma)\exp(-br^\gamma) \quad (13)$$

that has three zeros. One is at $\alpha = 0$ and one at $\alpha = \infty$. One finds the third zero by setting the second term from Eq. 13 equal to 0. That is also the absolute maximum of the equation and thus the mode radius r_c [µm].

$$r_c = \left(\frac{\alpha}{\gamma b}\right)^{\frac{1}{\gamma}} \quad (14)$$

The latter (r_c) represents the radius size of maximum frequency in the drop size distribution.

The modified gamma distribution is often also expressed by substituting b by

$$b = \frac{\alpha}{\gamma r_c^\gamma} \quad (15)$$

in the literature which yields to (Tampieri and Tomasi 1976):

$$n(r) = a r^\alpha \exp\left(-\frac{\alpha}{\gamma}\left(\frac{r}{r_c}\right)^\gamma\right) \quad (16)$$

As can be seen, the parameter b is characterized by mode radius r_c if α and γ are known.

With regard to the frequency of the radar at 94 GHz (= wavelength of 3.2 mm), the dominant scattering process is described by the Rayleigh-approximation. Therefore, the radar reflectivity Z can be written as the sixth moment of the continuous drop size spectrum (Danne 1996)

$$Z = \int_{r_1}^{r_2} n(r) r^6 dr \tag{17}$$

Inserting the drop size spectrum yields

$$Z = a \int_{r_1}^{r_2} r^{\alpha+6} \exp(-br^{\gamma})\, dr \tag{18}$$

An integration over the range of radii $r_1 \leq r \leq r_2$ with respect to Eq. 10 yields

$$Z = \frac{a}{\gamma} b^{-\left(\frac{\alpha+7}{\gamma}\right)} \Gamma\left(\frac{\alpha+7}{\gamma}\right) \tag{19}$$

The unit of radar reflectivity Z is either $mm^6\ m^{-3}$ or in a logarithmical unit according to

$$dBz = 10 \log_{10} \frac{Z}{Z_0} \tag{20}$$

with $Z_0 = 1\ mm^6\ m^{-3}$ (Danne 1996).

The determination of Z-LWC relations is directly based on the drop size distribution, because the liquid water content LWC [$g\ m^{-3}$] can be derived from the drop size spectrum and the mass of drops:

$$LWC = \int_{r_1}^{r_2} n(r) m(r) dr \tag{21}$$

with

$$m(r) = \frac{4}{3} \pi r^3 \rho_{H_2O} \tag{22}$$

where ρH_2O is the water density 1 $g\ cm^{-3}$ (Danne 1996).

As can be seen, the LWC is proportional to the third moment of the drop size spectrum. The integration of the LWC

$$LWC = \frac{4}{3} \rho_{H_2O} \pi a \int_{r_1}^{r_2} r^{\alpha+3} \exp(-br^{\gamma})\, dr \tag{23}$$

yields with the usage of Eq. 10

$$LWC = \frac{4}{3}\pi\rho_{H_2O}\frac{a}{\gamma}b^{-\left(\frac{\alpha+4}{\gamma}\right)}\Gamma\left(\frac{\alpha+4}{\gamma}\right) \times 10^{-6} \quad (24)$$

Consequently, the LWC-*Z* relation can be derived by dividing Eq. 24 by Eq.19.

$$\frac{LWC}{Z} = \frac{4}{3}\pi\rho_{H_2O}\frac{\Gamma\left(\frac{\alpha+4}{\gamma}\right)}{\Gamma\left(\frac{\alpha+7}{\gamma}\right)}b^{\frac{3}{\gamma}} \times 10^{-6} \quad (25)$$

The right part of the equation is defined as a proportionality factor Ω [g mm^{-6}] which enables a linear relationship between *Z* [mm^6 m^{-3}] and LWC [g m^{-3}].

$$LWC = \Omega \times Z \quad (26)$$

If the factor Ω can be determined for natural fog, it is possible to directly convert *Z* to LWC. Unfortunately, a universal value of the factor is not known and it is hypothesized that it varies with fog type and life cycle stage.

To investigate the behavior of Ω in different natural fogs, the radiative transfer code QuickBeam (Haynes et al. 2007) was adapted to the ground-based 94 GHz FMCW cloud radar. Major modifications included the increase of the spatial resolution to 4 m and the selection of the vertical path length of 2 km. According to Petterssen's classification of fog based on temperature, there are three types of fog (Petterssen, 1956). As our radar measurements are performed in central Europe mainly in spring and autumn, only liquid fog, defined by temperatures T > -10 °C, is of importance; mixed phase fog (-30 °C > T > -10 °C) and ice fog (T < -30 °C) are negligible. A major modification was the replacement of default drop size distributions by the freely adjustable modified gamma distribution for fog according to Deirmendjian (1964).

With the adapted radiative transfer code, a sensitivity study on the *Z*-LWC relation was conducted based on fog drop size distributions as taken from literature. In this study, the modified gamma distribution varied within typical ranges and the resulting radar reflectivity and liquid water content (and so, the *Z*-LWC relation) were calculated by the RTC. To find typical ranges of the drop size spectrum for different fog types and evolutionary stages, a literature survey was conducted to find respective field data. The results are displayed in Table 2.1. However, even more parameter sets were found, not all could be included because the level of information on fog occurrence was insufficient (e.g. Kalashnikova et al. 2002, Kim et al. 2001)

or because they were only recalculated from existing values (Hess et al. 1998, Awan et al. 2008).

TABLE 2.1. Parameter sets of the modified gamma distribution (a, α, b, γ) for the drop size spectrum. T&T is taken from Tomasi and Tampieri (1976), H from Harris (1995). N_t is the total number of drops per unit volume, r_c the mode radius and the LWC the liquid water content. Numbers in italic are calculated by the radiative transfer code

Fog type	DSD-model	a	α	γ	r_c [µm]	b	N_t [cm^{-3}]	LWC [g m^{-3}]	Source
Radiation fog	1	4.3239E+00	4	0.70	2.13	*3.36586*	249.93	6.137E-02	T&T
	2	7.4438E-03	4	1.23	4.98	*0.4514*	76.29	9.899E-02	T&T
	3	3.0410E-04	4	1.77	8.06	*0.05622*	35.85	1.379E-01	T&T
	4	7.5475E-06	5	1.62	12.22	*0.05351*	15.90	2.061E-01	T&T
	5	2.3730E-02	6	1.00	4.00	*1.5*	99.87	6.247E-02	H
	6	3.0375E+00	6	1.00	2.00	*3.0*	199.83	1.563E-02	H
Advection fog	1	4.9763E-01	4	0.85	2.75	*1.99163*	184.55	6.795E-02	T&T
	2	4.2028E-03	5	1.17	5.04	*0.64408*	78.75	9.534E-02	T&T
	3	8.1656E-03	3	1.05	6.20	*0.42065*	37.73	1.537E-01	T&T
	4	3.0861E-05	6	1.47	8.10	*0.18852*	36.13	1.348E-01	T&T
	5	8.9728E-08	5	3.09	21.16	*1.29768E-04*	6.50	3.059E-01	T&T
	6	1.3500E-03	3	1.00	10.00	*0.3*	20.00	3.724E-01	H
	7	3.4752E-03	3	1.00	7.89	*0.38*	18.99	1.740E-01	H
Evolutionary stage of valley fog									
Ground fog	1	1.3823E+00	1	0.89	0.86	*1.28501*	509.99	5.141E-02	T&T
Ground fog	2	2.0338E-01	1	2.04	2.22	*0.09634*	309.79	5.146E-02	T&T
Formation stage	1	5.6434E-02	3	1.26	3.49	*0.49294*	138.04	7.548E-02	T&T
Formation stage	2	2.1192E-04	5	1.40	7.50	*0.21269*	39.32	1.325E-01	T&T
Formation stage	3	4.0633E-05	5	1.69	9.07	*0.07124*	29.26	1.504E-01	T&T
Formation stage	4	5.1199E-05	4	2.17	10.82	*0.0105*	21.73	1.738E-01	T&T
Mature fog	1	4.0001E-02	1	1.93	4.99	*0.02329*	59.02	1.236E-01	T&T
Mature fog	2	1.5416E-03	4	1.14	7.12	*0.37439*	35.67	1.484E-01	T&T
Mature fog	3	6.1487E-05	5	1.47	9.00	*0.13456*	28.00	1.565E-01	T&T
Mature fog	4	1.3900E-02	1	4.39	9.10	*1.40392E-05*	34.68	1.450E-01	T&T
Mature fog	5	1.4085E-03	2	3.41	11.18	*1.55987E-04*	22.08	1.754E-01	T&T
Dissipation stage	1	3.3437E-03	4	0.94	6.92	*0.69061*	32.51	1.623E-01	T&T
Dissipation stage	2	8.0977E-05	4	2.00	10.10	*0.01961*	24.14	1.662E-01	T&T

Furthermore, we depicted the four parameter sets of Harris (1995) and not the original ones of Shettle and Fenn (1979), because the probability density function of the advection fog examples did not always result in 1.

It should be stressed that the selected fog types follow the classification of Tampieri and Tomasi, which referred to Eadie et al. (1971). The life cycle stages of fog are taken from Pilié's fog life cycle (Pilié et al. 1972, 1975a, b) and are: (a) ground fog, (b) formation stage, (c) mature fog and (d) dissipation stage.

In their bulk fog study, Pilié et al. (1975a, b) found typical patterns of fog evolution in the Chemung river valley, which can be accepted as generally valid. Ordinarily, preliminary plane ground fog (defined by visibility of less than 4000 m) appears before a deep fog event. It is characterized by a large total number of droplets (N_t = 100-200 cm^{-3}) with a low mean radius (2 μm < r < 4 μm), which results in a positive skewness of the drop size spectrum. In the so-called formation stage the visibility decreases as well as total number concentration down to 2 cm^{-3}. Therefore, the mean radius rises up to 6-12 μm, as does the LWC. The curve of the drop size distribution is typically almost parallel to the x axis, which stretches from 3 to about 25 μm. The very small droplets disappear during this stage. The visibility minimum after the first quarter of the fog life cycle delineates the formation stage of the mature fog stage. Its features are the reappearance of very small droplets (2 μm < r < 4 μm) and an enlargement of both the total number concentration (12 cm^{-3} < N_t < 25 cm^{-3}) and the LWC to between 0.05 to 0.15 mg m^{-3}. Both fluctuate synchronously with visibility. Consequently, a bimodal drop size distribution can be recorded with a mode radius from 2-3 μm and a mode from 6-12 μm. As fog thins out to a visibility above 1,000 m after three-fourths of the life cycle, the visibility rises continuously. This last evolutionary step is called the dissipation stage. Here, LWC, mean radius and total number concentration decrease continuously. However, the fog does not always disperse equally. In three out of eight examples measured, the drop size distribution could be described by a bimodal curve with a mode radius of 2-3 μm and one with 6-12 μm, another three out of eight measurements showed a curve with positive skewness. In the last two measurements the drop sizes seemed to be distributed randomly.

As is shown in Table 2.1, α is the only integer number and is in the range of 1-6. The other parameters of the modified gamma distribution are real numbers. The values of b are between 0.05351 and 3.36586. The minimum of γ is 0.7 and the maximum 2.17. The normalization factor a of the modified gamma distribution does not have to be taken into account, because it does not have an influence on the shape of the distribution but only on the slope. The mode radius r_c lies in the region between 0.86 and 12.22 μm. The total number of drops per unit volume of air is greater than

6.5 but smaller than 509.99 μm^{-1} cm^{-3}. The values of the measured LWC range from 0.016 to 0.37 g m^{-3}.

The values presented in Table 2.1 are taken as minimum and maximum boundaries for the sensitivity study. The parameters were iterated between the minimum and maximum values with the RTC, and the resulting Z and LWC were calculated. The increment for α is 1, for γ and Z 0.1 and for b 0.05. All different cases of the modified gamma distribution which could be taken into account were considered in four intertwined loops. The limits for Z were -25 and -85 dBz, which corresponds to the dynamic range of the radar.

The first parameter calculated by the RTC was the normalization factor a [g mm^{-6}] of the modified gamma distribution by resolving Eq. 19 for:

$$a = \frac{10^{\frac{Z}{10}} \times \gamma \times 10^{12}}{b^{-\left(\frac{\alpha+7}{\gamma}\right)}\Gamma\left(\frac{\alpha+7}{\gamma}\right)} \tag{27}$$

Afterwards, the mode radius r_c was calculated by means of Eq. 14. The total number of drops per unit volume of air N_t was computed by Eq. 9. The LWC was determined by Eq. 24.

In order to investigate different fog types in regards to their specific influence on the relationship between Z and LWC, the fogs were classified into two main groups, radiation and advection fog, after having been calculated by the RTC.

Furthermore, the calculated dataset was subdivided into four different stages of fog evolution according to the life cycles of valley fog identified by Pilié (et al. 1972, Pilié et al. 1975a, b).

This was done to investigate the relevance of the fog life cycle for the Z-LWC relationship. The resulting parameter sets are shown in Table 2.2.

For a better comparability of the parameter sets, the normalization factor a was recalculated for a probability function equal to 1. As Tomasi's and Tampieri's parameter sets were expressed in terms of r_c, the corresponding b had to be calculated by the usage of Eq. 14. The same equation was used for calculating r_c for the given parameter b in Harris' fog parameter sets.

TABLE 2.2. Ranges of the characteristic coefficients of fog. Fog events (all fogs) are separated by type (radiation fog, advection fog and valley fog) and by time (ground fog, formation stage, mature fog and dissipation stage). Differentiators are the three parameters of the drop size spectrum (α, b, γ), the mode radius, the total numbers of drops per unit volume and the LWC. The counts of fitting parameter-sets are also itemized as well

	All fog events	Radiation fog	Advection fog	Valley fog	Ground fog	Formation stage	Mature fog	Dissipation stage
α_{min}	1	4	3	1	1	3	1	4
α_{max}	6	6	6	5	1	5	5	4
b_{min}	0.05351	0.05351	0.18852	0.0105	0.09634	0.0105	0.02329	0.01961
b_{max}	3.36586	3.36586	1.99163	1.28501	1.28501	0.49294	0.37439	0.69061
γ_{min}	0.7	0.7	0.85	0.89	0.89	1.26	1.14	0.94
γ_{max}	2.17	1.77	1.47	2.17	2.04	2.17	1.93	2
$r_{c\ min}$ [μm]	0.86	2.13	2.75	0.86	0.86	3.49	4.99	6.92
$r_{c\ max}$ [μm]	12.22	12.22	10	10.82	2.22	10.82	9	10.1
$N_{t\ min}$ [cm^{-3}]	6.5	15.9	20	21.73	309.79	21.73	28	24.14
$N_{t\ max}$ [cm^{-3}]	509.99	249.93	184.55	509.99	509.99	138.04	59.02	32.51
LWC_{min} [g m^{-3}]	0.016	0.016	0.06795	0.05141	0.05141	0.07548	0.1236	0.1623
LWC_{max} [g m^{-3}]	0.37	0.2061	0.1537	0.1754	0.05146	0.1738	0.1565	0.1662
Counts	190,988	60,456	8,704	26,022	774	3,226	1,200	84

2.3 Results

Figure 2.1 illustrates the absolute frequency distribution of fog traits as extracted from the literature, related to radar reflectivity *Z*. The absolute number on the y axis is the frequency in terms of the parameter of the x axis. The population of parameter sets from the RTC equals 190,988. It can be shown that fog is generally characterized by small LWCs with a mode at 0.016 g m^{-3} and a tendency to smaller droplet number concentrations. Also, the mode radius is small, mostly below 6 μm. The parameter of the modified gamma distribution reveal a wide range of values, where *b* and *γ* show a mode at lower values (0.2 or 0.8), mainly oriented on the shape of the LWC and mode radius histograms, while the parameter α is monotonously increased in frequency with increasing value, inversely shaped to the histogram of number concentration. The consequences for the theoretically expectable radar reflectivity point to a bell-shaped histogram with a mode at –52.2 dBz and very low values of the *Z*-LWC relation (mode at 4231.18295).

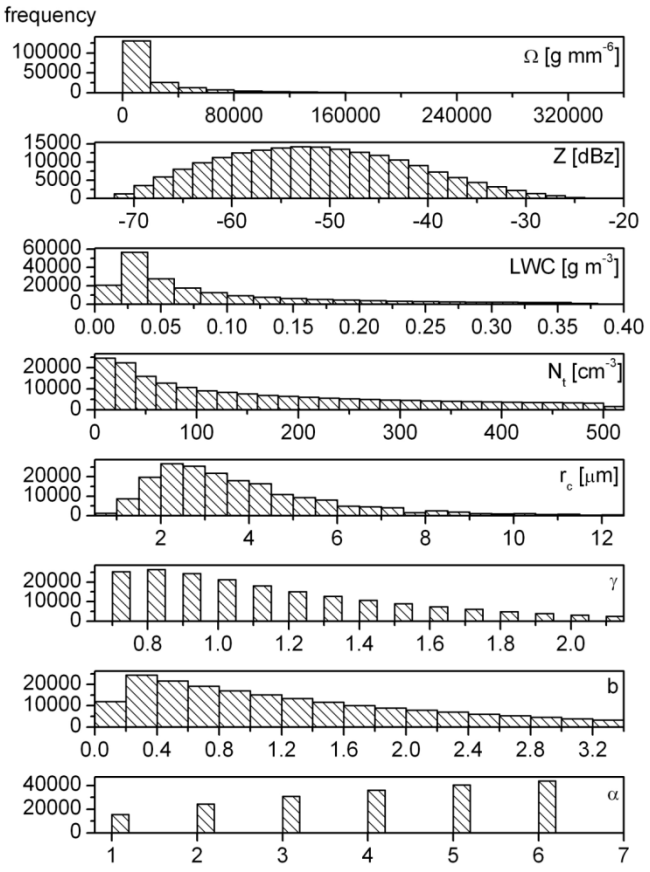

FIG. 2.1. Histogram of the characteristics for all (population = 190,988) computed fog types in the sensitivity study.

To derive a *Z*-LWC relation which can be used for the cloud radar, it is necessary to know how sensitive the relation is to variations in the three parameters. In order to address this uncertainty, the *Z*-LWC relationship factor Ω was plotted as a function of the three parameters of the modified gamma distribution in Fig. 2.2. Maximum values of Ω (3.2E+05 g mm^{-6}) can only be found for high values of both α and γ accompanied by smaller values of b. Minimum values of Ω (0 g mm^{-6}) occur in the entire range of α together with smaller values of γ almost independently of b. Ω remains fairly constant along the b and α axis at constant γ values. For fixed b values, Ω grows with increasing γ. Assuming fixed α, high values of γ and b result in high values of Ω, whereas high values of γ have priority. In total, the impact of α on Ω is higher than the impact of γ and b, as a maximum value of α is a necessary condition for a maximum value of Ω. Further, γ has priority to b as Ω grows with rising γ at constant values for α and b, whereas Ω stays nearly constant for fixed values for α and γ and variable b.

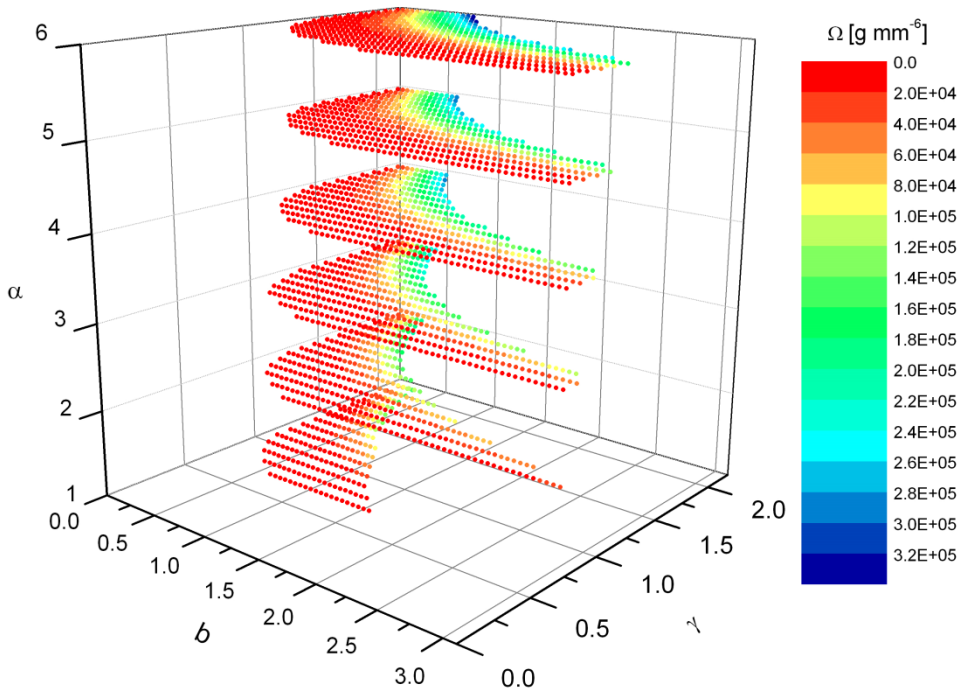

FIG. 2.2. Influence of the three parameters of the drops size spectrum γ, b, α on the LWC-Z relationship Ω for all computed fog types.

A second question is if the fog type has any specific impact on the *Z*-LWC relation when the main fog types considered are radiation and advection fog. To answer this question, *Z* and LWC for all simulations are

plotted for both fog types, whereby more information is available (Table 2.2; Fig. 2.3) for radiation fog. There are 60,456 calculated parameter sets for radiation and 8,704 for advection fog. It should be emphasized that the denser the plotted surface in Fig. 2.3 is, the more *Z*-LWC combinations lie in this range. The range of the *Z*-LWC-interaction factor Ω is according to Table 2.3 almost five times higher for radiation fog (142,584.59338) than for advection fog (21,110.49235), whereby the last range lies completely in the first one. For radiation fog it ranges from 253.43537 to 142,838.02875 g mm^{-6} and for advection fog from 521.57568 to 21,632.06803 g mm^{-6}. It can be stated that the values of Ω are widely spread.

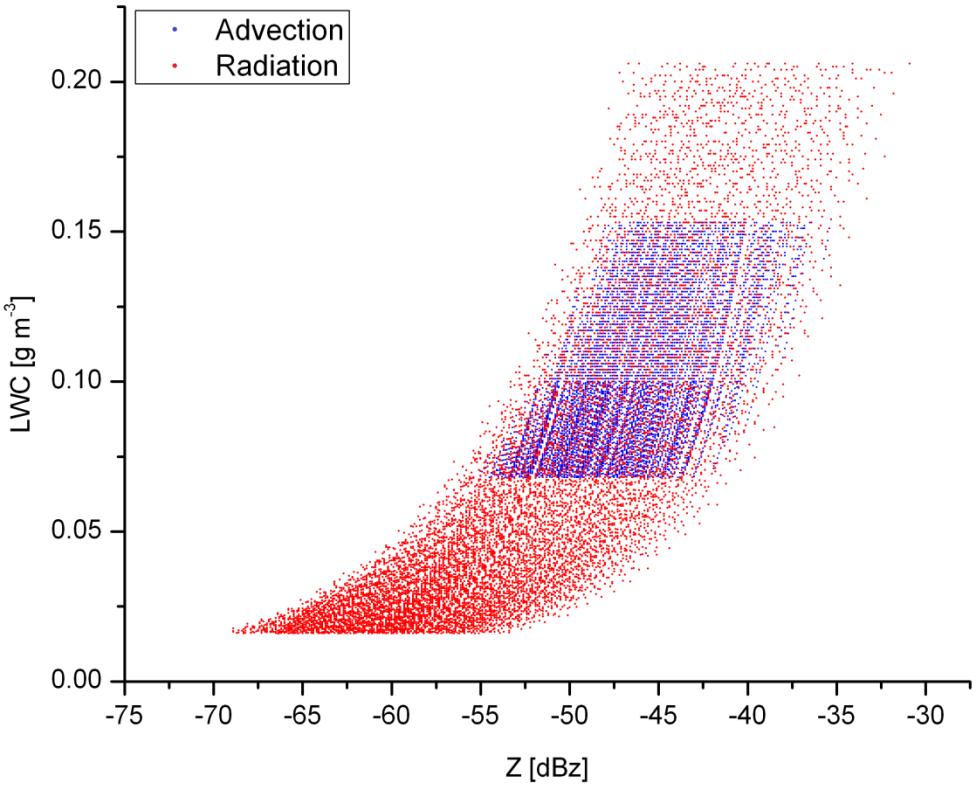

FIG. 2.3. Derived values of LWC from radar reflectivity dependent on type of fog. The plots for radiation fog were thinned out by a factor of 5.

Figure 2.3 also reveals that the range of the radar reflectivity for radiation fog has a broader range of *Z* - between -69.5 to -30.9 dBz - in comparison with advection fog, with *Z* ranging from -55.0 to -35.4 dBz. The same holds for the LWC which shows a broader range for radiation fog (0.016-0.206 g m^{-3}) than for advection fog (0.068-0.153 g m^{-3}). However, looking at the point density in Fig. 2.3 makes it clear that radiation fog is

most frequently characterized by smaller LWC values < 0.06 g m^{-3}, which is approximately the lower boundary of advection fog.

The last question is the relevance of the fog life cycle for the *Z*-LWC relation. Its impact on the *Z*-LWC interaction is presented in Fig. 2.4. Generally, the radar reflectivity shifts to higher values as a function of time in the course of the fog life cycle. With this, all four life cycle stages show a characteristic *Z*-LWC relation.

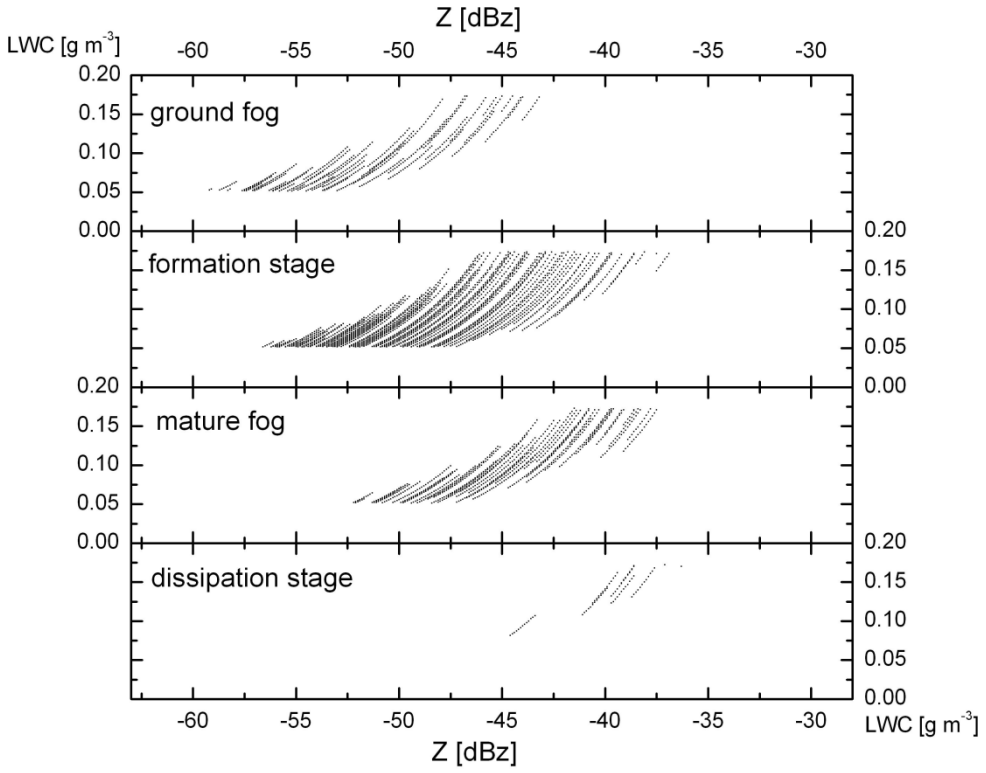

FIG. 2.4. Derived values of the LWC from Z relative to the evolutionary stage of fog. The temporal stages are listed in chronological order.

In the first three evolutionary stages (ground fog, formation stage, mature fog) the LWC values corresponding to a given radar reflectivity are spread over a wide range. Particularly in the formation stage, no unique LWC values can be derived from radar reflectivity. However, the dissipation stage features a narrow range of LWC values corresponding to a given radar reflectivity.

As can be seen in Table 2.3, the range of the *Z*-LWC relation factor Ω is initially very wide for a whole valley fog event (92,954.42255). A separation into the four characteristic states of a fog event results in smaller ranges of Ω. The Ω-intervals lessen with advancing time. While the Ω-range

amounts to 40,177.02082 during ground fog, the dissipation stage accounts only to 1,634.4085.

TABLE 3.3. Characteristic numbers (minimum, maximum, mode and range) of the Z-LWC relationship factor Ω depending on the type and evolutionary stage of fog

	Ω_{min} [g mm^{-6}]	Ω_{max} [g mm^{-6}]	Ω_{mode} [g mm^{-6}]	Ω_{delta} [g mm^{-6}]
All fog events	43.95566	336376.67707	4231.18295	336332.72141
Radiation fog	253.43537	142838.02875	4233.16494	142584.59338
Advection fog	521.57568	21632.06803	5248.0746	21110.49235
Valley fog	227.41854	93181.84109	6359.51148	92954.42255
Ground fog	3573.75354	43750.77436	8400.81409	40177.02082
Formation stage	836.98268	23594.8071	6214.75132	22757.82442
Mature fog	958.0055	8669.36576	2054.87482	7711.36026
Dissipation stage	725.18518	2359.59368	-	1634.4085

The same applies to the mode of Ω, which decreases with ongoing fog development (Fig. 2.5).

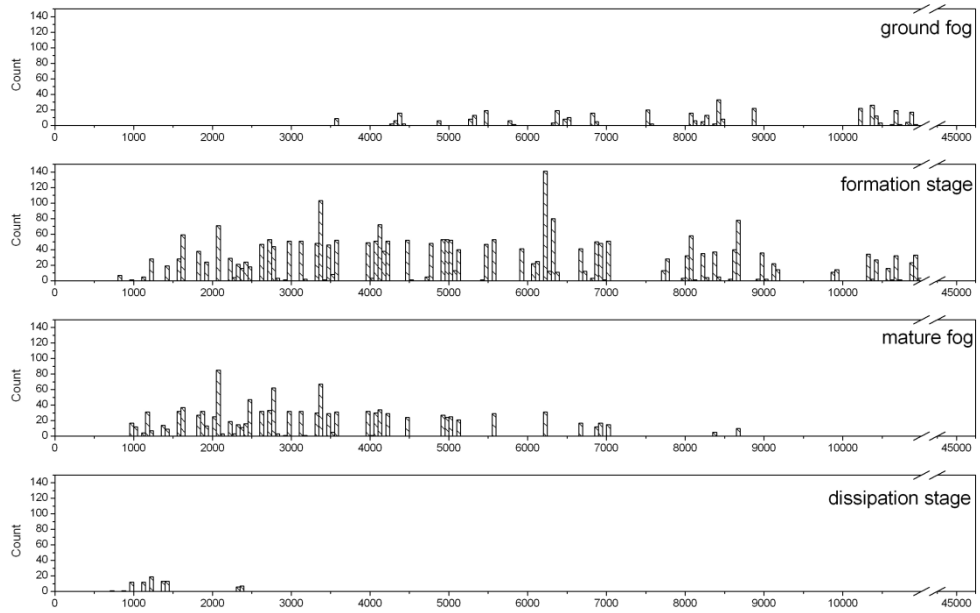

FIG. 2.5. Histogram of Ω dependent on evolutionary stage of fog.

The mode of Ω is 8,400.81409 for ground fog, 6,214.75132 for the formation stage and 2,054.87482 for mature fog. There is no clear mode value for Ω for the dissipation stage. However, the histogram in Fig. 2.5 suggests a shift of its Ω-mode to relatively low values in comparison to the Ω-modes in the preliminary stages.

2.4 Discussion

The development of a method for deriving LWC-profiles from radar reflectivity raised three questions.

The first one was how the drop size spectrum influences the relationship between radar reflectivity and LWC. Since there are three factors which determine its shape by means of the modified gamma distribution, their frequency was evaluated based on the measurement examples by Tomasi and Tampieri (1976). The first factor α showed a reverse behavior to the total number concentration N_t (Fig. 2.1). The two other factors b and γ determine, in concert with α, the mode radius of fog drops by Eq. 14. Thus, the radar reflectivity is not only influenced by the drop radius (represented by b and γ) but also by the total number concentration (represented by α). Figure 2.2 shows that both α and γ have a higher influence on the Z-LWC relationship than b because an individual change of their value resulted in a higher change of Ω compared to b. It can be observed that both α and γ have an important role on the Z-LWC interaction in relation to the mode radius r_c as computed by Eq. 14.

The second question was if the fog type influences the Z-LWC-interaction. Table 2.3 and Fig. 2.3 indicate not only that the range of the Z-LWC interaction factor Ω is much larger for radiation fog than for advection fog, but also that the Ω-values of advection fog lie completely in the range of radiation fog. This behavior is related to the total number of droplets and the mode radius, which can be higher in radiation fog (Table 2.2). Unfortunately, the intersection of the Ω-values of both fog types does not allow a strict classification of fog specific Ω-values. Although Fig. 2.3 reveals a strong accommodation of Ω-values for each fog type, advection fog has a strong concentration of Ω-values from about -55 to -43 dBz. This results in a LWC-range of 0.06795 to 0.1537 g m^{-3}. Radiation fog shows a strong concentration of Ω-values from -68 to -50 dBz, which results in a LWC-range from 0.016 to 0.2061 g m^{-3}. Comparing these ranges makes it apparent that the type of fog plays a very important role on the Z-LWC interaction.

The third question concerns the relevance of the fog life cycle for the Z-LWC relationship. To investigate this question, the parameter sets of valley fog were classified by valley fog's four development stages (Table 2.2). Regarding the fog event as a whole a wide range of 92,954.4225 g mm^{-6} was found for the relationship factor Ω (Table 2.3). Evidently it is difficult

to derive certain LWC-values from a given radar reflectivity without further specifications. Distinguishing the stage specific parameter sets from Table 2.2 for valley fog delivered narrower Ω ranges from Eq. 26. The Ω-interval decreases continuously from 40,177.02082 for ground fog to 1,634.4085 for the dissipation stage (Table 2.3). As can be seen in Fig. 2.4, the LWC-*Z* relationship could be specified for all four fog development stages, although the method is still in need of further improvement.

The radar reflectivity increases during the fog life cycle (Fig. 2.4). During ground fog the *Z* varies from -59.2 to -43.2 dBz. In the formation stage, it varies from -56.6 to -36.9 dBz. While *Z* ranges from -52.2 to -37.5 dBz during the mature stage, it varies from -44.6 to -36.3 dBz in the dissipation stage. A possible cause for the shift of *Z* to higher values with ongoing fog development might be the increasing drop radii. According to Eq. 18, bigger radii result in higher radar reflectivity. According to Eq. 23, bigger radii also result in higher LWC values. As the LWC is proportional to the drop size spectrum (a function of the drop radius) by the third moment and the radar reflectivity is proportional to DSD by the sixth moment, an increase of the radius results in smaller Ω values being the quotient, with LWC as the numerator and *Z* as the divisor. This also coincides with Table 2.3, where the mode of Ω decreases with advancing fog life cycle from 8,400.81409 for ground fog to 2,054.87482 for mature fog.

From the increasing radar reflectivity and the decreasing proportionality factor Ω with fog development, it can be concluded that the LWC stays constant or grows as well. This matches with Pilié's observations (Pilié et al. 1975a, b) of increasing LWC during fog events.

The narrower ranges of Ω in Table 2.3 for the consecutive fog stages imply clearer *Z*-LWC ratios as both factors determine the quotient Ω.

With regard to the three questions, there is a direct link between radar reflectivity and LWC even though it is not a direct one. For a more precise relationship between these two key figures, a fog differentiation by type and evolutionary stage in its life cycle promises good improvements.

2.5 Conclusion

The main purpose of the work was to show if it is possible to derive LWC-profiles from measured radar reflectivity of a new 94 GHz FMCW cloud radar. In order to answer this question, a radiative transfer model was developed considering the radar reflectivity as well as the LWC-profiles. Since both factors depend on the drop size spectrum, its influence on both factors was investigated. It could be shown that the parameters of the modified gamma distribution have a strong effect on their relationship, expressed by the proportionality factor Ω. Hence, the parameters of the modified gamma distribution (α, γ, b) were analyzed as a function of the fog

type and of the fog life cycle. Existing parameter sets of α, γ and b were elaborated from the relevant literature. The eligible parameter sets were separated into characteristic value ranges corresponding to the respective fog evolutionary stages. Next, new parameter sets for the drop size spectrum within these ranges were recalculated to obtain accommodated sets for specific fog cases and for error minimization. Both the fog type and the classification by time permitted a reduction of the contemplable parameter sets which fell within a narrower range of the *Z*-LWC-relation factor Ω. The results indicate a direct but nonlinear relation between LWC and radar reflectivity. Particularly the *Z*-LWC-relation factor Ω reveals characteristic ranges for the different life cycle stages. If a proper classification of the respective development stages in the field can be accomplished, it should be possible to apply appropriate *Z*-LWC relationships to calculate the LWC from the radar reflectivity for the respective fog life cycle stage. Microwave cloud radar profilers with the frequency modulated continuous wave technique are very well suited for monitoring fog and low stratus clouds. Because of the novelty of these radar devices, no published *Z*-LWC-relationships for fog and low stratus relying on direct radar and in situ measurements are available. Gultepe et al, (2009) derived *Z*-values from LWC- and r_{eff}-values that were measured with a fog measuring device during the FRAM-project. In their study they concluded that it is possible to obtain LWC and visibility from *Z* if r_{eff} is assumed to be constant. However, assuming a constant r_{eff} might not coincide with reality for most fog events. The results of this study indicate that r_{eff} cannot be taken as a constant (Fig. 2.1). According to Gultepe et al. (2009), the main reason for discontinuous r_{eff} values as well as varying *Z*-LWC- relationships is the large variability in fog drop size spectra.

Generally, the results imply that satellite and model diagnosing and forecasting applications relying on correct LWC profiles should be generally adapted to the life cycle stage of fog and fog type. Most fog diagnosing and nowcasting applications based on satellite information are reliant on passive instruments onboard operational polar-orbiting and geostationary weather satellite imagery (Gultepe et al. 2007). Since radiation in the wavebands of these instruments does not normally completely penetrate opaque cloud layers, it is only possible to observe the upper part of a potential fog layer, making the distinction between low stratus and ground fog a difficult task. As stated in the introduction, novel approaches were recently developed to overcome this problem (Bendix et al. 2005, Cermak and Bendix 2011). The major initialization parameter of these approaches is the LWC profile in a pixel. Due to the two-dimensional nature of the images, only the columnar liquid water path (LWP) can be retrieved (Nauß et al. 2005), which is not bijectively related to the LWC value or its profile. Different LWC profiles can occur, depending on LWP and geometrical depth of the fog layer. Because of hitherto lacking information,

it is assumed in the current ground fog detection schemes that LWP can be related to the respective LWC by a sub-adiabatic model of cloud microphysics (Cermak and Bendix 2011). It is obvious that this simplification must impose inaccuracies in the processing. A comprehensive investigation of the relation between LWC profiles and integrated LWP under different weather situations using the cloud radar-based *Z*-LWC relationships will be a clear step forward for a realistic initialization of the process. However, this will also require a proper estimate of fog type and life cycle in the satellite images or by ancillary data (as e.g. time of day). With regard to ground fog forecast models, proper LWC profiles are important for validation and model improvements (Gultepe and Milbrand 2007). Most models are initialized with standard meteorological parameters with poor vertical resolution, especially close to the ground (e.g. temperature, humidity etc.). Some studies show that the correct prediction of LWC as dependent on the vertical resolution of the models is hardly possible, thus (negatively) influencing important forecast parameters like ground visibility (Tardif 2007). Continuously measured LWC profiles based on the *Z*-LWC relation could particularly improve 1-D model results by initializing with LWC profiles with a high vertical resolution. This could also alleviate the common problem of fog modeling that reliable vertical humidity profiles used for data assimilation are often not available (Müller et al. 2007). With regard to straightforward, partly statistical fog models, it is obvious that those which rely directly on columnar LWC data (as e.g. Reudenbach and Bendix 1998) will benefit from cloud radar-based retrievals of LWC profiles.

Acknowledgements

The authors thank the University of Marburg for granting a PhD scholarship for F. Maier (03-06 2010) and the German Research Foundation DFG for funding the project (BE1780/14-1; TH1531/1-1). The work is also part of the COST action EG Climet.

2.6 References

Awan, M.S., Leitgelb, E., Muhammad, S.S., Marzuki, F.N., Khan, M.S., and Capsoni, C. 2008. Distribution function for continental and maritime fog for environments for optical wireless communication. doi: 10.1109/CSNDSP.2008.4610728, 260-264.

Bendix, J. 2002). A satellite-based climatology of fog and low-level stratus in Germany and adjacent areas. *Atmospheric Research* **64**, 3-18.

Bendix, J., Thies, B., Cermak, J., and Nauss, T. 2005. Ground fog detection from space based on MODIS daytime data – a feasibility study. *Weather and Forecasting* **20**, 989-1005.

Bennett, A. J., Gaffard, C., Oakley, T. and Moyna, B. 2009. Cloud radar – initial measurements from the 94 GHz FMCW cloud radar. *Proceedings of the 8th International Symposium on Tropospheric Profiling 19–23 October*, Delft, 1-8.

Boers, R., Russchenberg, H., Erkelens, J., Venema, V., Van Lammeren, A., Apitule, A., Pituley, A., and Jongen, S. 2000. Ground-based remote sensing of stratocumulus properties during CLARA, 1996. *Journal of Applied Meteorology* **39**, 169–181.

Cermak, J., Schneebeli, M., Nowak, D., Vuilleumier, L., and Bendix, J. 2006. Characterization of low clouds with satellite and ground-based remote sensing systems. *Meteorologische Zeitschrift* **15**, 65-72.

Cermak, J., Bendix, J., 2011. Detecting ground fog from space – a micro-physics-based approach. *International Journal of Remote Sensing* **32**, 3345–3371. doi:10.1080/01431161003747505.

Clothiaux, E.E., Miller, M.A., Albrecht, B.A., Ackermann, T.P., Verlinde, J., Babb, D.M., Peters, R.M., and Syrett, W.J. 1995. An evaluation of a 94 GHz radar for remote sensing of cloud properties. J*ournal of Atmospheric and Oceanic Technology* **12**, 201–229.

Danne, O. 1996. *Messungen physikalischer Eigenschaften mit stratiformer Bewölkung mit einem 94 GHz-Wolkenradar*. *Dissertation*, University of Hannover, Hannover, pp. 1-117.

Deirmendjian, D. 1964. Scattering + polarization properties of water clouds + hazes in the visible + infrared. *Applied Optics* **3**, 187-196.

Deirmendjian, D. 1969. *Electromagnetic scattering on spherical polydispersions*. Elsevier Scientific Publishing, New York, pp. 1-290.

Donovan, D.P., and Van Lammeren, A.C.A.P. 2001. Cloud effective particle size and water content profile retrievals using combined lidar and radar observations 1. Theory and examples. *Journal of Geophysical Research-Atmospheres* **106**, 27425–27448.

Eadie, W.J., Kocmond, W.C., Leonard, R.P., Mack, E.J., and Pilié, R.J. 1971. Investigation of warm fog properties and fog modification concepts. *NASA Contractor Report* **1731**, Washington D.C.

Engelbart, D.A.M., Monna, W.A., Nash, J., and Mätzler, C. (eds). 2008. *Integrated ground-based redmote sensing stations for atmospheric profiling*. COST Action 720 final report, Final Report. COST office, Luxembourg, pp. 1-422.

Flatau, P.J., Tripoli, G.J., Verlinde, J., and Cotton, W.R. 1989. The CSU-RAMS cloud microphysics module: general theory and code documentation, Colorado State University. *Atmospheric Science Paper* **45**.

Frisch, A.S., Fairall, C.W., and Snider, J.B. 1995. Measurement of stratus cloud and drizzle parameters in ASTEX with a K_α-band Doppler radar and a microwave radiometer. *Journal of the Atmospheric Sciences* **52**, 2788–2799.

Frisch, A.S., Fairall, C.W., Feingold, G., Utal, T., and Snider, J.B. 1998. On cloud radar microwave radiometer measurements of stratus cloud liquid water profiles. *Journal of Geophysical Research* **103**, 23195–23197.

Fox, N.I., and Illingworth, A.J. 1997. The retrieval of stratocumulus cloud properties by ground-based cloud radar. *Journal of Applied Meteorology* **36**, 485-492.

Görsdorf, U. 2008. Cloud radar, In: Engelbart et al. (eds) COST Action 720. *Integrated ground-based redmote sensing stations for atmospheric profiling*. Final Report. COST office, Luxembourg, pp. 148-166.

Gradshteyn, I.S., and Ryzhik, I.M. 1980. *Table of integrals, series, and products*. Academic Press Inc, New York, pp. 1-1248.

Gultepe, I., Muller, M.D., and Boybeyi, Z. 2006. A new visibility parameterization for warm-fog applications in numerical weather prediction models. *Journal of Applied Meteorology and Climatology* **45**, 1469–1480.

Gultepe, I., and Milbrandt, J.A. 2007. Microphysical observations and mesoscale model simulation of a warm fog case during FRAM project. *Pure and Applied Geophysics* **164**, 1161–1178.

Gultepe, I., Tardif, R., Michaelides, S.C., Cermak, J., Bott, A., Bendix, J., Mueller, M.D., Pagowski, M., Hansen, B., Ellrod, G., Jacobs, W., Toth, G., and Cober, S.G. 2007. Fog reasearch: A review of past achievements and future perspectives. *Pure and Applied Geophysics* **164**, 1121-1159.

Gultepe, I., Pearson, G., Milbrandt, J.A., Hansen, B., Platnick, S., Taylor, P., Gordon, M., Oakley, J.P., and Cober, S.G. 2009. The fog remote sensing and modeling field project. *Bulletin of the American Meteorological Society* **90**, 341-359.

Haynes, J.M., Marchand, R.T., Luo, Z., Bodas-Salcedo, A., and Stephens, G.L. 2007. A multipurpose radar simulation package: QuickBeam. *Bulletin of the American Meteorological Society* **88**, 1723-1727.

Harris, D. 1995. The attenuation of electromagnetic-waves due to atmospheric fog. *International Journal of Infrared and Millimeter Waves* **16**, 1091-1108.

Hess, M., Koepke, P., and Schult, I. 1998. Optical properties of aerosols and clouds: The software package OPAC. *Bulletin of the American Meteorological Society* **5**, 831-844.

Huggard, P.G., Oldfield, M.L., Moyna, B.P., Ellison, B.N., Matheson, D.N., Bennett, A.J., Gaffard, C., Oakley, T., and Nash, J. 2008. 94 GHz FMCW cloud radar. In: *Proceedings of the SPIE symposium on millimetre wave and terahertz sensors and technology*, 15-18 September 2008, Cardfiff, pp. 1-6.

Jacobs, W., Nietosvaara, V., Bott, A. Bendix, J., Cermak, J., Michaelides, S., and Gultepe, I. (eds). 2008. *Short range forecasting methods of fog, visibility and low clouds*, COST Action 722 final report, Brussels, Office for official publications of the European Communities, pp. 1-489.

Kalashnikova, O.V., Heinz, A.W., and Mayhew, L.M. 2002. Wavelength and altitude dependence of laser beam propagation in dense fog. doi: 10.1117/12.464103, pp. 278-287.

Kim, I.I., McArthur, B., and Korevaar, E. 2001. Comparison of laser beam propagation at 785 nm and 1550 nm in fog and haze for optical wireless communications. doi: 10.1117/12.417512, pp. 1-12.

Khain, A., Pinsky, M., Magaritz, L., Krasnov, O., and Russchenberg, H.W.J. 2008. Combined observational and model investigations of the Z–LWC relationship in stratocumulus clouds. *Journal of Applied Meteorology and Climatology* **47**, 591-606.

Kollias, P., Clothiaux, E.E., Miller, M.A., Albrecht, B.A., Stephens, G.L., and Ackerman, T.P. 2007. Millimeter-wavelength radars - New frontier in atmospheric cloud and precipitation research. *Bulletin of the American Meteorological Society* **88**, 1608-1624.

Liao, L., and Sassen, K. 1994. Investigation of relationships between Ka-band radar reflectivity and ice and liquid water contents. *Atmospheric Research* **34**, 231–248.

Löhnert, U., Crewell, S., Simmer, C., and Macke, A. 2001. Profiling cloud liquid water by combining active and passive microwave measurements with cloud model statistics. *Journal of Atmospheric and Oceanic Technology* **18**, 1354–1366.

Löhnert, U., Crewell, S., and Simmer, C. 2004. An integrated approach toward retrieving physically consistent profiles of temperature, humidity, and cloud liquid water. *Journal of Applied Meteorology* **43**, 1295-1307.

McFarlane, S.A., Evans, K.F., and Ackerman, A.S. 2002. A Bayesian algorithm for the retrieval of liquid water cloud properties from microwave radiometer and millimeter radar data. J*ournal of Geophysical Research-Atmospheres* **107**, 4317-4338.

Meyer, M.B., Lala, G.G., and Jiusto, J.E. 1986. FOG-82 - A cooperative field study of radiation fog. *Bulletin of the American Meteorological* Society **67**, 825-832.

Müller, M.D., Schmutz, C., and Parlow, E. 2007. A one-dimensional ensemble forecast and assimilation system for fog prediction. P*ure and Applied Geophysics* **164**, 1241-1264.

Nauß, T., Kokhanovsky, A., Nakajima T.Y., Reudenbach, C., and Bendix, J. 2005. The intercomparison of selected cloud retrieval algorithms. *Atmospheric Research* **78**, 46-78.

Nowak, D., Ruffieux, D., Agnew, J.L., and Vuilleumier, L. 2008. Detection of fog and low cloud boundaries with ground-based remote sensing systems. *Journal of Atmospheric and Oceanic Technology* **25**, 1357-1368.

Pagowski, M., Gultepe, I., and King, P. 2004. Analysis and modeling of an extremely dense fog event in southern Ontario. *Journal of Applied Meteorology* **43**, 3-16.

Petterssen, S. 1956. *Weather analysis and forecasting*. McGraw-Hill, New York, pp. 1-428.

Pilié, R.J., Eadie, W., Mack, E.J., Rogers, C., and Kocmond, W.C. 1972. Project Fog Drops. Part 1: Investigations of warm fog properties. Washington D.C., *NASA Contractor Report*. Buffalo, New York: Cornell Aeronautical Laboratory, Inc., 1-149.

Pilié, R. J., Mack, E. J., Kocmond, W. C., Rogers, C. W., and Eadie, W.J. 1975a. The life-cycle of valley fog. 1. Micrometeorological characteristics. *Journal of Applied Meteorology* **14**, 347-363.

Pilié, R. J., Mack, E. J., Kocmond, W. C., Eadie, W. J., and Rogers, C. W. 1975b. The life-cycle of valley fog. 2. Fog microphysics. *Journal of Applied Meteorology* **14**, 364-374.

Reudenbach, C., and Bendix J. 1998. Experiments with a straightforward model for the spatial forecast of fog/low stratus clearance based on multi-source data. *Meteorological Applications* **5**, 205-216.

Ruffieux, D. Nash, J., Jeannet, P., and Agnew, J.L. 2006- The COST 720 temperature, humidity, and cloud profiling campaign: TUC. *Meteorologische Zeitschrift* **15**, 5-10.

Sauvageot, H., and Omar, J. 1987. Radar reflectivity of cumulus clouds. *Journal of Atmospheric and Oceanic Technology* **4**, 264–272.

Schulze-Neuhoff, H. 1976. Detailed analysis of fog based on additional 420 weather stations. *Meteorol. Rundsch*. **29**, 75-84.

Shettle, E.P., and Fenn, R.W. 1979. Models for the aerosols of the lower atmosphere and the effects of humidity variations on their optical properties. *Environmental Research Paper* **676**, 1-94.

Siebert, J., Bott, A., and Zdunkowski, W. 1992a. Influence of a vegetation-soil model on the simulation of radiation fog. *Contributions to Atmospheric Physics/Beiträge zur Physik der Atmosphäre* **65**. 93–106.

Siebert, J., Bott, A., and Zdunkowski, W. 1992b. A one-dimensional simulation of the interaction between land surface processes and the atmosphere. *Boundary-Layer Meteorology* **59**, 1–34.

Tampieri, F., and Tomasi, C. 1976. Size distribution models of fog and cloud droplets in terms of the modified gamma function. *Tellus* **28**, 333-347.

Tardif, R. 2007. The impact of vertical resolution in the explicit numerical forecasting of radiation fog. A case study. *Pure and Applied Geophysics* **164**, 1221-1240

Terradellas, E., and Bergot, T. 2007. Comparison between two single-column models designed for short-term fog and low-clouds forecasting. *Física de la Tierra* **19**, 189-203.

Tomasi, C., and Tampieri, F. 1976. Features of the proportionality coefficient in the relationship between visibility and liquid water content in haze and fog. *Atmosphere* **14**, 61-76.

Welch, R.M., and Ravichandran, M.G. 1986. Prediction of quasi-periodic oscillations in radiation fogs. 1. Comparison of simple similarity approaches. *Journal of the Atmospheric Sciences* **43**, 633-651.

von Glasow, R. and Bott, A. 1999. Interaction of radiation fog with tall vegetation. *Atmospheric Environment* **33**, 1333–1346.

Wendisch, M., Mertes, S., Heintzenberg, J., Wiedensohler, A., Schell, D., Wobrock, W., Frank, G., Martinsson, B.G., Fuzzi, S., Orsi, G., Kos, G., and Berner, A. 1998. Drop size distribution and LWC in Po Valley fog. *Contributions to Atmospheric Physics/Beiträge zur Physik der Atmosphäre* **71**, 87-100.

WMO, (ed.). 1992. *International Meteorological Vocabulary*. Vol. 182. Geneva: WMO; pp. 1-276.

3. Development and application of a method for the objective differentiation of fog life cycle phases

Frank Maier, Jörg Bendix and Boris Thies

Faculty of Geography, University of Marburg, Marburg, Germany

---

Printed in

TELLUS B (2013)

Tellus B, **65**, 19971

Published online May 2013

DOI: 10.3402/tellusb.v65i0.19971

(Received 10/25 2012, Printed 05/15 2013)

Abstract

An objective classification of radiation fog in distinct evolutionary stages during its life cycle based on reliable criteria is essential for various applications, e.g. for numerical fog modeling and fog forecasting. However, there are up to now merely qualitative approaches for the distinction of different evolutionary stages in radiation fog. Measurements of the microphysical fog properties with an optical particle counter from Droplet Measurement Technologies together with recordings of the horizontal visibility (VIS) are statistically analyzed to determine individual evolutionary stages of radiation fog with consistent microphysical properties. The developed three-stage approach is based on a statistical change point analysis of the double sum curves of the VIS, the liquid water content, the droplet concentration, and the mean radius of the drop size distributions. It could be shown that each of the three recorded radiation fog occurrences could be split in three consecutive phases from formation to dissipation, regardless whether the VIS or the microphysical properties were considered. Having featured consistent microphysical patterns, it could be assumed that the three separated phases of the single fog occurrences could be aggregated for radiation fog. Although this classification is statistically reliable, the dataset still has to be extended for a generalization concerning the separated evolutionary stages.

3.1 Introduction

The phenomenon of fog is referred to horizontal visibility below 1 km (WMO, 1992). Due to low visibility during fog events they have a great impact on human life and on society with increasing air, marine, and road traffic. Following Gultepe et al. (2007, 2009) the total economic loss, related to fog, is comparable with that for tornadoes and even with that for hurricanes or winter storms in some situations.

Fog forms under specific weather situations and its evolution and structure are related to local conditions, like terrain and ecological environment. Many factors, for example radiation cooling, air mass advection, and precipitation, can affect the formation and the duration of fog. Based on primary factors that affect fog formation, maturation, and dissipation Gultepe et al. (2007) classified fogs into radiation fog, high-inversion fog, advection–radiation fog, advection fog, and steam fog.

The most studied fog type is that associated with radiative cooling. Radiation fog forms when ground-level temperatures decrease below dew point as a result of nocturnal long-wave emission of the earth's surface and turbulent fluxes. It usually forms near the surface under clear skies in stagnant air in association with anticyclonic conditions (Gultepe et al., 2007). However, the mechanisms of radiation fog formation, development and dis-

sipation are very complex and have been extensively studied with a series of numerical simulations and comprehensive observational programs including in-situ measurements (Meyer et al., 1986; Fitzjarrald and Lala, 1989; Fuzzi et al., 1992, 1998; Gultepe et al., 2007; Zhou and Ferrier, 2008; Liu et al., 2011; Dupont et al., 2012;). Recently, field experiments have been conducted to investigate dynamic, thermodynamic, microphysical, and radiative processes in Beijing and Nanjing, China (Liu et al., 2011), in Canada (Gultepe et al., 2009), and in Paris, France (Haeffelin et al., 2010; Dupont et al., 2012).

The balance between radiative cooling and turbulent mixing seems to be a primary factor in the development of radiation fog (Roach et al., 1976; Nakanishi, 2000; Terradellas and Bergot, 2008). Beside radiative cooling as a main mechanism the upward soil heat flux as well as the warming effects and moisture losses through dew deposition from turbulent mixing strongly influence the formation, the structure and the life cycle of radiation fog (Lala et al., 1975; Pilié et al., 1975b; Brown and Roach, 1976; Roach et al., 1976; Findlater, 1985; Turton and Brown, 1987; Fitzjarrald and Lala, 1989; Bergot and Guédalia, 1994; Duynkerke, 1999).

As a result of the complex mechanisms of radiation fog development and dissipation fog properties differ greatly, depending on the synoptic situation, the mode of formation, and the geographic conditions. These diverse factors contribute to the present inability to forecast the occurrence and severity of radiation fog with an acceptable accuracy. Still lacking is a detailed understanding of the processes that control the evolution of radiation fog.

However, radiation fog shows a remarkable diurnal variation. It forms mostly at sunset or midnight, and lifts after sunrise or at noon. The development of radiation fog is often described as a typical life cycle regarding fog properties with consecutive evolutionary stages (e.g. Lala et al., 1982; Stewart and Essenwanger, 1982; Juisto and Lala, 1983). Variations in the microphysical character of radiation fog have been tied to various stages defining the life cycle of radiation fog. Gultepe et al. (2007) separated the fog life cycle into three distinct development stages. The formation stage is characterized by an increase in the liquid water content (LWC), the droplet concentration (N_t), and the mean droplet size (r_{mean}). Gultepe et al. (2007) stressed that during the mature stage LWC and N_t stay nearly constant and r_{mean} decreases gradually. When the fog dissipates all three microphysical parameters decrease. Pilié et al. (1972, 1975a, 1975b) distinguished four separate stages in the life cycle of fog by analyzing the horizontal visibility, N_t, LWC, and r_{mean}. The prefog phase began when VIS < 4 km and ended when VIS < 1 km for the first time. The initiation phase lasted until the first minimum in VIS. N_t and LWC increase to a maximum at the same time. r_{mean} increases to near maximum between the first observable visibility decrease and the first minimum. During the following mature phase VIS remains nearly constant. N_t and LWC fluctuate synchronously with VIS. r_{mean}

gradually decreases after the maximum in the initiation phase and remains almost constant through the mature phase. In the dissipation phase VIS gradually increases. N_t and LWC decrease drastically. On average r_{mean} also decreases at the time of dissipation.

For a radiation fog event in Nanjing, China Liu et al. (2011) identified four development phases: formation, development, mature, and dissipation phases, depending on microstructure and VIS.

Wendisch et al. (1998) identified two characteristic phases for the observed fog events during the CHEMDROP experiment in the Po Valley (Northern Italy). The first "initial" phase is characterized by a strong increase of the number of small droplets. During the second phase, which is called "mass transfer phase" the water mass for the large drops increases drastically, whereas the small droplets remain nearly unchanged. Price (2011) analyzed the droplet spectra for several fog events in Cardington, UK. In accordance to Wendisch et al. (1998), he identified an initial phase with small drop sizes and a mature phase with the appearance of larger drop sizes.

The existing studies on radiation fog development accordingly indicate the existence of distinct evolutionary stages during the fog life cycle. However, they differ with respect to the number and the characterization of the identified phases. This might be due to the differing conditions under which the fog events occurred. Another important aspect is the missing quantitative and consistent criteria that would allow a reproducible separation of the fog events into concurrent stages from the initiation to the dissipation together with the missing consistency in the analyzed parameters. An objective classification method by means of quantitative criteria can help to separate differing radiation fog events in a consistent manner.

The consistent recognition of distinct phases of fog evolution is important for the interpretation of governing physical processes. The microphysical characteristics associated with the identified phases can be used as verification criteria for numerical fog modeling and can help to improve the accuracy of fog forecasting. At present existing microphysical model schemes do not account for the evolution of microphysical properties during the lifetime of radiation fog. In this context the identified and characterized evolutionary stages can help to improve the microphysical parameterizations in the models.

The aim of the present study is therefore to introduce a statistical method based on change point (CP) analysis of time series for the objective separation of radiation fog events into distinct life cycle phases. The classification is based on microphysical properties of three radiation fog occurrences during October and November 2011 as liquid water content (LWC), the total number of droplets per cubic centimeter (N_t) and the mean and mode radius (r_{mean}, r_c) as well as the prevailing VIS.

It is hypothesized that the measured time series of the microphysical parameters show a characteristic temporal course from the initiation to the dissipation, which can be separated into distinct development phases. It is further hypothesized that the statistical CP analysis of time series allows the objective and quantitative separation into distinct development phases and that there is an accordance between the separated phases of each fog event especially with respect to the microphysical characteristics.

The structure of the article is as follows. The measurement site and equipment together with the prevailing weather situation are introduced in Section 3.2. This is followed by a description of the developed statistical method to detect quantitatively definable evolutionary stages in the radiation fog life cycle. The results of the analysis are presented in Section 3.3. A discussion of the results, also with respect to existing results from the literature is given in Section 3.4. The paper closes with a conclusion in Section 3.5.

3.2 Materials and Methods

3.2.1 Measurement site and equipment

The field measurements were carried out in autumn 2011 at the Marburg Ground Truth and Profiling Station (50.53304 °N/ 8.68535 °E, 172 m a.s.l.). The measuring site is located in the flood plain of the Lückebach-creek. The rural valley is surrounded by small hills extending up to 250 m a.s.l. In consequence of the topographic position and the warm-moderate rain climate of the mid-latitudes the study area is known for its high fog frequency in autumn months (Schulze-Neuhoff, 1976; Bendix, 1998, 2002). The Marburg Ground Truth and Profiling Station encompasses the measuring instruments according to Table 3.1.

The measured horizontal visibility in 2 m height was the criterion for the occurrence of fog (< 1 km) (WMO, 1992). Fog-specific drop size distributions cause extinction of visible light since the extinction coefficient of fog droplets is a function of LWC and N_t. The reduction of light can be detected by optical measuring devices (Gultepe et al., 2006). The top height of fog was derived from radar reflectivity of a 94 GHz FMCW radar (Huggard et al., 2008; Bennett et al., 2009). In case of a lifting fog layer, the cloud base height was detected by a Ceilometer. The core instrument of the field measurements was an Optical Particle Counter (OPC) from Droplet Measurement Technologies (DMT). The device allowed a particle-by-particle measurement and detected drop size spectra within a range from 2 µm to 50 µm in 30 size bins and in a 1-second-cycle (DMT, 2012). The microphysical parameters LWC, N_t, r_{mean}, and r_c were derived from the volume-corrected counts per cubic centimeter of the individual 30 size bins. The fog microphysical measurements were conducted 2 m above ground.

For the analysis the gathered raw data from the meteorological and microphysical instruments were synchronized on a 1-min-time-interval. The time series were reduced to the time range of the fog event when the horizontal visibility fell the first time below 1 km and finally exceeded 1 km in the dissipation phase.

TABLE 3.1. Applied instruments on the Marburg Ground Truth and Profiling Station

Instrument	Measured parameter	Time interval	Manufacturer
94 GHz FMCW Radar	Altitude of cloud top	10 [sec]	Rutherford Appleton Laboratory, UK
Ceilometer (CL31)	Altitude of cloud base	20 [sec]	Vaisala, Finland
Optical Particle Counter (CDP)	Drop size spectrum[b]	1 [sec]	Droplet Measurement Technologies, USA
Climatological Station	• Temperature[a] • Precipitation[b] • Pressure[b] • Relative Humidity[a] • Wind direction[a] • Wind speed[c]	5 [min]	Campbell Scientific, USA
Present Weather Sensor (HSS VPF-730)	Horizontal visibility[a]	20 [sec]	Biral, UK

[a] measured at 2 m and 10m height
[b] measured at 2 m height
[c] measured at 10m height

3.2.2 Weather situation during the fog events

The three fog events analyzed in this paper occurred from 26-27 October 2011, 31 October-1 November 2011 and 13-14 November 2011. The prevailing synoptic weather regimes over Europe and the North East Atlantic were recorded by the German Weather Service (DWD, 2011) referring to the classification of Hess and Brezowsky (1977). The general weather situations are summarized in Fig. 3.1 with respect to the general classification of James (2007).

a) Cyclonic south-easterly: 10/26/2011 - 10/27/2011

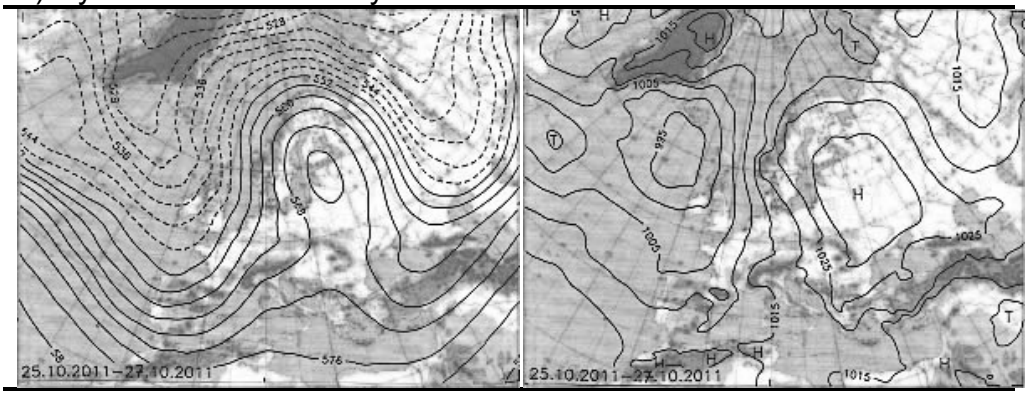

b) Change from zonal ridge across Central Europe 10/31/2011 to anticyclonic southerly 11/01/2011

Zonal ridge across Central Europe (10/28/2011-10/31/2011)

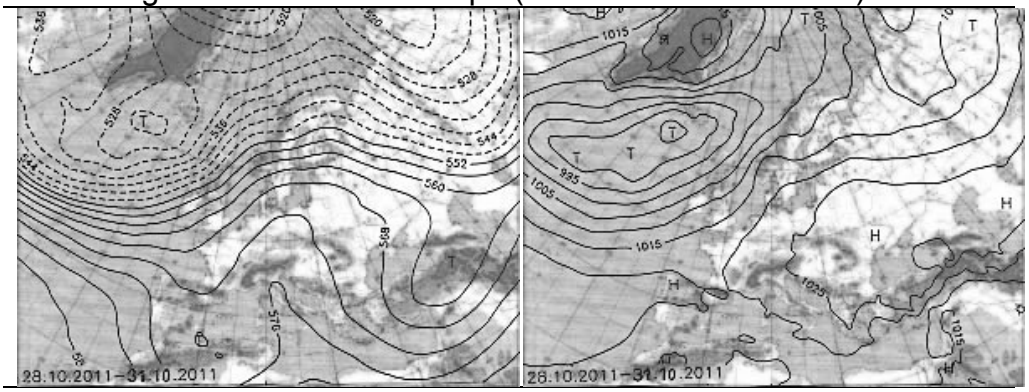

Anticyclonic southerly (11/01/2011-11/05/2011)

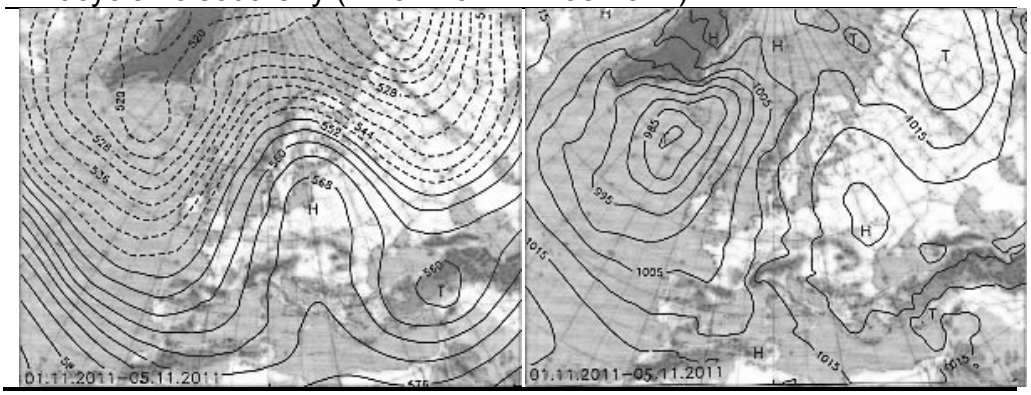

c) Icelandic high, ridge Central Europe 11/13/2011 - 11/14/2011

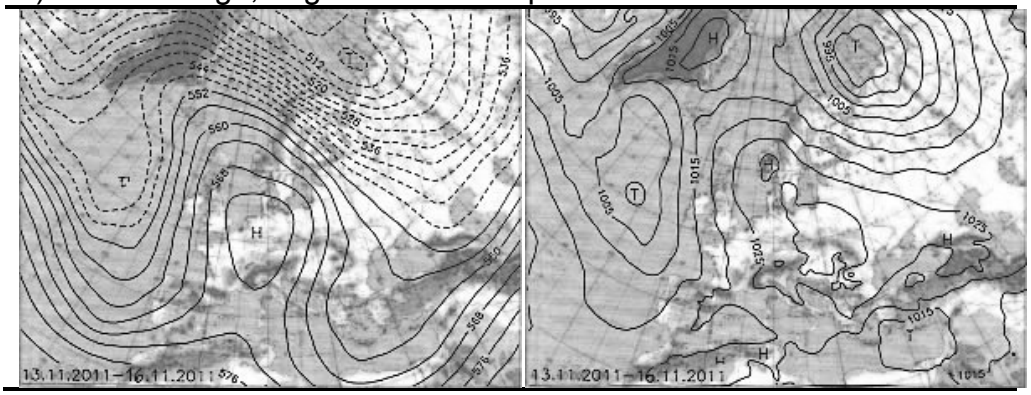

FIG. 3.1. Synoptic weather regimes during the three fog events referring to Hess and Brezowsky (1977) and James (2007) (DWD, 2011). a) first fog event: 26-27 October 2011, b) second fog event: 31 October 2011-1 November 2011, c) third fog event: 3-14 November 2011. Left column: 500 hPa level, right column: surface pressure level.

The first fog event occurred during a cyclonic weather situation, generally at south-easterly streamflow from 25 to 27 October 2011 but accompanied by a strong high pressure area over Russia and Central Europe. Negative temperature and precipitation anomalies compared to the seasonal averages were recorded due to cold and dry maritime polar air mass intrusions to the study area.

The second fog event featured a transition in the general weather conditions from a zonal ridge type across Central Europe (28-31 October 2011) to an anticyclonic southerly (11 January 2011-11 May 2011) situation. During this process, a temporary ridge of high pressure between a high over the Azores and a Russian continental high disappeared and was replaced by a frontal zone, preliminary in the northwestern part of the ridge. The result was a meridional streamflow transporting warmer and more humid air masses to Central Europe.

The general weather condition during the third fog event was characterized by an Icelandic high and a high pressure ridge over Central Europe from 13 to 16 November 2011. Both, temperature and precipitation were below average for the season.

3.2.3 Detection of the fog development stages

For the detection and the classification of the different fog evolutionary stages during its life cycle a statistical method was developed that is based on double sum curve analysis as used for hydrological analyses of

flood water flows (AK KLIWA, 2002). The analysis of double sum curves is a method for finding inhomogeneities in time series (Hansel and Schäfer, 1970). Figure 3.2 reveals the three steps that had to be undertaken for the detection of potential CPs within the times series of the microphysical parameters and VIS of the three recorded fog occurrences. A detailed explanation of the statistical approach is given in Appendix (Section 3.6).

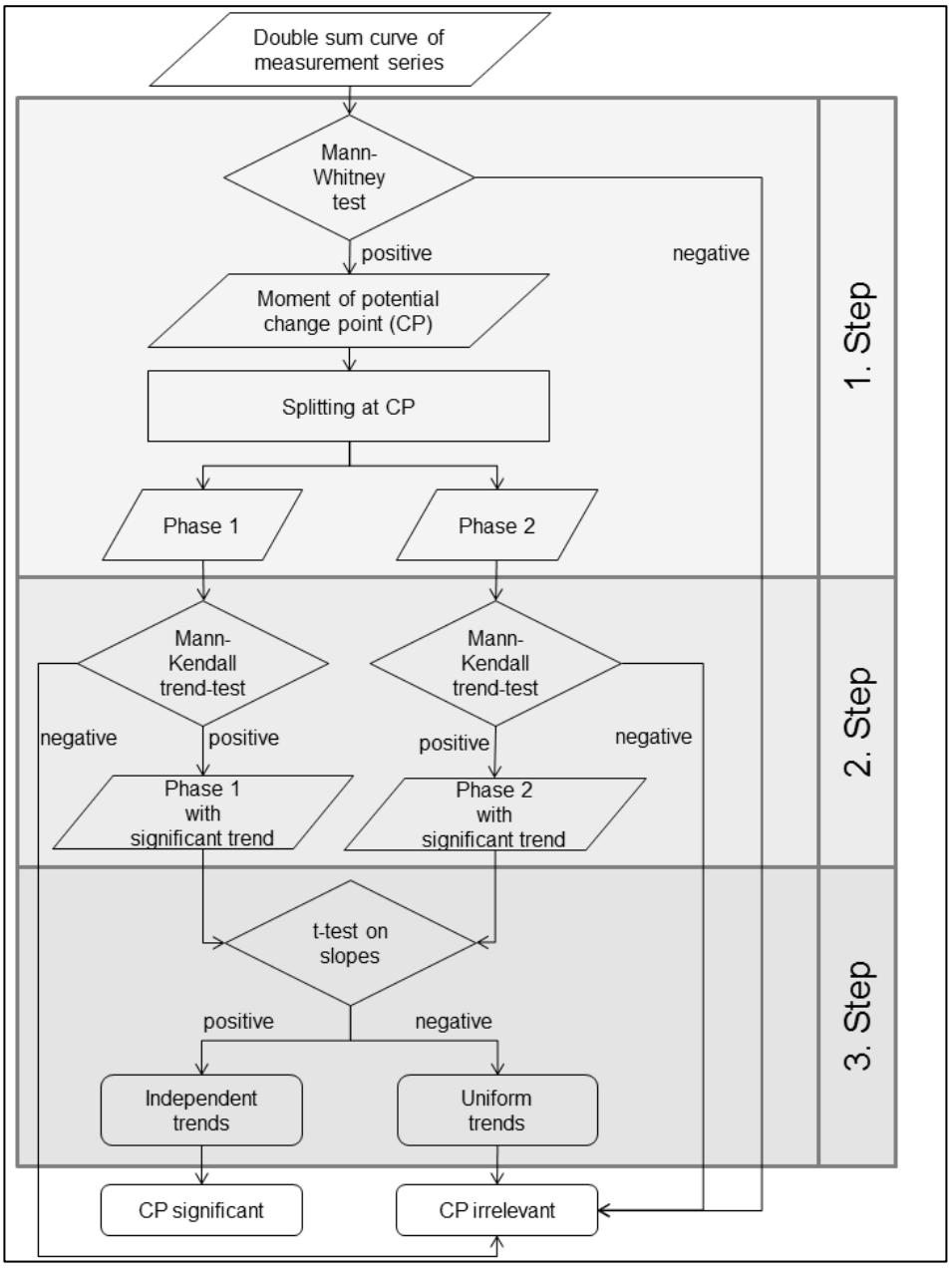

FIG. 3.2. Flowchart of the statistical approach for the detection and statistical proof of change point (CP) in double sum curves of measurement series.

3.3 Results

3.3.1 Detected life cycle phases

The results of the statistical analysis for the three fog events are summarized in Tables 3.2 and 3.3. Table 3.2 shows the potential CPs of step 1 found for the analyzed parameters VIS, LWC, N_t, r_c and r_{mean} for each fog event found by the Mann-Whitney homogeneity test.

The calculated time of the CPs were the same for all five parameters. Therefore, Table 3.2 contains only one value for each CP which is representative for the five measurement parameters. The two CPs of a double sum curve separate the time series of a fog event in three sub-time series.

The test statistics $\hat{z}$ of the Mann-Kendall trend-tests were very low (< 0.0001) for all identified phases and for each parameter (VIS, LWC, N_t, r_{mean}, r_c) revealing a very high statistical significance level (99.99%). Thus, H_0 ($\mu_x(t) = \text{const}$) can be denied in the benefit of H_A, meaning that there is an uniformly increasing trend for each parameter during each identified phase of the three fog events.

The results from the two-sided t-test on the slopes of the parameters VIS, LWC, N_t, r_c, and r_{mean} for each identified evolutionary stage of the three fog events (step 3) are shown in Table 3.3.

Apart from the low significance level obtained for the LWC in the first phase of the third fog event, all five parameters featured a high significance level of 99.99% for each evolutionary stage. Hence, H_A ($B_{x1t1} \neq B_{x2t2}$) can be accepted at the cost of H_0 ($B_{x1t1} = B_{x2t2}$), implying that there was always a significant change of the slopes at the CPs between the phases.

TABLE 3.2. Found potential change points (CP) of the three fog events from the homogeneity test of Mann-Whitney for the cumulative sum of VIS, LWC, N_t, r_c and r_{mean}

Fog event	Duration	CP1	CP2	Phase 1		Phase 2		Phase 3	
				Period	n	Period	n	Period	n
1	10/26, 19:21 – 10/27, 08:05	10/27, 01:50	10/27, 06:00	10/26, 19:21 – 10/27, 01:50	390	10/27, 01:51 – 10/27, 06:00	250	10/27, 06:01 – 10/27, 08:05	125
2	10/31, 17:38 – 11/01, 07:55	10/31, 19:17	11/01, 01:57	10/31, 17:38 – 10/31, 19:17	100	10/31, 19:18 – 11/01, 01:57	400	11/01, 01:58 – 11/01, 07:55	358
3	11/13, 18:48 – 11/14, 08:15	11/13, 23:47	11/14, 06:27	11/13, 18:48 – 11/13, 23:47	300	11/13, 23:48 – 11/14, 06:27	400	11/14, 06:28 – 11/14, 08:15	108

TABLE 3.3. Two-sided t-test on the slopes of the phases regarding the microphysical parameters and VIS from the three measured fog events

		VIS		LWC		N_t		r_{mean}		r_c	
Fog event	Change point	t	p [%]	t	p [%]	t	p [%]	t	p [%]	t	p [%]
1	1	23.57	99.99	37,83	99.99	49,59	99.99	29.27	99.99	34.54	99.99
	2	19.59	99.99	20.09	99.99	10.96	99.99	46.61	99.99	43.72	99.99
2	1	35.94	99.99	12.00	99.99	13.20	99.99	8.71	99.99	11.40	99.99
	2	64.30	99.99	54.54	99.99	33.11	99.99	101.12	99.99	96.74	99.99
3	1	123.77	99.99	7.56	75	1.14	99.99	47.13	99.99	36.62	99.99
	2	40.09	99.99	14.33	99.99	15.15	99.99	19.09	99.99	20.21	99.99

3.3.2 Description of the derived life cycle stages

The development of the microphysical and meteorological measurement parameters in terms of the identified phases of the three fog events will be described in detail for the first (26-27 October 2011) and second fog event (10 October 2011-1 November 2011). The characteristics of the third fog event (13-14 November 2011) are very similar to those of the first fog event. Therefore, the development of the microphysical and meteorological measurement parameters of the third fog event are not described in detail; but are given in the appropriate Table 3.4 and Fig. 3.3.

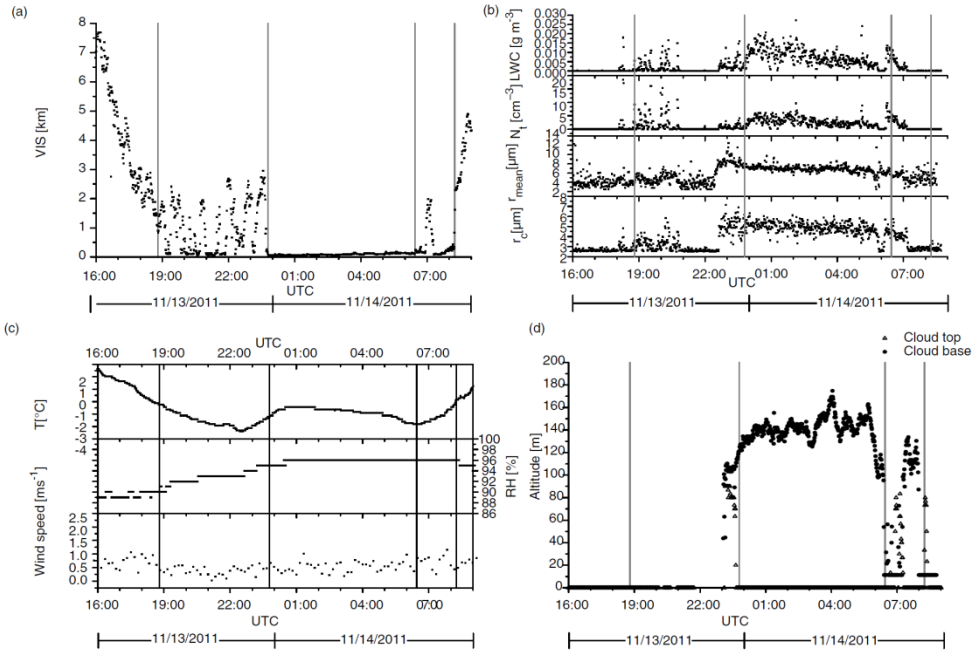

Fig. 3.3. Measured data during third fog event: 13-14 November 2011. (a) Horizontal visibility (VIS); (b) Microphysical properties: liquid water content (LWC), total number of droplets per cubic centimeter (N_t), mean droplet radius (r_{mean}), modal droplet radius (r_c); (c) Meteorological properties: temperature (T), relative humidity (RH), wind speed; (d) Cloud ceilings. The first and last vertical line represent the time when VIS is the first and last time below 1 km during the fog event. The other two vertical lines signify the change points (CPs) determined by the statistical approach.

TABLE 3.4. Overview of the microphysical properties of the three fog measurements differentiated by evolutionary stages: liquid water content (LWC), total amount of droplets N_t, arithmetic mean of radius r_{mean}, modal value of radius r_c, minimum value of radius r_{min}, maximum value of radius r_{max}, range between minimum and maximum value within a drop size spectrum

	Min	Max	Mean	Standard deviation	Median	Min	Max	Mean	Standard deviation	Median	Min	Max	Mean	Standard deviation	Median
	Formation stage of 26 October-27 October 2011					Formation stage of 31 October -1 November 2011					Formation stage of 13 November-14 November 2011				
LWC [g m^{-3}]	0.00	0.09	0.01	0.02	0.00	0.00	0.06	0.02	0.02	0.01	0.00	0.02	0.00	0.00	0.00
N_t [cm^{-3}]	0.02	115.69	11.04	17.83	2.79	0.05	50.72	12.23	11.53	7.85	0.00	16.11	1.24	2.65	0.14
r_{mean} [µm]	3.15	9.50	4.94	1.25	4.54	3.02	7.61	5.36	0.91	5.27	2.50	12.45	5.44	2.06	4.95
r_c [µm]	2.50	7.08	3.82	0.97	3.52	2.50	4.70	3.37	0.59	3.31	2.50	7.13	3.45	1.10	2.93
r_{min} [µm]	2.50	5.21	3.08	0.58	2.89	2.50	4.20	2.75	0.31	2.63	2.50	10.95	4.00	1.38	3.75
r_{max} [µm]	3.38	22.47	10.98	5.71	11.15	3.43	22.70	16.12	4.35	16.69	2.50	16.56	7.93	4.01	7.18
dr [µm]	0.00	19.97	7.90	6.11	8.15	0.44	20.20	13.38	4.58	13.99	0.00	13.18	3.93	3.86	3.12
	Mature fog of 26 October-27 October 2011					Mature fog of 31 October-1 November 2011					Mature fog of 13 November-14 November 2011				
LWC [g m^{-3}]	0.00	0.05	0.01	0.01	0.01	0.00	0.06	0.01	0.01	0.01	0.00	0.03	0.01	0.00	0.01
N_t [cm^{-3}]	0.20	38.28	2.15	3.25	1.47	0.01	41.43	4.58	6.98	1.90	0.00	9.66	2.73	1.71	2.42
r_{mean} [µm]	4.03	11.22	8.63	1.62	8.97	3.20	13.13	6.54	1.88	6.40	2.50	11.50	6.82	0.79	6.89
r_c [µm]	2.58	10.25	5.99	1.56	5.93	2.50	7.24	3.71	0.91	3.53	2.50	6.31	4.80	0.65	4.86
r_{min} [µm]	2.50	7.46	3.58	0.99	3.25	2.50	12.25	3.45	1.40	2.91	2.50	11.50	3.25	0.89	3.00
r_{max} [µm]	6.34	23.07	17.10	2.61	17.25	3.38	22.05	14.25	3.99	14.81	2.50	18.72	13.88	2.44	14.16
dr [µm]	3.46	20.57	13.52	3.12	13.69	0.33	19.55	10.80	4.50	11.56	0.00	16.17	10.63	2.96	11.06
	Dissipation stage of 26 October-27 October 2011					Dissipation stage of 31 October-1 November 2011					Dissipation stage of 13 November-14 November 2011				
LWC [g m^{-3}]	0.00	0.03	0.01	0.01	0.00	0.00	0.03	0.00	0.00	0.00	0.00	0.01	0.00	0.00	0.00
N_t [cm^{-3}]	0.14	5.66	1.57	1.33	1.07	0.00	33.78	0.75	3.58	0.05	0.00	5.43	0.89	1.41	0.02
r_{mean} [µm]	4.85	9.63	7.56	0.98	7.50	2.50	5.97	3.88	0.69	3.75	2.75	8.14	5.10	1.04	5.10
r_c [µm]	2.72	7.30	4.98	0.92	4.96	2.50	3.95	2.89	0.30	2.78	2.52	5.74	3.34	0.79	2.91
r_{min} [µm]	2.50	5.14	3.45	0.74	3.29	2.50	5.62	3.50	0.59	3.44	2.53	8.14	4.33	1.21	4.22
r_{max} [µm]	5.96	21.13	14.61	3.64	14.49	2.50	17.18	4.73	2.27	4.04	2.75	13.76	6.58	2.80	5.42
dr [µm]	1.91	18.57	11.16	4.22	10.96	0.00	14.68	1.22	2.38	0.47	0.00	11.14	2.24	3.36	0.18

3.3.2.1 First fog event (26-27 October 2011)

Before VIS dropped below < 1 km for the first time at 19:21 LT, more than two hours after sunset, it had decreased relatively continuously (Fig. 3.4a). Then it oscillated with wide fluctuations till the first CPs at 01:50 LT. The first evolutionary stage lasted over 50% of the whole life cycle. Hereafter, VIS remained constantly low around 0.2 km during the secondary evolutionary stage which lasted 33% of the whole fog life cycle. Not until the second CP at 06:00 LT during sunrise it exceeded 1 km. After having had a local maxima with > 1 km, VIS dropped again below 1 km, before it finally rose > 1 km at around 08:00 LT in the last phase. The dissipation stage persisted 16% of the whole fog event.

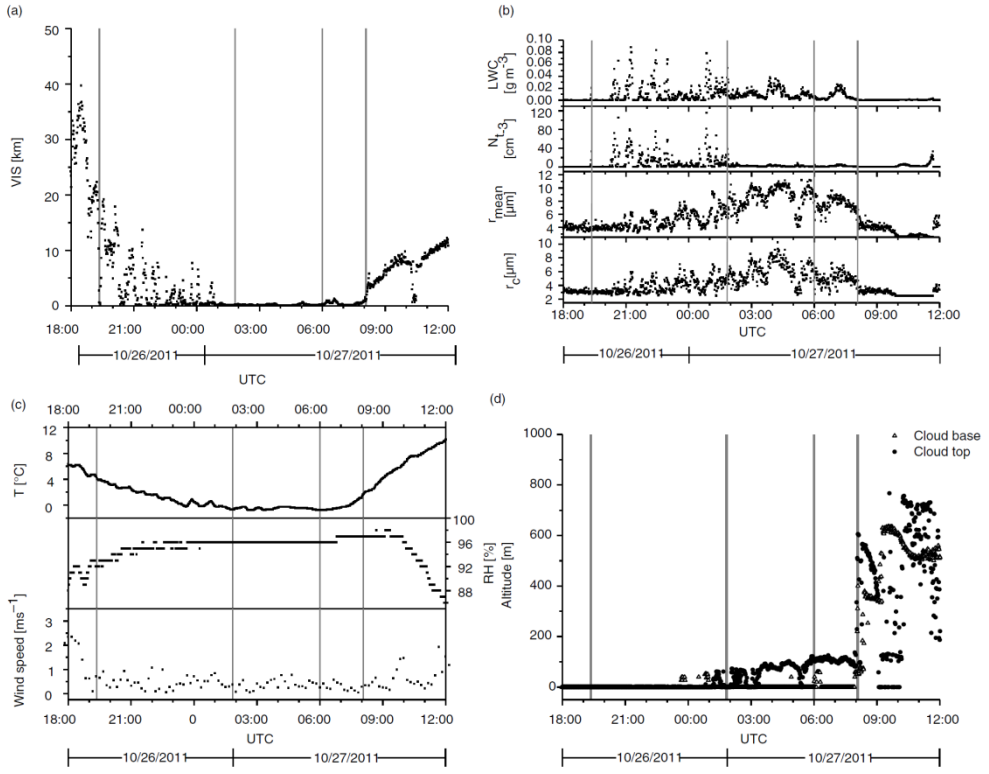

FIG. 3.4. Measured data during first fog event: 26-27 October 2011. (a) Horizontal visibility (VIS); (b) Microphysical properties: liquid water content (LWC), total number of droplets per cubic centimeter (N_t), mean droplet radius (r_{mean}), modal droplet radius (r_c); (c) Meteorological properties: temperature (T), relative humidity (RH), wind speed; (d) Cloud ceilings. The first and last vertical line represent the time when VIS is the first and last time below 1 km during the fog event. The other two vertical lines signify the change points (CPs) determined by the statistical approach.

Initial measureable values of all microphysical parameters were recorded at the time when VIS became < 1 km for the first time. Prior to the first CP, they strongly oscillated during the formation stage, whereby LWC and N_t reached maximal values with 0.09 g m^{-3} or 116 cm^{-3}. Both, r_{mean} and r_c had a slight tendency to increasing values. In between the two CPs (mature phase) all microphysical parameters but N_t continued fluctuating with r_{mean} and r_c reaching maximum values for the whole fog event with 11.2 µm and 10.3 µm. Meanwhile, N_t decreased at first and stayed hereafter constant at a low level with 2.1 cm^{-3}. During the last evolutionary phase (dissipation stage), between the second CP and the time when VIS became > 1 km again, all microphysical parameters had local maxima. Subsequently, their values decreased to a level of zero.

Temperatures steadily decreased from sunset to the first CP by more than 6 K whereas relative humidity increased up to 96%. Within the two CPs, temperature as well as relative humidity stayed on a constant low ($T \approx$ 0 °C) and high level (RH ≈ 96%), respectively. After sunrise both meteorological parameters increased again whereas RH featured a reversal of the trend at around 09:30 LT. Air pressure was almost constant around 1016 hPa during the whole fog event. Air speed during the fog occurrence (vv ≈ 1 m s^{-1}) was lower than before and after it (vv > 2 m s^{-1}). During the whole fog event neither drizzle nor precipitation was recorded.

With the beginning of the formation stage a cloud top formed at 50 m altitude that expanded up to 120 m with some interruptions. When VIS was < 1 km for the last time at 08:05 LT, a formation of a solid cloud base could be observed. Hereafter, both, cloud base and cloud top rose simultaneously up to 750 m and 500 m respectively.

3.3.2.2 Second fog event (1 October 2011-1 November 2011)

After sunset at 16:04 LT, VIS has decreased continuously until it became < 1 km for the first time at 17:40 LT (Fig. 3.5a). Then it oscillated with an amplitude of up to 3 km till the first CP at 19:17 LT. The formation of the fog lasted only 12% of the whole event. As far as the second CP at 01:57 LT VIS stayed then < 1 km at a constant level of around 0.1 km. The second stage of the whole life cycle lasted 45%. More than four hours before sunrise at 06:16 VIS increased > 1 km at 01:57 LT during the second CP with VIS = 4.1 km. Afterwards VIS decreased anew below 1 km, before it finally rose constantly above 1 km at 07:55 LT. The last phase persisted 42% of the whole fog occurrence.

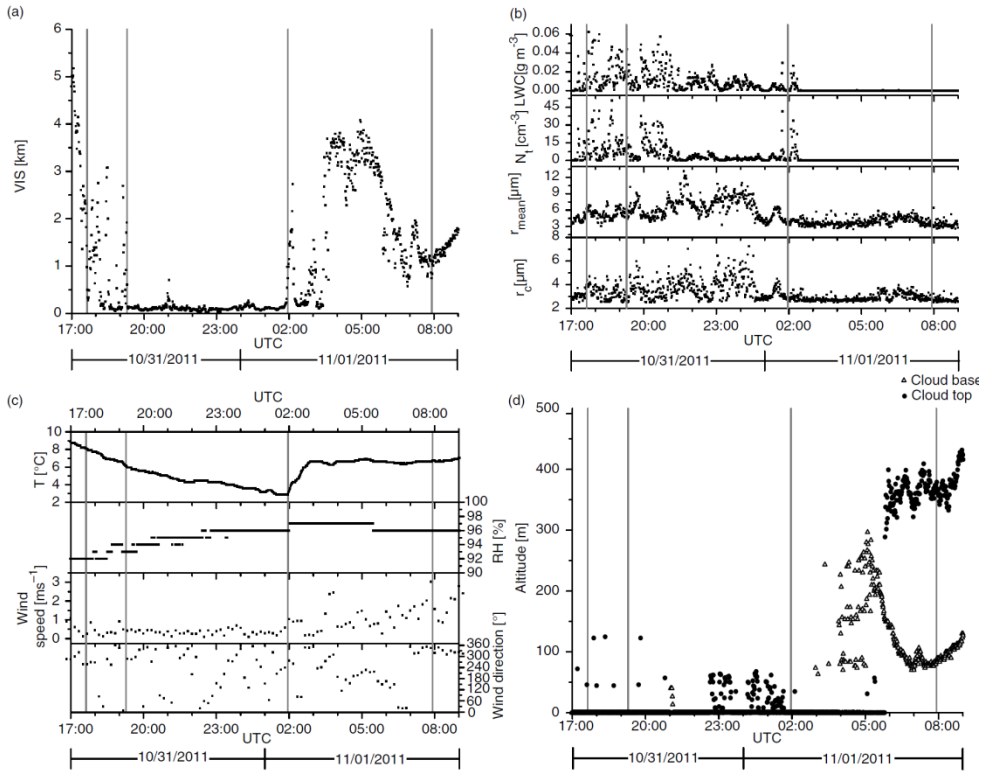

FIG. 3.5. Measured data during second fog event: 31 October 2011-1 November 2011. (a) Horizontal visibility (VIS); (b) Microphysical properties: liquid water content (LWC), total number of droplets per cubic centimeter (N_t), mean droplet radius (r_{mean}), modal droplet radius (r_c); (c) Meteorological properties: temperature (T), relative humidity (RH), wind speed, wind direction; (d) Cloud ceilings. The first and last vertical line represent the time when VIS is the first and last time below 1 km during the fog event. The other two vertical lines signify the change points (CPs) determined by the statistical approach.

Unlike the previous fog event, initial measurable values of the microphysical parameters could be recorded even before VIS < 1 km for the first time. Similarly to the first phase of the first fog event, the highest values of LWC (0.06 g m^{-3}) and N_t (51 cm^{-3}) were also recorded during this phase of the second fog event. Not only in the first phase but also in the second evolutionary stage r_{mean} and r_c revealed fluctuations with an increasing tendencies from 5.3 µm to 6.5 µm, respectively from 3.4 µm to 3.7 µm. Their maximum values of the whole fog event were also recorded in this secondary evolutionary stage with 13.1 µm or 7.2 µm. At the same time LWC and N_t continued oscillating as well, though with a much smaller amplitude as in the beginning, maximal values attained almost 0.06 gm^{-3} or 41 cm^{-3}. During the last evolutionary stage LWC and N_t exhibited one last local

maxima, followed by a sudden decrease to zero. In contrast r_{mean} and r_c revealed coincidently fluctuations even though on a much lower level (3.9 µm or 2.9 µm).

While temperatures continued decreasing from sunset on ($\Delta T \approx$ -6 K), relative humidity increased from 92% up to 94% till the second CP at 01:57 LT. From then on temperatures revealed a strong increase until the second CP ($\Delta T \approx$ +4 K) and beyond. Meanwhile, relative humidity initially increased slightly, before it featured a steady reversal trend. Air pressure fluctuated around 1016 hPa during the whole fog event. Wind speed started on a low level (0.5 m s^{-1}) in the beginning and remained low till the second CP. Subsequently, during the dissipation stage, wind speed rose permanently up to 3 m s^{-1}. Furthermore, the main wind direction veered coincidently from northwest to southeast at the same time. During the whole fog event neither drizzle nor precipitation was recorded.

During the first phase a perforated cloud top formed at 50 m height which vanished before having reached the second CP. Though, the cloud top signal reoccurred in the dissipation stage, accompanied by the formation of a stable cloud base at 250 m altitude. At the end of the fog event, the cloud ceilings enlarged vertically to 100 m and 450m above the ground.

3.4 Discussion

The applied statistical based approach detected very significant CPs for all tested parameters in their double sum curves of the recorded three fog events. As the changes occurred at the same time for each parameter, they can be taken as feasible criteria for classification of radiation fog in three different phases.

In the context of existing classifications of different fog life cycle phases and considering the two identified CPs, together with the resulting three phases, the analyzed fog events can be classified into three phases. The first phase (formation stage) lasted from the time when VIS became < 1 km for the first time until the first CP, the second phase (mature stage) in between the first and the second CP and the last phase (dissipation stage) from the second CP till the time when VIS became > 1 km.

In the following, the three evolutionary stages, derived from the performed CP analysis of the three analyzed radiation fog events shall be compared with two existing fog models from the literature. Pilié's (Pilié et al., 1972, 1975a, 1975b) model for the evolution of radiation fog (PFM) consists of four phases and Gultepe's (Gultepe et al., 2007) fog model (GFM) distinguishes three evolutionary stages. These two models of fog development were chosen, because they provide quantitative criteria for each separated phase that could be compared with our results.

According to Gultepe et al. (2007) the three stages of a fog life cycle can be characterized by the progress of their microphysical properties in

detail. The formation stage shows gradually upward trends of LWC, N_t and r_{mean}. During mature fog LWC and N_t stay on a nearly constant level while r_{mean} decreases gradually. With the beginning of the dissipation stage all three parameters decrease again. If one expands the three stage classification by another phase that takes place right before the actual fog event, one gets the PFM (Pilié et al., 1972, 1975a, 1975b). The so-called ground fog or pre-fog phase in the PFM starts when VIS < 4 km and lasts till VIS < 1 km for the first time. This mist consists of up to 200 drops per cubic centimeter with a range between 1 and 10 µm and a mean from 2 to 4 µm. In the formation stage VIS decreases until it reaches its first minimum – mostly after 12% of the whole life cycle. From then on, VIS increases till the end of the fog event. All three microphysical parameters (LWC, N_t and r_{mean}) increase during the formation stage whereas r_{mean} already reaches its absolute maximum. The first minimal VIS is also the criterion for the transition to mature fog and the time of maximal values of LWC and N_t. Furthermore, very small drops disappear shortly before this point and reappear afterwards. During mature fog LWC and N_t fluctuate synchronously with VIS whereby the latter either stays constant or subjects to large fluctuations. r_{mean} stays constant once it has decreased gradually in the beginning of mature fog. The shift to the last phase, dissipation stage, occurs after 75% of the life cycle when all microphysical parameters decrease drastically with some exceptions for r_{mean}.

VIS as criterion for the differentiation between formation stage and mature fog is not suitable for the three measured fog events because very low values were spread over all three stages of evolution. Their absolute minima lay in the middle of the formation stage with 0.05667 km at 04:07 LT during the first fog event and with 0.02 km at 22:17 LT during the second fog event; the VIS-minimum of the third fog occurrence was situated earlier in the formation stage with 0.05333 km at 21:19 LT. Besides, VIS revealed large fluctuations in the formation and in the dissipation stage, different from PFM. Also, the time intervals of the classified formation stages did not coincide with Pilié's (Pilié et al., 1972, 1975a, 1975b) declaration (25% of the total life cycle). During the first fog event the formation stage lasted longer than 50% of the whole fog event, while it lasted about 10% of the whole fog event during the second fog event and 37% of the third fog event. The increasing trend of all microphysical properties could be seen during the formation stages as in GFM and PFM, however with larger fluctuations and prior maximum values of LWC (0.09 g m^{-3}/ 0.06 g m^{-3}) and N_t (116 cm^{-3}/ 51 cm^{-3}/ 18 cm^{-3}). Only the maximum LWC of the third fog event lay in the mature fog with 0.03 g m^{-3}.

The mature fog episodes did not always exhibit constant values for LWC and N_t, but rather unsteady values. Unlike the specification of GFM and PFM, r_{mean} did not show a decreasing, but rather a constant or an increasing trend. In return, high values of r_{mean} at the end of the first fog event

agreed with the exception for that phase of the PFM. Maximum r_{mean} values of 11 µm were reached at the transition to the dissipation stage of the first fog event. In contrast, maximum r_{mean} values of about 13 µm occurred in the middle of the mature fog stage during the second fog event and in the formation stage of the third fog event.

The dissipation stages set in after 85% (first fog event) and after 60% (second and third event) of the whole fog event. This corresponds well with the PFM which states the beginning of the dissipation stage after 75% of the whole fog event.

Even though the separation of the investigated fog events in three evolutionary stages seems to be appropriate, featuring the same main trends in the microphysics as the GFM and the PFM; Pilié's criteria (Pilié et al., 1972, 1975a, 1975b) for stage classification as minimum VIS or maximum values of microphysical properties did not match with the statistical based CPs of the three observed fog events.

Another aspect that has to be clarified is the representation of the measured microphysical values of the three fog events. In a former study Maier et al. (2012) compiled published measurement values of LWC, N_t, r_c from different authors depending on the type and evolutionary stage of fog (Table 3.5). For a comparison with our measurements the extremes of LWC, N_t and r_c were aggregated for the whole data set of all three fog events. Thereby, the phase-specific minimum as well as the phase-specific maximum of the microphysical parameters was selected and opposed with the phase-specific extreme values from Maier et al. (2012). Additionally, the marginal values of the parameters were assembled without consideration of the evolutionary stage for the whole measured values from the three fog events. Considering the aggregated microphysical values from the three investigated fog events without a differentiation into evolutionary stages, they agree well with the values from other studies. According to Gultepe et. al (2009) continental fog events feature a mean LWC of about 0.02 – 0.03 g m^{-3} and a mean N_t of 90 cm^{-3}. Compared to the measured values of LWC and N_t during summery marine fog cases (Gultepe et al., 2009), the presented measurements for both microphysical properties feature mostly smaller values (Fig. 3.6).

TABLE 3.5. Comparison of the measured microphysical parameters (LWC, N_t, r_c) with values from literature compiled in Maier et al. (2012)

	LWC [g m^{-3}]				Nt [cm^{-3}]				r_c [µm]			
	Measurements		Maier et al. 2012		Measurements		Maier et al. 2012		Measurements		Maier, 2012	
	min	max	min	max	min	max	min	max	min	max	min	max
Whole data set of measured radiation fog events	0.00	0.09	0.02	0.21	0.00	115.69	15.90	249.93	2.50	10.25	2.13	12.22
Formation stage	0.00	0.06	0.08	0.17	0.05	50.72	21.73	138.04	2.50	4.70	3.49	10.82
Mature fog	0.00	0.06	0.12	0.16	0.00	41.43	28.00	59.02	2.50	10.25	4.99	9.00
Dissipation stage	0.00	0.03	0.17	0.16	0.00	33.78	24.14	32.51	2.50	7.30	6.92	10.10

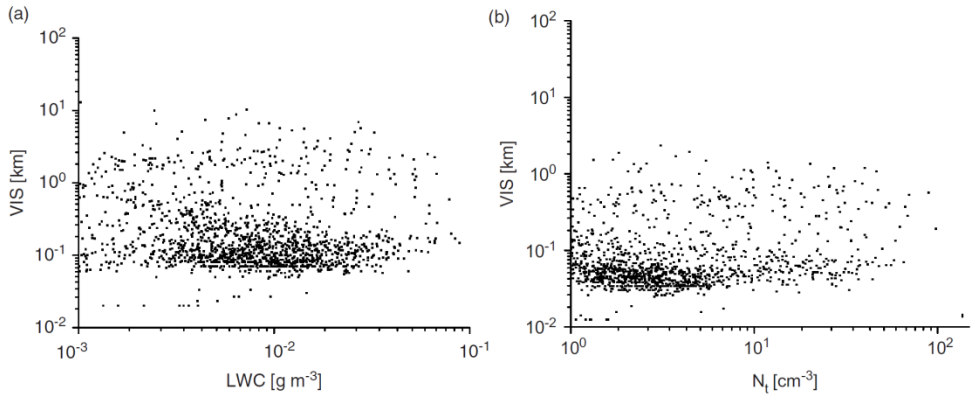

FIG. 3.6. Horizontal visibility (VIS) as a function of (a) liquid water content (LWC) and (b) total number of droplets per cubic centimeter (N_t) for all three fog events.

The differences of the microphysical properties can be ascribed to the different types of fog as well as the diverse location of the measurement sites. The Marburg Ground Truth and Profiling Station is located in a region featuring a warmer continental climate than in Canada where Gultepe et al. (2009) accomplished their fog measurements under a colder maritime influence. Furthermore the used time-intervals differ by a factor of 60 which results in further anomalies.

If the values are separated into the different evolutionary stages some differences become apparent in comparison with the parameter values from the literature. All maxima of measured LWC are lower than the LWC minima from the literature for all evolutionary stages. In return, all recorded maximal values of N_t and r_c are in the published ranges. Only maximal N_t values during the dissipation stage and maximal r_c values during the mature stage are slightly above the released figures. Regarding that no clear criteria for the phase-specific classification were given in literature, measured values of the microphysical properties of the three fog occurrences fit quite well with the known ones. Also one should note that the values from the literature are assembled from different, older instruments with different time resolutions, however, the compliances are quite good.

Whether the three evolutionary stages of the three measured fog events, found by the statistical approach, can be aggregated, will be discussed next. The longest phase was the mature stage with about half of the whole life cycles. However, there is no coincidence for the two other evolutionary stages. During the first and last fog events, the formation stage lasted about a third and the dissipation stage about 15% of the whole fog events. In contrast, the last phase of the second fog occurrence was over 40% of the fog duration and its formation stage only 12%. Overall, the separation of the evolutionary stages as a function of time has to be seen crucial.

Although the arithmetic mean of phase-specific LWC of the three fog events show a slight increase from formation to mature stage with a strong decrease to the dissipation stage, maximum values of LWC were found in the two initial phases for the first two fog events that decreased over the fog life cycle (Table 3.4). Averaged values of N_t over the three phases decreased from formation (7.5 cm^{-3}) over mature (3.3 cm^{-3}) till dissipation stage (1.0 cm^{-3}). Maximum values of droplets were always in the formation stage (115.7 cm^{-3}/ 50.7 cm^{-3}/ 16.1 cm^{-3}) and minimum peak values of N_t in the dissipation stage (5.7 cm^{-3}/ 33.8 cm^{-3}/ 5.4 cm^{-3}). The arithmetic means of the phase-specific r_{mean} and r_c of the three fog occurrences showed consistent tendencies. From the initial phase to mature stage r_{mean} and r_c averaged over all separated phases increased from 5.2 µm (3.6 µm) to 7.1 µm (4.7 µm) and decreased again to 4.9 µm (9.6 µm) during the dissipation stage and thereby below the values at the beginning of fog formation. Phase-specific arithmetic averaged values of r_{max} show also uniform trends. Table 3.4 reveals that there was an increase from formation (11.0 µm/ 16.1 µm/ 8.0 µm) to dissipation stage (17.1 µm/ 22.1 µm/13.9 µm) and then a decrease to dissipation stage (14.6 µm/ 4.7 µm/ 6.6 µm) for all three fog events. Regarding the phase-specific microphysical properties the derived evolutionary stages by the developed statistical approach show good agreements.

For a more precise understanding of the development of radiation fog the meteorological processes have to be included which determine the microphysical parameters in a relevant manner and therewith also the formation of the three consecutive evolutionary stages. The dynamic basis of the three fog events from 26-27 October 2011 (cyclonic south-easterly), 31 October 2011-1 November 2011 (change from zonal ridge across Central Europe to anticyclonic southerly) and 13-14 November 2011 (anticyclonic southerly) were high pressure (> 1016 hPa) situations over the study site (Fig. 3.1). An increasing high relative humidity > 90%, low wind speeds < 2 m s^{-1} (Figs. 3.3c, 3.4c, 3.5c) and a clear sky (Figs. 3.3d, 3.4d, 3.5d) predominated after sunset, shortly after 16:00 LT. Persistent radiative cooling of the surface resulted in constantly decreasing temperature of the ground. First small droplets formed when dew point had been reached and consequently VIS decreased. Small droplets evaporated and recondensed again. When wind speed continued decreasing down to 0.5 m s^{-1} the conditions for lasting drops were given, together with further radiative cooling and increasing humidity. VIS became below 1 km for the first time. Turbulent fluxes, indicated by fluctuating wind speeds, disturbed the growth process of the fog layers. Thereby, the up and down of the microphysical parameters as well as VIS can be explained. When temperatures reached even lower degrees, the dew point fell too, permitting a stable growth of drops. Maximum drop sizes and minimal VIS-values were observable while the number of droplets decreased and stayed at a low constant level. The dispersal of the three fog

occurrences came along with a change of temperature. As far as the second CPs the temperatures had decreased to a (local) minimum level. From that time on, temperatures got an increasing tendency and relative humidity ascended slightly once again. Striking are the different times of the second CPs and thus, the beginning of the dissipation stages. The first and the third fog event featured it simultaneously with sunrise around 06:00 LT while for the second fog event the dissipation stage began in the middle of the night at 01:57 LT. Because of increasing temperatures, turbulent fluxes increased as well by which vertical mixing was enhanced and droplets evaporated after having shrank to a critical size. Supporting measurements of radiation fluxes were not available. Comparable studies such as Gultepe et. al (2009) showed that reduced incoming shortwave radiation fluxes (up to -300 W m^{-2}) may result in temperature decreases of up to -9 K as a consequence of fog effects. The mixing and shifting of air masses could be seen in an increase from air speed during the end of the first fog event from around 0.5 m s^{-1} up to 2 m s^{-1} (Fig. 3.4c). Furthermore, the cloud ceilings from this event (Fig. 3.4d) indicate a take-off of the fog. At once, when a formation of the cloud base was recorded at 20:00 LT, the fog top shifted to a higher altitude. After three more hours a stratus cloud with distinct cloud ceilings prevailed 500 m above the ground. However, the energy for droplet evaporation during the second fog event from 31 October 2011 to 1 November 2011 could not have come from solar insolation after sunrise. The nocturnal growth of wind speed from around 0.5 m s^{-1} up to 2 m s^{-1} had a different cause, namely a change of general weather conditions (Section 3.2.2, Fig. 3.1b). Overnight a zonal ridge across Central Europe was replaced by an anticyclonic southerly, accompanied by an inflow of warmer air masses from the south. These did not only originate with a sudden increase of wind speed from 0.5 to 2.5 m s^{-1}, but also a change of wind direction form mainly northwest to southeast (Fig. 3.5c). Hence, ground temperatures rose suddenly after the second CP at 01:57 LT from ca. 3 °C up to 7 °C and stayed constantly at this level. Due to the inflow of warmer air masses over colder and moisture air masses the dew point rose and fog droplets evaporated. As a result, the fog dissolved and VIS rose consequently. The humid air masses from the ground shifted upwards and recondensed at 06:00 LT at a height of about 100 m, from where they spread up to 400 m (Fig. 3.5d).

An additional analysis of the meteorological standard parameters exposed the presumable cause. Increasing temperatures as principal source of fog dissipation originated for two occurrences from insolation with beginning of sunrise (26-27 October 2011 and 13-14 November 2011) and for one from a change of the principal weather conditions from zonal ridge across Central Europe to anticyclonic southerly (31 October 2011-1 November 2011) midway through the fog event. Thus, two differing mechanism of fog dissipation proceeded which affected the evolution of microphysical and meteorological parameters. In total, the first time series of the

three examples showed an increase of all three microphysical parameters with maximal values of N_t and LWC. The second phase of the three fog events revealed a further growth of r_{mean} reaching maximum values whereas N_t and LWC decreased and leveled off at a lower standard. The last phase could be described with an omnipresent downward tendency of all three microphysical parameters which subsequently reached zero, mostly attended by a last local maximum.

3.5 Summary and Conclusion

The intention of the presented study was the development of an objective statistical method for the separation of fog events into individual life cycle phases. For this purpose the statistical approach of double sum curves was applied to three fog events in autumn 2011 in central Germany. By use of the homogeneity-test of Mann-Whitney, two potential CPs per double sum curves of measured time series of microphysical fog properties and horizontal visibility could be identified. The following trend-tests of Mann-Kendall and the two-sided t-tests on the slopes of the three phases per fog event provided the statistical significance of the CPs. As the CPs of the microphysical properties and the corresponding VIS coincided at the same points in time, the latter can be used as a reliable criterion for the separation of measurement series of LWC, N_t and r_{mean} in different evolutionary stages during the fog life cycle. With respect to the obtained results it can be stated that an objective method with distinct criteria for the investigation and classification of radiation fog incorporating the different evolutionary stages could be derived. However, the analyses were limited to only three fog events. For more representative results, further fog events have to be analyzed with the presented method.

By comparing the three distinguishable phases, derived from the developed statistical approach with existing classifications of radiation fog, good agreements have been found with the GFM discriminating three stages and the PFM with four evolutionary stages. Their criteria for the separation of the evolutionary stages, as the predetermined points in time of VIS within the fog duration did not correspond with our findings. However, the general trends of the phase-specific microphysical properties are in good agreement with our results. Almost all measured values of N_t and r_{mean} lay in the published ranges of the three evolutionary stages, merely LWC was underestimated during the formation stage.

A comparison of the separated phases between the three fog events revealed that the characteristic microphysical properties in each phase correspond well between the three fog events.

It seems possible to characterize the evolutionary stage of the respective fog event by stage-specifically averaged values of the measured microphysical parameters over all three fog events. However, for substantiated

results in this direction, much more measurements and analyses of radiation fog events are needed. In this context, the presented method is a valuable method for the required statistical analyses.

Even though different mechanisms are responsible for the fog development, as seen by the two diverse synoptic situations responsible for fog dissipation (26-27 October 2011 vs. 31 October 2011- 1 November 2011) the applied statistical approach seems to work well. The differentiation between mature fog and dissipation stage at the second CPs fit well with the changing tendencies of the microphysical and meteorological parameters.

3.6 Appendix

For the discrimination of fog life cycle phases CPs in time series *(t)* of microphysical parameters and VIS (x) were used. In more detail, the cumulative sum of the latter (x_t) till time step t was plotted as a function of the cumulative sum of time ($1 \leq t \leq T$; with T end time of time series). On condition that the time series was homogeneous, it revealed a unique slope, meaning a constant arithmetic average all along the double sum curve. In case of inhomogeneities in a time series, a change of slope in the double sum curve could be observed. Consequently, its double sum curve was split in separate curve segments $x_1(t_1)$ to $x_n(t_n)$ with diverging slopes and arithmetic means for each segment derived. In three consecutive tests CPs in the double sum curves could be found and their statistical reliability be tested.

1. Step: Identifying potential CPs with the homogeneity test of Mann-Whitney

For finding CPs in the calculated double sum curves of the microphysical parameters and VIS the non-parametric test of Mann-Whitney (Mann and Whitney, 1947), later modified by Pettitt (1979), was used as suggested by the WMO (2003). The rank-test yielded the most possible points in time within time series where changes occurred. However, no information about the significance of the CPs can be derived with this procedure. The test statistic $(U_{t,T})$ is defined as

$$U_{t,T} = \sum_{i=1}^{t} \sum_{j=t+1}^{T} sgn(x_i - x_j) \tag{1}$$

and

$$sgn(x_i - x_j) = \begin{cases} +1 & (x_i - x_j) > 0 \\ 0 & \text{if} \quad (x_i - x_j) = 0 \\ -1 & (x_i - x_j) < 0 \end{cases} \tag{2}$$

The most possible CP t_{CP} is the point where $U_{t,T}$ becomes maximum.

$$K_T = \max_{1 \le t \le T} |U_{t,T}| \tag{3}$$

The derived CP split the double sum curve segment in two different trend curves defined by

$$\hat{x}_1 = A_{x1t1} + B_{x1t1}t \quad \text{and} \quad \hat{x}_2 = A_{x2t2} + B_{x2t2}t \tag{4}$$

Their slopes B_{x1t1} and B_{x2t2}

$$B_{xt} = \frac{s_{xt}}{s_t^2} = \frac{\frac{1}{n-1}\sum(x_i - \bar{x})(t_i - \bar{t})}{\frac{1}{n-1}(t_i - \bar{t})^2} \tag{5}$$

and intercepts A_{x1t1} and A_{x2t2}

$$A_{xt} = \bar{x} - B_{xt}\bar{t} \tag{6}$$

were calculated by linear regression (Schönwiese, 2006) whereby s_{xt} was the covariance of the time and the measured quantities, s_t^2 was the variance of the time and n the number of time steps.

If a CP was found, the result of step 1 is the segmentation of the double sum curve in two curve segments separated by a CP. It should be noted, that the double sum analysis is conducted several times for every curve segment derived from a previous analysis step.

2. Step: Mann-Kendall trend-test

Once the potential CPs were determined, the separated two curve segments had to be tested for homogenous (and significant) trends in a second step to warrant that the found segments were consistent. For this, the non-parametric trend-test according to Mann (1945) and Kendall (Kendall and Stuart, 1969) was utilized. The Mann-Kendall test statistic is

$$Q = \sum_{i=1}^{n-1}\sum_{j=i+1}^{n} sgn(x_i - x_j) \tag{7}$$

where i, j are successive points in time.

If the number of considered time steps $n > 10$, Q could be considered as standard normal distributed with an arithmetic mean of zero and a variance of

$$s_Q^2 = \frac{1}{18}(n(n-1)(2n+5)) \tag{8}$$

Consequently, the standard normal distributed test statistic is

$$\hat{z} = \frac{Q}{s_Q} \tag{9}$$

that could be used for a two-sided test on significance with H_0 ($\mu_x(t)$ = const) and H_A ($\mu_x(t)$ decreases or increases with time). Thus, the split time series were determined which featured homogenous trends.

3. Step: Two-sided t-test for compatibility of the slopes of the evolutionary stages

As mentioned above, the homogeneity-test of Mann-Whitney only provided possible positions of CPs in the measurement series of the examined parameters. However, it could not give evidence of its statistical significance. In order to test if a CP split a double sum curve at the right place in two significantly different curve segments the consistency of their slopes had to be tested with H_0 ($B_{x1t1} = B_{x2t2}$) and H_A ($B_{x1t1} \neq B_{x2t2}$). Thereby, different slopes represented different mean values in both curve segments. A change of the slope at the CP in the double sum curve was validated by a two-sided t-test on the slopes of the two curve segments with the following test statistic (Schönwiese, 2006)

$$\hat{t} = \frac{|B_{x1t1} B_{x2t2}|}{\sqrt{\frac{s^2_{x1*t1}(n_1-2)+s^2_{x2*t2}}{n_1+n_2-4}\left(\frac{1}{Y_{x1}}+\frac{1}{Y_{x2}}\right)}} \tag{10}$$

with

$$Y_{x1} = \sum_{i=1}^{n}(x_{1\,i} - \overline{x_1})^2 \quad \text{and} \quad Y_{x2} = \sum_{i=1}^{n}(x_{2\,i} - \overline{x_2})^2 \tag{11}$$

and s^2_{x1*t1} , s^2_{x2*t2} being the residual variances and n_1, n_2 representing the number of time steps in the time series before or after the CP. The corresponding degrees of freedom was given by

$$DF = n_1 + n_2 - 4 \tag{12}$$

Provided that a point in time within the double sum curve of a measurement series passed all three listed tests, it was regarded as a statistically significant CP.

Acknowledgements

The authors thank the German Research Foundation DFG for funding the project (BE1780/14-1; TH1531/1-1). The work is also part of the COST action EG Climet. The authors are also thankful to Sebastian Achilles for his support during the measurements.

3.7 References

AK KLIWA. 2002. Long-run behaviour of flood flows in Baden-Württemberg and Bavaria. In: *KLIWA-reports 2* (ed. AK KLIWA). Stork Druck, Karlsruhe, pp. 1-98.

Bendix, J. 1998. Ein neuer Methodenverbund zur Erfassung der klimatologisch-lufthygienischen Situation von Nordrhein-Westfalen. Untersuchungen mit Hilfe boden- und satellitengestützer Fernerkundung und numerischer Modellierung. In: *Bonner Geographische Abhandlungen* **98** (ed. W. Schenk). E-Ferger Verlag, Bonn, Germany, pp. 1-183.

Bendix, J. 2002. A satellite-based climatology of fog and low-level stratus in Germany and adjacent areas. *Atmosph. Res.* **64**, 3-18.

Bennett, A. J., Gaffard, C., Oakley, T. and Moyna, B. 2009. Cloud radar – initial measurements from the 94 GHz FMCW cloud radar. *Proceedings of the 8th International Symposium on Tropospheric Profiling 19–23 October, Delft,* 1-8.

Bergot, T. and Guédalia, D. 1994. Numerical forecasting of radiation fog. Part I. Numerical model and sensitivity tests, *Mon. Weather Rev.* **122**, 1218–1230.

Brown, R. and Roach, W. T. 1976. The physics of radiation fog. II. A numerical study. *Q. J. Roy. Meteor. Soc.* **102**, 335-354.

DMT. 2012. Cloud Droplet Probe (CDP). Manual. DOC-0029. Rev N-3. Boulder, USA, 1-55.

Dupont, J. C., Haeffelin, M., Protat, A., Bouniol, D., Boyouk, N. and Morille, Y. 2012. Stratus–Fog Formation and Dissipation. A 6-Day Case Study. *Bound.-Lay. Meteorol.* **143**, 207-225.

Duynkerke, P.G. 1999. Turbulence, radiation and fog in Dutch stable boundary layers. *Bound.-Lay. Meteorol.* **90**, 4477-477.

DWD. 2011. General weather situations of Europe. Online at: http://www.dwd.de/GWL. Last page view: 10/24/2012.

Findlater, J. 1985. Field investigations of radiation fog formation at outstations. *Meteorol. Mag.* **114**, 187-201.

Fitzjarrald, D. R. and Lala, G. G. 1989. Hudson Valley Fog Environments. *J. Appl. Meteorol.* **28**, 1303-1328.

Fuzzi, S., Facchini, M. C., Orsi, G., Lind, J. A., Wobrock, W., Kessel, M., Maser, R., Jaeschke, W., Enderle, K. H., Arends, B. G., Berner, A., Solly, A., Kruicsz, C., Reischl, G., Pahl, S., Kaminski, U., Winkler, P., Ogren, J. A., Noone, K. J., Hallberg, A., Fierlinger-Oberlinninger, H., Puxbaum, H., Marzorati, A., Hansson, H.-C., Wiedensohler, A., Svenningsson, I. B., Martinsson, B. G., Schell, D. and Georgii, H. W. 1992. The Po Valley fog experiment 1989. An overview. *Tellus* **44B**, 448–468.

Fuzzi, S., Laj, P., Ricci, L., Orsi, G., Heintzenberg, J., Wendisch, M., Yuskiewicz, B., Mertes, S., Orsini, D., Schwanz, M., Wiedensohler, A., Stratmann, F., Berg, O. H., Swietlcki, E., Frank, G., Martinsson, B. G., Günther, A., Dierssen, J. P., Schell, D., Jaenschke, W. Berner, A., Dusek, U., Galambos, Z., Kruisz, C., Mesfin, N. S., Wobrock, W., Arends, B. and Tenb, H. 1998. Overview of the Po Valley fog experiment 1994 (CHEMDROP). *Contr. Atmos. Phys.***71**, 3–19.

Gultepe, I., Pearson, G., Milbrandt, J. A., Hansen, B., Platnick, S., Taylor, P., Gordon, M., Oakley, J. P. and Cober, S. G. 2009. The fog remote sensing and modeling field project. *B. Am. Meteorol. Soc.* **90**, 341–359.

Gultepe, I., Tardif, R., Michaelides, S. C., Cermak, J., Bott, A., Bendix, J., Mueller, M. D., Pagowski, M., Hansen, B., Ellrod, G., Jacobs, W., Toth, G. and Cober, S. G. 2007. Fog research. A review of past achievements and future perspectives. *Pure Appl. Geophys.* **164**, 1121–1159.

Gultepe, I., Müller, M.D. and Boybeyi, Z. 2006. A new visibility parameterization for warm-fog applications in numerical weather prediction models. *J. Appl. Meteorol. Clim.* **45**. 1469-1480.

Haeffelin M., Bergot, T., Elias, T., Tardif, R., Carrer, D., Chazette, P., Colomb, M., Drobinski, P., Dupont, E., Dupont, J.-C., Gomes, L., Musson-Genon, L., Pietras, C., Plana-Fattori, A., Protat, A., Rangognio, J., Raut, J.-C., Rémy, S., Richard, D., Sciare, J. and Zhang, X. 2010. PARISFOG. Shedding new light on fog physical processes. *B. Am. Meteorol. Soc.* **91**, 767–783.

Hansel, N. and Schäfer, U. 1970. The double sum analysis. *Water management-water technology* **20**, 145-149.

Hess, P. and Brezowsky, H. 1977. Catalog of the general weather situations of Europe (1881-1976). *Reports of the German Weather Service* **113**, 1-54.

Huggard, P.G., Oldfield, M. L., Moyna, B. P., Ellison B.N., Matheson, D. N., Bennett, A. J., Gaffard, C. Oakley, T. and Nash, J. 2008. 94 GHz FMCW cloud radar. *Proceedings of the SPIE symposium on millimetre*

wave and terahertz sensors and technology, 15–18 September 2008, Cardfiff, 1-6.

James, P. M. 2007. An objective classification method for Hess and Brezowsky Grosswetter-lagen over Europe. *Theor. Appl. Climatol.* **88**, 17-42.

Juisto, J. E. and Lala, G. G. 1983. The Fog project - 1982. *Proceedings. of 9th Conference on Aerospace and Aeronautical Meteorology, AMS, 6-9 June 1983, Omaha, NE,* 95-98.

Kendall, M. G. and Stuart, S. 1969. *Advanced theory of statistics. Part 1. Distribution theory*. (ed. Kendall, M G.). Griffin, London, 1-439.

Lala, G. G., Mandel, E. and Jiusto, J. E. 1975. A numerical investigation of radiation fog variables. *J. Atmos. Sci.* **32**, 720–728.

Lala, G. G., Jiusto, J. E., Meyer, M. B. and Komfein, M. 1982. Mechanisms of radiation fog formation on four consecutive nights. *Preprints of Conference on Cloud Physics, Nov. 15–18, 1982, Chicago, IL, AMS, Boston, MA, 9–11.*

Liu, D., Yang, J., Niu, S. and Li, Z. 2011. On the evolution and structure of a radiation fog event in Nanjing. *Adv. Atmos. Sci.* **28**, 223-237.

Maier, F., Thies, B. and Bendix, J. 2012. Simulating Z–LWC relations in natural fogs with radiative transfer calculations for future application to a cloud radar profiler. *Pure Appl. Geophys.* **169**, 793-807.

Mann, H. B. 1945. Nonparametric tests against trend. *Econometrica* **13**, 245-259.

Mann, H. B. and Whitney, D. R. 1947. On a test of whether one of two random variables is stochastically larger than the other. *Ann. Math. Stat.* **18**, 55-60.

Meyer, M. B., Lala, G. G. and Jiutso, J. E. 1986. FOG-82. A cooperative field study of radiation fog. *B. Am. Meteorol. Soc.* **67**, 825–832.

Nakanishi, M. 2000. Large-eddy simulation of radiation fog. *Bound.-Lay. Meteorol.* **94**, 461-493.

Pettitt, A. N. 1979. A non-parametric approach to the change-point problem. *J. R. Stat. Soc.* **28**, 126-135.

Pilié , R., Eadie, W., Mack, E., Rogers, C. and Kocmond, W. 1972. Project fog drops. Part 1. Investigations of warm fog properties. *NASA Contractor Report*, No. **2078**. Buffalo, New York: Cornell Aeronautical Laboratory, Inc., 1-149.

Pilié, R. J., Mack, E. J., Kocmond, W. C., Rogers, C. W. and Eadie, W. J. 1975a. The life cycle of valley fog. Part I. Micrometeorological characteristics. *J. Appl. Meteorol.* **14**, 347-363.

Pilié, R. J., Mack, E. J., Kocmond, W. C., Eadie, W. J. and Rogers, C. W. 1975b. The life cycle of valley fog. Part II. Fog microphysics. *J. Appl. Meteorol.* **14**, 364-374.

Price, J. 2011. Radiation fog. Part I. Observations of stability and drop size distributions. B*ound.-Lay. Meteorol.* **139**, 167–191.

Roach, W. T., Brown, R., Caughey, R., Garlands, J. and Readings, C. J. 1976. The physics of radiation fog. I. A field study. *Q. J. Roy. Meteor. Soc.* **102**, 313-333.

Schönwiese, C. D. 2006. *Applied statistics for meteorologists and earth scientists.* Bornträger, Berlin, pp. 1-302.

Schulze-Neuhoff, H. 1976. Detailed analysis of fog based on additional 420 weather stations. *Meteorol. Rundsch*. **29**, 75-84.

Stewart, D. A. and Essenwanger, O. M. 1982. A survey of fog and related optical propagation characteristics. *Review of Geophysics* **20**, 481-495.

Terradellas, E. and Bergot, T. 2008. Comparison between two single-column models designed for short-term fog and low-clouds forecasting. *Fisica de la Tierra* **19**, 189–203.

Turton, J. D. and Brown, R. 1987. A comparison of a numerical model of radiation fog with detailed observations. *Q. J. Roy. Meteor. Soc.* **113**, 37-54.

Wendisch, M., Mertes, S., Heintzenberg, J., Wiedensohler, A., Schell, D., Wobrock, W., Frank, G., Martinsson, B. G., Fuzzi, S., Orsi, G., Kos, G. and Berner, A. 1998. Drop size distribution and LWC in Po Valley Fog. *Contr. Atmos. Phys.***71**, 87–100.

WMO. 1992. International meteorological vocabulary. Vol. 182. (ed. WMO). Geneva, 1-276.

WMO. 2003. The WCDMP „guidelines“ series. *Technical Document 1186*, 1-50.

Zhou, B. B. and B. S. Ferrier. 2008. Asymptotic analysis of equilibrium in radiation fog. *J. Appl. Meteorol.* 47, 1704-1722.

4. Vertical distribution of microphysical properties in radiation fogs - a case study

Sebastian Egli, Frank Maier, Boris Thies and Jörg Bendix

Faculty of Geography, University of Marburg, Marburg, Germany

---

Submitted to

ATMOSPHERIC RESEARCH (2013)

Abstract

The present study investigates the validity of a theoretical liquid water content (LWC) profile in fog layers currently used for satellite based ground fog detection, with a special focus on the temporal dynamics during fog life cycle. For this purpose, LWC profiles recorded during two different fog events by means of a tethered balloon borne measurement system are presented and discussed. The results indicate a good agreement in trend and gradient between measured and theoretical LWC profiles during the mature stage of the fog life cycle. The profile obtained during the dissipation stage shows less accordance with the theoretical profile. To improve the agreement between theoretical and measured LWC profiles, the evolutionary stages during the fog life cycle should be incorporated. However, the variability within the prenoted measurements points out that more LWC profiles during a great variety of different fog events have to be collected for a well-justified adaptation of the theoretical LWC profile, considering fog life cycle phases in future. In general, this underlines the existing knowledge gap regarding the vertical distribution of microphysical properties in natural fogs.

4.1 Introduction

Fog is internationally defined as a visible aggregate of small water droplets or ice crystals in the air, reducing horizontal visibility (VIS) to less than 1 km (Glickman, 2000). Its impact on the human sphere has increased significantly during the modern era - mainly due to obstructions of marine, air and road traffic or the solution and deposition of air pollutants (Bendix et al., 2011). As fog strongly influences the heat fluxes in the atmospheric boundary layer and the Earth's radiation budget by forming persistent low level temperature inversions trapping air pollutants, it also often has a negative impact on the air quality in industrial agglomerations during inverted weather conditions (Nemery et al., 2001). All these effects ultimately lead to financial losses or even human casualties that are comparable to effects from other severe weather situations like tornadoes or winter storms (Gultepe et al., 2007). In contrast to its negative effects on the environment, fog is often considered as a positive element in ecology and hydrology as it can supply otherwise arid ecosystems with moisture (Bendix et al., 2011; Bruijnzeel et al., 2006; Pinto et al., 2001).

Hence, much effort has been put into the development of fore- and nowcasting methods by means of numerical models and satellite data (see Gultepe et al. (2007) and Jacobs et al. (2008) for an overview). The fog-forecasting-quality of numerical weather prediction (NWP) models is limited due to their low horizontal and vertical resolution as well as deficiencies in the parameterization of the microphysics (Bergot et al., 2007; Ronda

et al., 2011). Several studies suggest that a better understanding of fog microphysics is needed to develop more accurate forecasting models (Gultepe et al., 2007; Pagowski et al., 2004; Tardif, 2007). The results of Terradellas and Bergot (2007) indicate a high sensibility of 1-D models to the incorporated microphysics and the vertical resolution. Since these models are computationally very intensive, parameterized versions of the detailed 1-D fog microphysics models can be used in 3-D models to improve the forecast results (Gultepe et al., 2006, 2007; Pagowski et al., 2004). As a consequence, several models explicitly simulate fog microphysics as e.g. PFOG (Bott and Trautmann, 2002). In several experiments, Thoma et al. (2012) could show that an initialization or nudging with observational data (visibility, vertical profiles of temperature and specific humidity) could significantly improve forecast quality. However, the authors stated that especially the integration of measured fog droplet spectra over the fog layer would be necessary to properly simulate fog formation, dissipation and fog vertical extent.

The potential of fog detection techniques based on polar orbiting satellite systems like NOAA/AVHRR (Advanced Very High Resolution Radiometer) and Terra & Aqua/MODIS (Moderate Resolution Imaging Spectroradiometer) has been widely investigated (Bendix, 2002; Bendix et al., 2005, 2006; Eyre et al., 1984; Turner et al., 1986). Due to improvements in the spectral resolution of the new generations of geostationary satellites, this methodology has also been successfully transferred to the GOES (Geostationary Observational Environmental Satellites) and the SEVIRI systems (Spinning Enhanced Visible and Infrared Imager) aboard MSG (Meteosat Second Generation) satellites (Cermak and Bendix, 2007; Ellrod, 1995). However, the common problem of these techniques persists: The distinction between low stratus (LS) layers and ground fog which is based on information about cloud top altitude and geometrical thickness. Various methods for the deduction of cloud geometrical thickness as a precondition to discriminate between LS and ground fog have been proposed using simple parameterizations (Ellrod, 1995), adiabatic approximations (Iwabuchi and Hayasaka, 2002) and pseudosounding approaches (Chang and Li, 2002). However, these methods perform not always well for low stratus layers and fog (Bendix et al., 2005; Cermak, 2006). Hutchison (2002) estimated cloud thickness and cloud-base heights assuming constant vertical liquid water content (LWC) profiles for stratus clouds. Brenguier et al. (2000) applied an adiabatically stratified LWC profile to estimate cloud thickness. Minnis et al. (1997) developed an empirical relationship between cloud geometrical thickness and cloud optical thickness. Cermak and Bendix (2011) recently developed a technique on the basis of the European geostationary satellite system MSG-SEVIRI that takes greater account of the microphysical properties in fogs. In their model they assume a three-layered stratification of an LS/fog layer with the following characteristics:

1. The lowermost part of the cloud/fog layer shows a linear shift from adiabatic to subadiabatic conditions with increasing height.
2. Liquid water content (LWC) in the central region of low stratus and fog layers rises with altitude (Pruppacher and Klett, 1997). The emerging LWC profiles generally follow a sub adiabatic gradient. This is due to the fact that most stratiform cloud formations are characterized by very weak turbulence which, in turn, leads to a higher saturation point and consequently to LWC values that diverge from the adiabatic profile (Betts, 1982).
3. Near the fog/stratus top r_{eff} and thus LWC values decrease linearly. In very low stratus layers this starts at about 80% to 90% of the cloud height and can be attributed to the entrainment of dry air at the top of the fog/stratus layer (Boers and Mitchell, 1994; Roach et al., 1982; Wieprecht et al., 2005).

The validation results of Cermak and Bendix (2011) show an overall good performance of the ground fog detection methodology which points to the general validity of the underlying theoretical LWC profile. However, the scatter obtained during validation also pointed out that the assumptions might not hold for all fog events and/or fog life cycle phases. This is why the development of fog is often described as a typical life cycle with varying microphysical properties during consecutive evolutionary stages (Gultepe et al., 2007; Liu et al., 2011; Pilié et al., 1972, 1975b, a; Wendisch et al., 1998). Maier et al. (2013), for instance, classified three development stages with characteristic changes in the LWC at the ground level. However, it is obvious that LWC not only varies at the ground but also in the vertical profile during the different development stages. Thus, the validity of the remote sensing approach, but also of advanced simulation models like PAFOG might be strongly depending on the availability of varying vertical profiles of LS/fog properties.

Unfortunately, there is only little data concerning the vertical distribution of fog microphysics, particularly during the different life cycle stages, that would allow to investigate the validity of the theoretical LWC profile and/or properly initialize numerical models. In situ airborne measurements for the investigation of low level stratocumulus clouds (Hayasaka et al., 1995; Slingo et al., 1982; Wang et al., 2009) are hardly permitted and not even possible during fog situations. Studies using balloon-borne systems with suitable sensors for profile measurements are rare. Okita (1962), for instance, investigated the LWC profile of four radiation fogs in Japan. Pinnick et al. (1978) measured the vertical profile during a fog event in West Germany. However, the recorded profiles did not completely cover the whole fog column. During the Po Valley and the Chemdrop experiment the vertical structure during fog events was measured with a 50 m high tower (Fuzzi et al., 1992, 1998), also not capturing the whole vertical LS/fog pro-

file. Beside the small dataset about fog LWC profiles there is no information available about fog evolutionary stages during the different profile measurements. This information, however, is necessary to be able to account for the expected changes in the LWC profiles during the different development stages of the fog (Maier et al., 2013) and to verify the validity of the theoretical assumptions made by Cermak and Bendix (2011) especially throughout the whole fog life cycle.

The aim of the present study is to compensate the lack of data and knowledge by measuring LWC profiles during selected fog events with a special focus on their temporal evolution during the fog life cycle, particularly to assess the validity and applicability of the theoretical profile used in Cermak and Bendix (2011).

The paper is structured as follows: Section 4.2 describes the balloon borne measurement system together with other ground based measurement devices and introduces the necessary data processing steps. In section 4.3 first measurement results are presented and compared to the theoretical profile.

4.2 Instrumentation and Data Processing

4.2.1 Instrumentation

Vertical profiles of fog characteristics were recorded at the Marburg ground truth and profiling station in Linden, Germany (50.533 °N, 8.685 °E, 172 m a.m.s.l). The site is located in a rural valley, surrounded by flat hills extending up to 250 m a.m.s.l. These topographic conditions cause a high frequency of fog events during spring and autumn months when weather situations with boundary-layer inversions frequently occur (Bendix, 2002; Schulze-Neuhoff, 1976). The measurements are based on a tethered balloon borne composition of meteorological and microphysical instruments, including a novel optical particle counter. Via controlled ascending and incremental descending meteorological and microphysical data profiles were recorded during the respective ground fog events with the following instrumentation (Table 4.1).

Drop size distributions (DSD) were measured using the Cloud Droplet Probe (CDP) developed and manufactured by Droplet Measurement Technologies, Inc., Boulder, CO, USA. The instrument uses a 658 nm laser to illuminate particles in a specific volume of air and measures their size by capturing the intensity of the scattered light. Using this technique it was possible to detect drops at 30 intervals within the size range of 2 µm to 50 µm at a sampling frequency of 1 Hz (DMT, 2009). To analyze the vertical fog structure, liquid water content (LWC), droplet number concentration (N_t) and effective particle radius (r_{eff}) were calculated from the recorded DSD at each measurement height.

Temperature, pressure and relative humidity as well as the altitude of the instruments were measured with the wireless Smart Tether system distributed by Anasphere Inc., Bozeman, Montana, USA (Anasphere, 2012).

Besides the tethered balloon observations, several instruments at ground level support the study. For the distinction between fog and non-fog phases, visibility data was obtained with the HSS VPF-730 Visibility and present weather sensor developed at the Bristol Industrial and Research Associates Limited Company, England. It uses forward scatter meter technology to determine the extinction coefficient (EXCO) of a specific volume of air and calculates the meteorological optical range (MOR) on the basis of the measured data, thus providing visibility-data. The instrument is installed 2 m above ground and measures horizontal visibility every 20 s (Biral, 2012).

Additional profile information about fog depth and density could be acquired using a Frequency Modulated Continuous Wave cloud radar profiler (FMCW radar) which has been developed by the STFC Rutherford Appleton Laboratory, Great Britain (Huggard et al., 2008). The system operates at a frequency of 94 GHz which makes it highly sensitive to cloud and fog droplets while the signal's attenuation in the relevant atmospheric range is relatively low. The temporal resolution of the device was set to 10 s with a vertical resolution of 3.9m and a total range of 2.0 km. The complete instrumentation is listed in Table 4.1.

TABLE 4.1. Instrumentation. DMT: Droplet Measurement Technologies; RAL: Rutherford Appleton Laboratories; BIRAL: Bristol Industrial and Research Associates Limited Company

Instrument	Parameter	Unit	Interval	Manufacturer
Cloud Droplet Probe (CDP)	Drop Size Distribution (DSD)	[$\mu m^{-1}/cm^{-3}$]	1 s	DMT, USA
Smart Tether	• Temperature • Pressure • Rel. Humidity • Altitude	[°C] [mbar] [%] [m]	1 s	Anasphere, USA
94 GHz FMCW radar	Fog top height	[m]	10 s	RAL, GB
VPF 730	Horizontal visibility at 2 m altitude (VIS)	[km]	20 s	BIRAL, GB

4.2.2 Data Processing

In a first preprocessing step, all parameters were averaged over 1 minute intervals in order to get a consistent temporal resolution throughout the whole dataset.

As mentioned above, the microphysical parameters LWC, N_t and r_{eff} were calculated from the measured DSD. This was realized by applying the modified gamma distribution (MGD) as a probability density function (PDF) to the raw data. In this way the expected total spectrum was accounted for during the derivation of the fog microphysics. The MGD is given by Deirmendjian (1969) as

$$f(r) = ar^{\alpha}\exp(-br^{\gamma}) \tag{1}$$

where a, b and γ are positive real numbers and α is a positive integer. a is called the normalization factor as it ensures that the integral of the MGD over all radii equals the total drop count. The shape of the MGD is determined by b and α which are the slope and shape parameter respectively. It has two zeros, one at $r = 0$ and one at $r = \infty$. The MGD has been fitted to the DSD of each measurement using a least squares method implemented by Garbow et al. (1980) following the Levenberg-Marquardt algorithm. By this means the MGD parameters a, α, b and γ were derived.

According to Gradshteyn and Ryzhik (2007) the moments of the MGD can be written as

$$m_i = \frac{a}{\gamma} b^{-\frac{(\alpha+1+i)}{\gamma}} \Gamma\left(\frac{\alpha+1+i}{\gamma}\right) \tag{2}$$

with the gamma function

$$\Gamma(x) = \int_0^{\infty} t^{x-1} \exp(-t)\, dt \tag{3}$$

The 1st moment of the DSD gives total drop count N_t [cm^{-3}] while effective radius r_{eff} [µm] can be derived via the 2nd and 3rd moment (Danne, 1996; Maier et al., 2011):

$$N_t = \frac{a}{\gamma} b^{-\left(\frac{\alpha+1}{\gamma}\right)} \Gamma\left(\frac{\alpha+1}{\gamma}\right) \tag{4}$$

and

$$r_{eff} = \frac{b^{-\left(\frac{\alpha+4}{\gamma}\right)}\Gamma\left(\frac{\alpha+4}{\gamma}\right)}{b^{-\left(\frac{\alpha+3}{\gamma}\right)}\Gamma\left(\frac{\alpha+3}{\gamma}\right)} \quad (5)$$

Assuming a spherical drop shape and only liquid water within the fog layer, LWC [g m^{-3}] values can be calculated using the third moment of the DSD (Maier et al., 2011):

$$LWC = \frac{4}{3}\pi\varrho_{H_2O}\frac{a}{\gamma}b^{-\left(\frac{\alpha+4}{\gamma}\right)}\Gamma\left(\frac{\alpha+4}{\gamma}\right) \times 10^{-6} \quad (6)$$

where ρ_{H_2O} is the approximate water density of 1 g cm^{-3} at the expected temperatures.

To determine the fog top altitude for the balloon borne measurements (section 4.3.3), VIS values were calculated from the DSD data using the following formula modified after DMT (2009) and Biral (2012):

$$VIS = 3(\pi \sum_{i=1}^{n} Qc_i r_i^2)^{-1} \quad (7)$$

with n being the count of radius intervals. Q is the extinction efficiency after van de Hulst (1957), c_i is the number concentration of hydrometeors in size category i and r_i is the average radius of size category i.

To account for the fog's evolutionary stages during the analysis of the profile records, 2 m VIS data of the different fog events were separated into different development phases using the breakpoint analysis proposed by Maier et al. (2013). Fog start and end date were defined as the first/last point in time when VIS decreased below 1 km.

To assess the validity of the theoretical LWC in comparison with the measured LWC profiles, the LWC and temperature values measured at ground level as well as the fog top height derived from the calculated VIS were used to compute the theoretical LWC profiles following the method described by Cermak and Bendix (2011).

4.3 Results and Discussion

In the following subsections, measurement results for two fog events are presented and compared to the theoretical profile. First, the vertical fog structure derived during the fog event on October 28/29 2011 (three profiles) is described. This will be followed by the presentation of the results obtained during the fog event on November 19/20 2012 (six profiles). All times are specified in UTC.

4.3.1 Observations on October 28/29, 2011

As presented in DWD (2013b), the synoptic weather regime in Europe during October 28/29, 2011 was characterized by a zonal ridge across Central Europe, following the classification of Hess and Brezowsky (1977), translated by James (2006). Troughs from a depression over the North Atlantic were not reaching over Central Europe and the weather in Linden was mainly influenced by a strong high pressure system over Eastern Europe (see Fig. 4.1). As a consequence, clouds were absent and wind conditions remained calm at the study site during the whole measurement period.

A relatively thin and short-lived fog layer formed on October 28, 2011 at 23:23. It lasted 6 h 28 min with its top not exceeding 100m altitude. Sunrise was at 06:11. The fog dissipated shortly before, at 05:50.

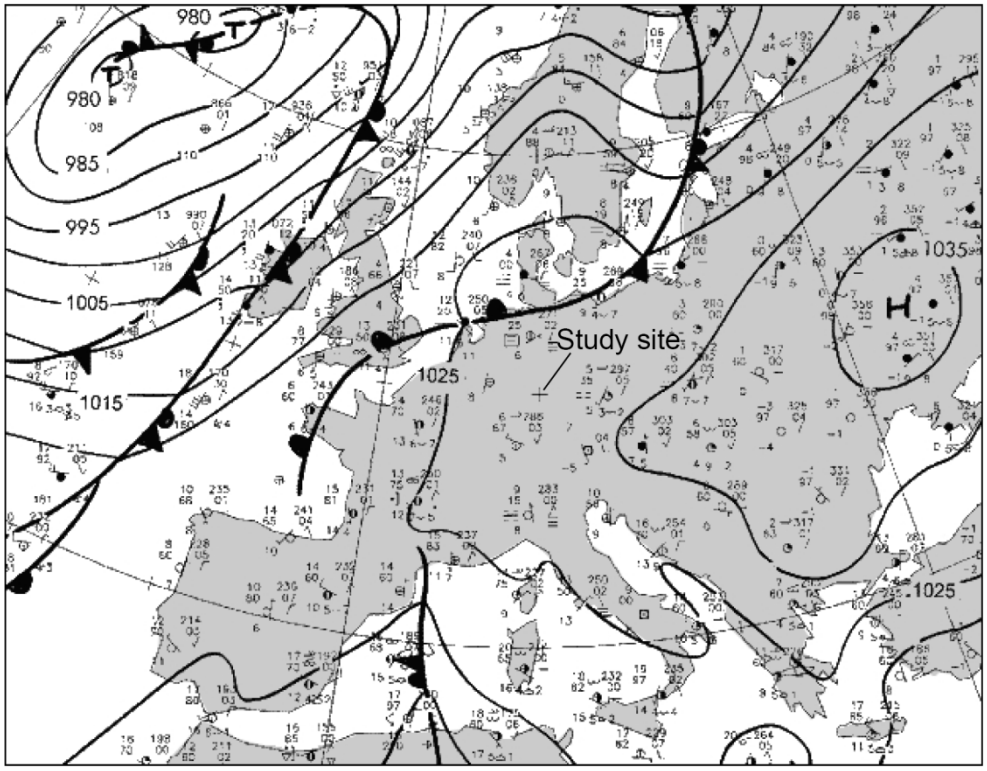

FIGURE 4.1: Synoptic weather situation in Central Europe for October 29, 2011: 00:00 UTC. Modified after DWD (2013a).

Figure 4.2 gives an overview of the boundary layer conditions at Linden during October 28/29, 2011. Following the terminology used in Maier et al. (2013), the first black vertical line marks the transition from formation to mature phase while the second line denotes the transition from mature phase to dissipation. While profile 1a was recorded at the end of the mature phase, dissipation has already started during the measurements of profile 1b and 1c.

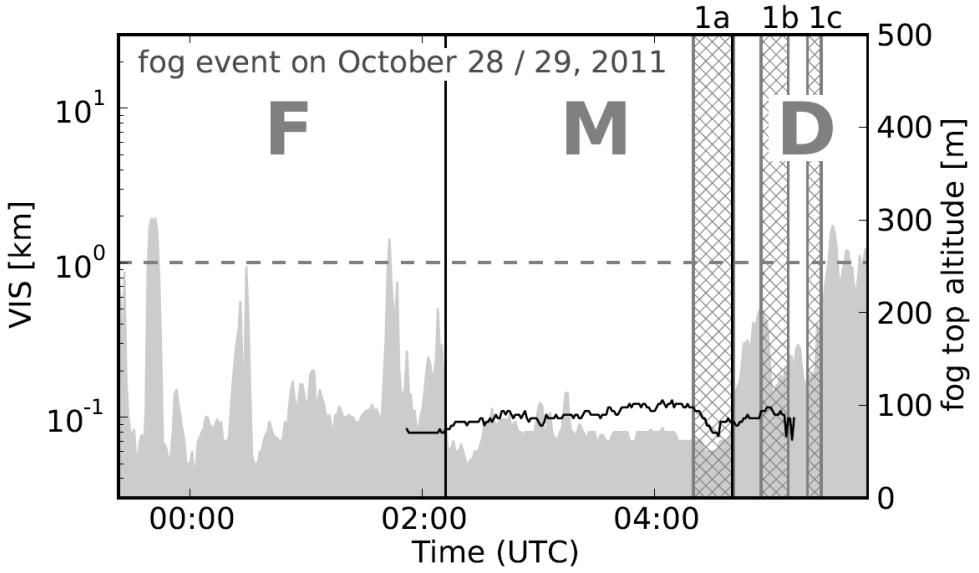

FIGURE 4.2. VIS (grey area) & radar derived fog top altitude (black line) between 23:23 October 28, 2011 and 05:50 October 29, 2011. Hatched stripes mark periods of profile measurements and are labelled corresponding to the following profile plots. Measurement periods were 04:16-04:37 for 1a, 04:41-05:05 for 1b and 05:15-05:22 for 1c. Black vertical lines mark phase transitions. The horizontal grey dashed line represents 1 km VIS. F: Formation, M: Mature fog, D: Dissipation.

The meteorological data along the fog vertical profiles presented in Fig. 4.3 give first insights into the conditions of the lower atmosphere during this event. Temperature distributions indicate the existence of a strong groundtouching inversion layer up to approx. 110 m for profile 1a. In profile 1b the inversion has already been lifted from the ground and ranged from 50 m to 125 m altitude. Above the inversion layer, both profiles showed constant temperature values with averages of 7.7 °C in 1a and 8.3 °C in 1b. Until the recording of profile 1c, temperature values have further increased, only the uppermost part (above 150 m) showing a slight decrease. Isother-

mal conditions were thus only prevalent closely above the inversion layer at this point in time. The general temperature increase between the profile measurements can be ascribed to the increasing long-wave downward radiation reflected at the fog layer, especially during the mature stage when the fog layer was densest.

The RH profiles showed a steep decline towards higher altitudes within the inversion layer which can be attributed to the temperature rise at these heights. Above and below the inversion layer, the profiles showed comparably constant values with an exception in profile 1a where up to 60 m altitude RH gradually declined with height. A general increase of RH could be identified between profile 1a and 1b, likely resulting from an intensified evaporation of fog droplets due to the onset of the dissipation phase between both profile measurements. Profile 1c shows, that RH values generally declined afterwards which can be attributed to the contemporaneous temperature rise.

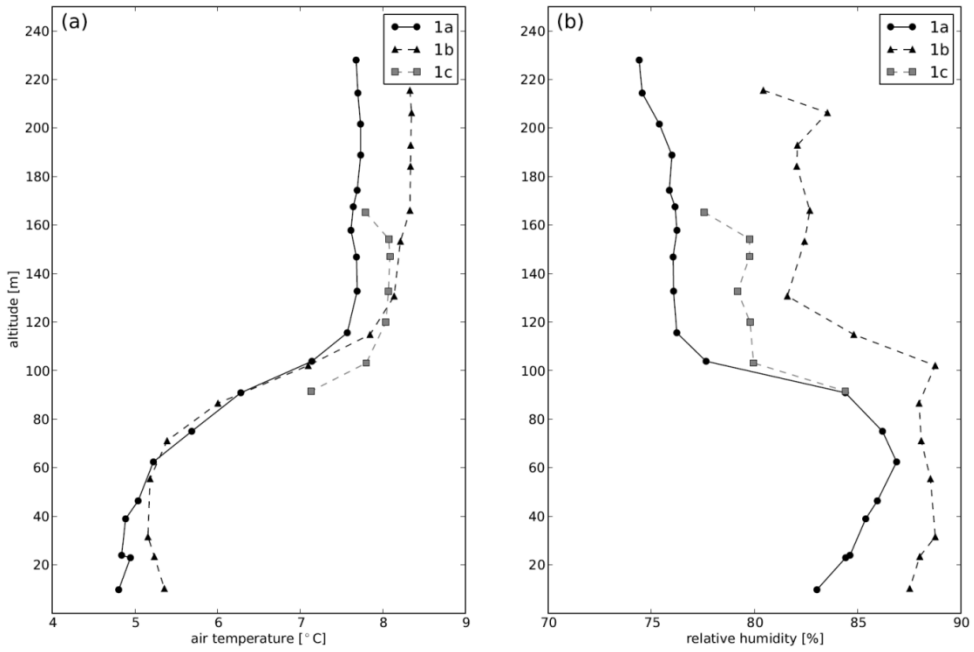

FIGURE 4.3. Profiles of meteorological parameters of October 29, 2011: (a) air temperature, (b) relative humidity.

The corresponding LWC values are depicted in Fig. 4.4a. Most values stayed below 0.1 g m^{-3} which underlines the weakness of this fog event when compared to records of LWC in radiation fogs from other authors (Choularton et al., 2007; Okita, 1962; Pinnick et al., 1978; Wobrock et al., 1992) with values reaching up to 1.0 g m^{-3}. Apart from that, there was no

general conformity between the different profile measurements of this study. Values in Profile 1a rose towards higher altitudes and reached their maximum of 0.14 g m^{-3} at approx. 100 m height with small r_{eff} but high N_t values. Above, LWC values never exceeded 0.01 g m^{-3}. This obviously can be attributed to the fact that the fog's top was exceeded for this part of the profile. Profile 1b reached its maximum of 0.08 g m^{-3} already at 32 m and, contrary to 1a, showed less oscillating values within the fog layer. Towards higher altitudes the values then slowly declined. In profile 1c LWC was reduced close to zero at all altitudes.

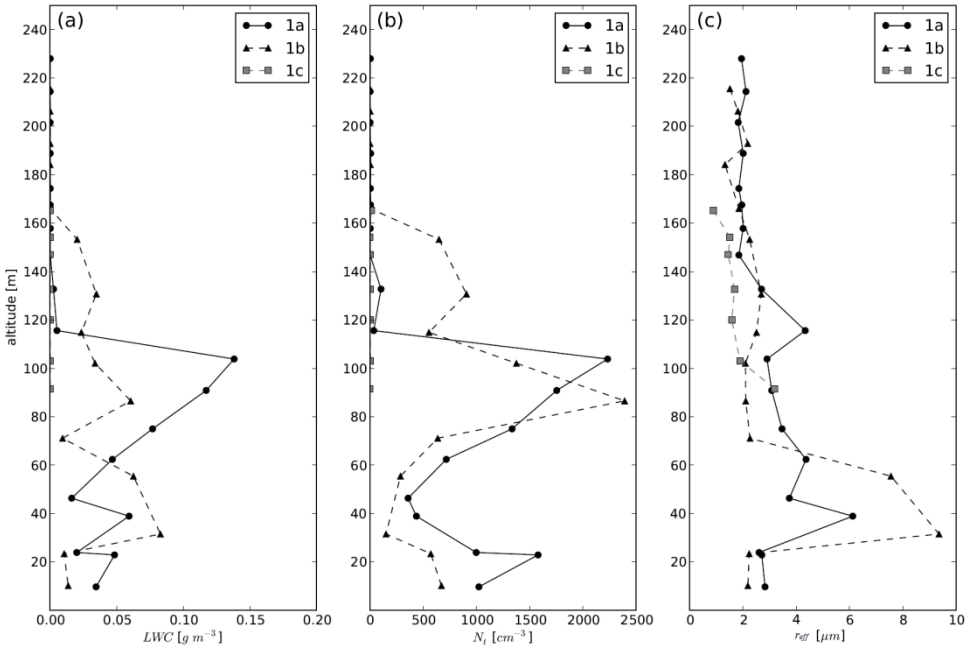

FIGURE 4.4. Profiles of microphysical parameters of October 29, 2011: (a) LWC, (b) N_t, (c) r_{eff}.

The N_t and r_{eff} profiles of Figs. 4.4b and 4.4c give further explanations for the shapes of the LWC profiles. N_t values of profiles 1a and 1b showed similar distributions with maxima of 2231 cm^{-3} and 2390 cm^{-3} close to the fog top and second maxima near the ground. r_{eff} values generally rose towards the ground but declined to approx. 2 µm at the very bottom of the profiles. Profile 1b showed a distinct rise in r_{eff} between 25 m and 70 m up to 9.4 µm. While the LWC values of profile 1a were thus mainly driven by total drop counts, in profile 1b the change in drop radii played an equipollent role in the vertical distribution of the DSD, resulting in high LWC values between 20 m and 60 m. In profile 1c drop counts remained close to zero at all measurement heights.

The main condensation layer of profile 1a can be located around 100 m height where high drop counts and small drop radii resulted in large LWC values. Above, RH values indicated a saturation deficit and consequently a rapid decrease of LWC and N_t. Towards the central fog levels, condensation and coalescence of larger particles gained in importance, manifesting themselves in growing r_{eff} and shrinking N_t values. Concurrent value increases of temperature and RH in the lowermost part of profile 1a (up to 60 m) may be ascribed to an increased evaporation of small droplets in these heights caused by the temperature increase. This is reflected in a peak of r_{eff} and a collapse of N_t values at the respective altitudes.

The microphysical parameters of profile 1b indicate a clear vertical development of the fog layer. Above the lower parts (> 30 m), clearly increasing LWC and r_{eff} values, as well as decreasing N_t values, point to distinctly stronger droplet growth by coalescence than in the central part of profile 1a. This increase coincided with a change in the temperature profile (see Fig. 4.3) from a temperature decrease with height in the lowermost levels towards an isothermal stratification developing into a temperature inversion. Highest fog density is therefore related to the formed inversion base in 1b (uplifted inversion base at 50 m) which typically indicates a shift of the outgoing infra-red radiation maximum at ground level during the measurement of profile 1a (concomitant with a true ground inversion) towards the fog top with maximum cooling and condensation (1b). Above 50 m, temperature increased while r_{eff} and LWC decreased. Although r_{eff} values did not exceed 2.7 µm for the rest of the profile, LWC values only marginally decreased due to significantly higher drop counts towards the inversion base and another peak of N_t above the inversion layer. The slow LWC decline indicates a far-reaching intrusion of the overlying warm air masses into the upper parts of the fog layer which itself induced slow fog dissipation from top to bottom. In profile 1c the dissipation process has already led to N_t and LWC values close to zero at all altitudes.

In summary, the profiles showed considerable changes in their vertical microphysical structure caused by the onset of dissipation. While the LWC values of profile 1a increased with altitude, profile 1b showed an inverted situation with decreasing LWC values towards the fog top, most likely resulting from evaporation and drop settling processes at this stage. In profile 1c the fog's dissipation has already advanced to a complete disappearance of the fog manifesting itself in LWC and N_t values close to zero at all measured altitudes.

4.3.2 Observations on November 19/20, 2012

On November 19, 2012 the synoptic weather regime over central Europe is described as anticyclonic south-westerly with a well formed high pressure system over Eastern Europe (DWD, 2013b). As a consequence, shortwave troughs approaching from the Atlantic were slowed down over Western Europe and pushed into North-East direction towards Scandinavia. The weather at Linden was thus dominated by the strong high over Eastern Europe throughout the complete measurement period, thus providing adequate preconditions for fog formation (see Fig. 4.5).

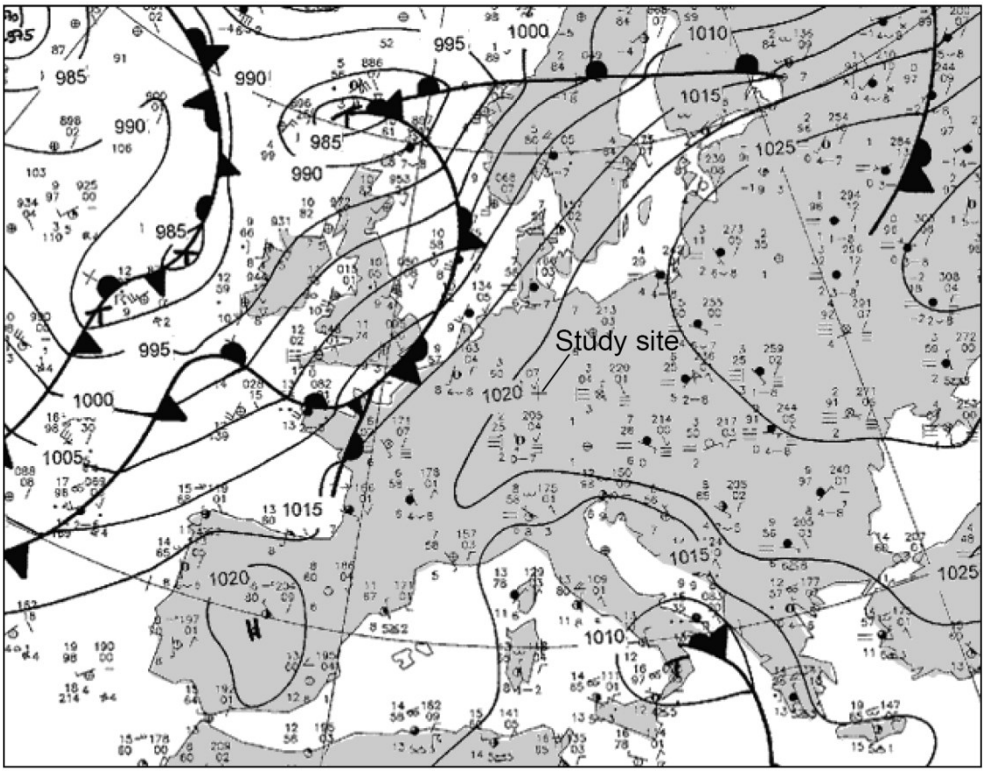

FIGURE 4.5. Synoptic weather situation in Central Europe for November 20, 2012: 00:00 UTC. Modified after DWD (2013a).

At 16:21 a dense and long lasting ground fog formed. Its thickness steadily rose to approx. 200 m until 05:15 on the next morning when it rapidly started increasing in height up to 500 m. After 15 h 53 min it finally lifted from the ground at 08:13 to form an LS layer shortly after sunrise (06:49). During the long lasting mature phase (20:27 - 06:23) VIS never exceeded 1 km. For a detailed overview of VIS, fog top altitude and measurement periods see Fig. 4.6.

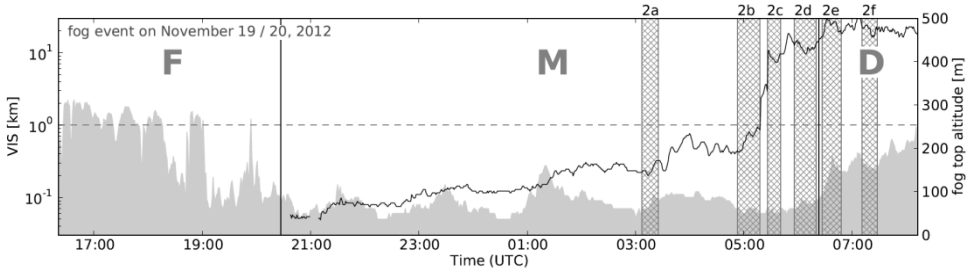

FIGURE 4.6. VIS (grey area) & radar derived fog top altitude (black line) between 16:21 November 19, 2012 and 08:13 November 20, 2012. Hatched stripes mark periods of profile measurements and are labelled corresponding to the following profile plots. Measurement periods were 03:03-03:21 for 2a, 04:49-05:14 for 2b, 05:22-05:37 for 2c, 05:52-06:16 for 2d, 06:23-06:44 for 2e and 07:07-07:24 for 2f. Black vertical lines mark phase transitions. The horizontal grey dashed line represents 1 km VIS. F: Formation, M: Mature fog, D: Dissipation.

In total, six vertical profiles were recorded - four at the end of the mature phase and two during dissipation. Temperature values of each profile are depicted in Fig. 4.7a. The profiles are depicted in chronological order, illustrating the general shift towards warmer temperatures during the measurement period. Profile 2a showed a pronounced inversion above 120 m but temperatures slowly started to rise already at 60 m. In profile 2b the inversion layer has been lifted up to altitudes above 140 m with a strong temperature increase starting at 180 m. Below the inversion layer, temperatures decreased with height in 2a and 2b. Profiles 2c to 2f were mainly isothermal and did not show a comparable temperature decrease/increase which can be attributed to a rapid lifting of the inversion layer after 05:15. Mature phase conditions were thus mainly affected by a general temperature decline with minima just below the inversion layer. This is caused by the fog top acting as main emitter of long-wave thermal radiation while the lower fog layers reflect thermal radiation emitted from the surface, consequently feeding the lower parts with additional heat. Fog dissipation, on the other hand, was characterized by isothermal conditions at lower levels. Here, longwave downward radiation started to cease due to thinning of the fog layer, resulting in less heat adduction close to the surface.

The relative humidity profiles give further insight to the properties of the studied fog event (see Fig. 4.7b). Most of the profiles varied between 96% and 98% in all altitudes with no substantial outliers. Only profile 2a and 2b showed distinct shifts in the values of the uppermost part. Due to the beginning temperature increase at 60 m in 2a and 140 m in 2b, RH values began to decline, reaching their minima of 91.7% and 94.5% at 120 m and

170 m respectively. These heights coincided with rapid temperature increases in both profiles, marking the lower boundary of the inversion layer. Above, RH values rapidly increased towards the profile tops, reaching maxima of 100% and 97.1 %. These increases can directly be ascribed to the beginning evaporation processes of fog droplets in these altitudes as will be affirmed by the microphysical parameter distributions. Profiles 2c to 2f did not show comparable temperature and RH shifts as they did not reach up to the inversion at the top of the fog layer.

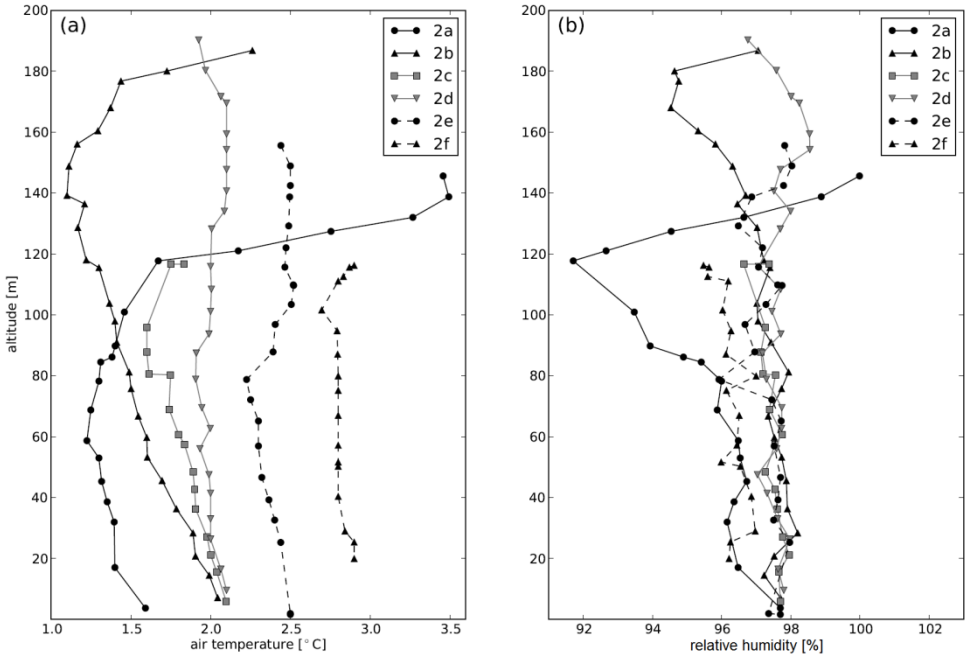

FIGURE 4.7. Profiles of meteorological parameters of November 20, 2012: (a) air temperature, (b) relative humidity.

Microphysical parameters (LWC, N_t and r_{eff}) of the profiles recorded during mature fog are presented in Fig. 4.8. The profiles recorded during dissipation are depicted in Figure 4.9. Compared to the fog event investigated on October 28/29, 2011 the data indicated a significantly denser fog with higher LWC and r_{eff} values but smaller total drop counts.

All LWC profiles showed some minor common characteristics but the absolute values differed considerably. In profile 2a LWC values stayed below 0.06 g m^{-3} up to 50 m height but changed their average level to 0.1 g m^{-3} between 50 m and 120 m altitude. Above 120 m and close to the fog top, the CDP measured rapidly decreasing LWC values. Profile 2b showed considerably larger LWC values throughout the whole measurement but otherwise comparable characteristics. The lower part of the profile had values fluctuating around 0.2 g m^{-3}, a maximum of 0.44 g m^{-3} at 130 m and

constantly decreasing values towards the fog top. These value distributions are in good agreement with the meteorological profiles: Maximum LWC values were reached at minimal temperatures and the decline of LWC values with intrusion into the inversion layer is reflected in growing RH values due to progressive evaporation of fog droplets at these heights.

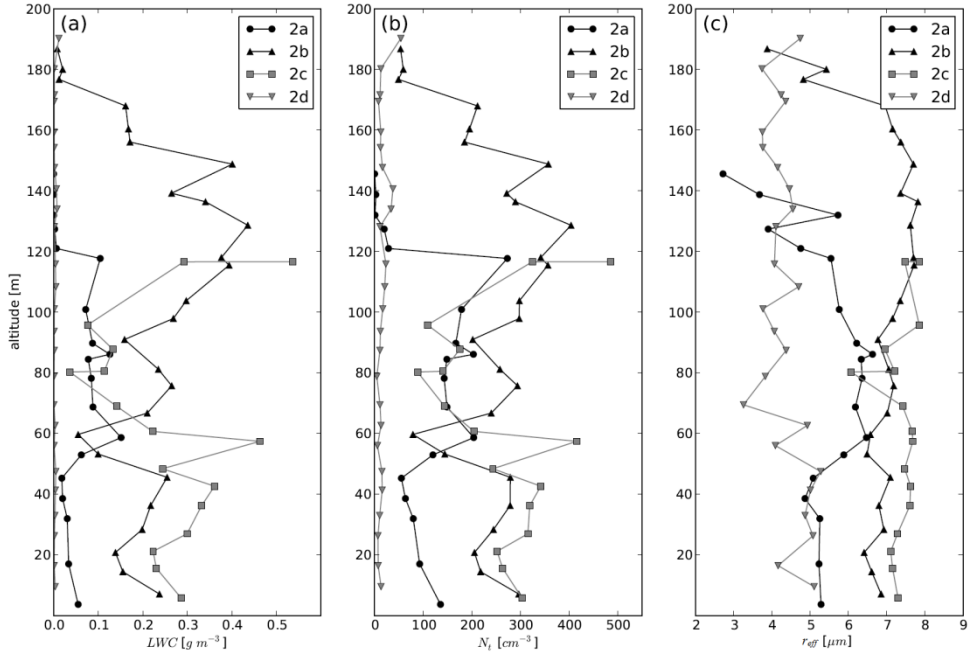

FIGURE 4.8. Profiles of microphysical parameters of November 20, 2012 (Mature fog): (a) LWC, (b) N_t, (c) r_{eff}.

In profile 2c the curve below 50 m was similarly shaped to 2b with slightly higher LWC values. Above 50 m the values suddenly declined and reached a minimum of 0.04 g m^{-3} at 80 m whereas the maximum of this profile was already reached at 116 m with 0.54 g m^{-3}. It is, however, important to consider that the maximum height during this measurement was also reached at 116 m and thus the profile did not represent the whole fog column as its vertical extent exceeded 400 m at this time (see Fig. 4.6). Apart from the strong decrease of LWC between 60 m and 100 m, profile 2c may also have shown similar characteristics to 2a and 2b but due to the missing upper part of the profile it was not possible to derive information for the whole fog column. Surprisingly, in profile 2d LWC values stayed below 0.01 g m^{-3} throughout all altitudes although it was recorded during the mature phase. A possible reason for the strong decline in values may be the rapid increase of the fog's vertical extent shortly before, resulting in a smaller density of condensed particles per volume of air. However, a final explanation for this phenomenon could not be determined yet. Profile 2e

and 2f showed similar characteristics to 2a although the total fog depth recorded by the radar was considerably higher and thus the profiles did only represent the lower third of the respective fog column.

N_t values (see Fig. 4.8b) lay clearly below the values of the October fog event. The shapes of most profiles closely resembled the shapes of the corresponding LWC profiles. Maxima of profiles 2a and 2b were measured towards the fog top with 203 and 404 drops per cm^3 and a decline towards higher altitudes. Profile 2c showed highest drop counts with more than 500 drops per cm^3 whereas profile 2d was characterized by values close to zero throughout all altitudes. Profiles 2e and 2f (see Fig. 4.9b) showed values comparable to the other profiles for heights above 50 m but considerably smaller values close to the ground. This indicates the emerging uplift of the fog layer from the surface during the measurement of these profiles as a consequence of the onset of dissipation at that time.

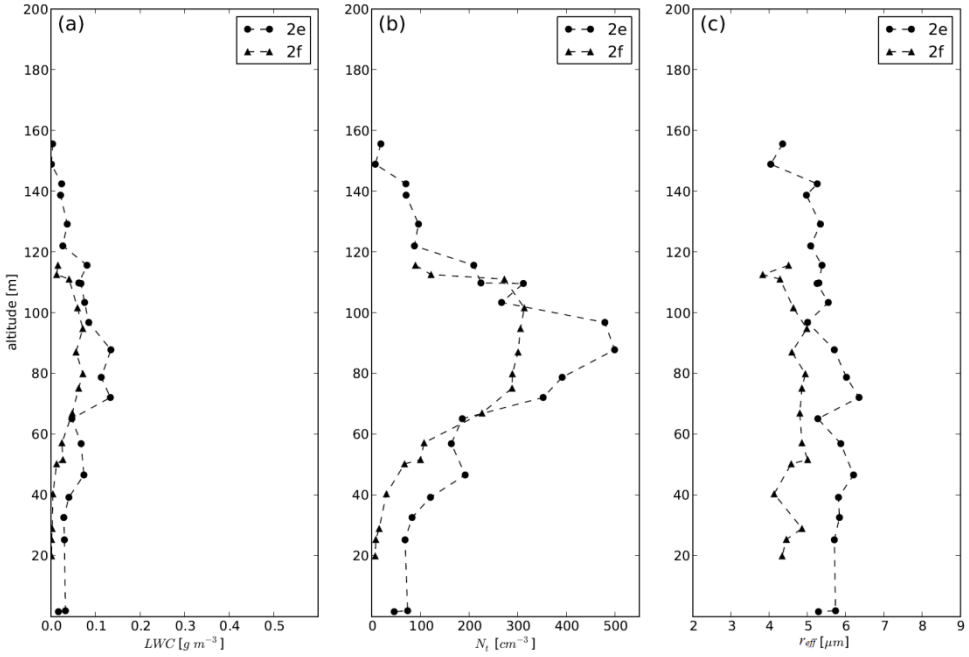

FIGURE 4.9. Profiles of microphysical parameters of November 20, 2012 (Dissipation): (a) LWC, (b) N_t, (c) r_{eff}.

All recorded r_{eff} profiles were characterized by very little vertical variability but considerable shifts between the different profiles. For profiles 2c to 2f no vertical trends could be identified. Only profile 2a and 2b showed a slight increase in the central region and a distinctive decrease towards the respective profile tops. In conjunction with decreasing N_t values, shrinking drop sizes were thus jointly responsible for the diminishing LWC

values at the fog top. Due to rising temperatures within the inversion layer, the fog top layer during mature stage was characterized by strong evaporation processes affecting both, small and large drops (decrease of N_t due to dissipation of small drops and decrease of r_{eff} due to beginning evaporation of large drops).

In summary, all presented parameters showed changes in the microphysical characteristics within small temporal and vertical intervals. The shapes of the recorded N_t profiles closely matched the curves of the respective LWC profiles whereas r_{eff} values did not show noticeable similarities except for profile 2a and 2b. Vertical changes in LWC within one profile could thus mainly be ascribed to changes in the distribution of total drop counts and not to changes in their size. On the other hand, the apparent differences of r_{eff} values between the profiles led to the conclusion that drop growth and shrinking were responsible for long term temporal changes in LWC over the whole fog column. However, phase-dependent profile characteristics were hard to detect in this fog event as they were superimposed by the short term changes that manifested themselves primarily in shifts of r_{eff} values throughout the whole fog column.

4.3.3 Comparison between theoretical profiles and measurements

To investigate the validity of the theoretical assumptions about the vertical LWC distribution made by Cermak and Bendix (2011), suitable profiles, covering the whole fog column, were compared to their theoretical equivalent. Fog top altitude information was derived for each profile by deriving VIS values from measured drop size distributions via Eq. 7.

Figure 4.10 depicts the investigated profiles together with their theoretical equivalents. Profile 1a (mature phase) showed broad agreement between LWC measurements and theoretical expectations, leading to a mean absolute error (MAE) of 0.024 g m^{-3} and a difference of 21.2% in the derived liquid water paths (LWP, defined as the integrated LWC over the whole fog column in g m^{-2}). Apart from some minor deviations in the central part, shape and maximum of the theoretical profile were closely resembled by the CDP records. However, the distribution of N_t and r_{eff} values (see Figs. 4.4b and 4.4c) showed, that increases in LWC values could mainly be ascribed to increases of drop counts and not to particle growth.

In contrary, the measurements of profile 1b (dissipation phase) did not match the theoretical distribution (Fig. 4.10b). The LWC profile rather showed an inverted shape with slowly decreasing values towards the fog top and a fast increase at the bottom. This led to LWC values that persisted at lower values compared to the theoretical profile, especially at higher altitudes. An MAE of 0.055 g m^{-3} and an LWP difference of 57.3% supported this perception. While N_t values followed a similar distribution compared to those of profile 1a, r_{eff} values were generally smaller except for the range

between 25 m and 70 m where they were higher, causing the reported increase of LWC values at the bottom of the fog. A possible explanation for the difference between theoretical and measured profile can be found in the onset of the dissipation phase shortly before the measurement of this profile. The Smart Tether data support the assumption, that mixing and subsequent evaporation processes from above have already set in at this point. These processes may then have led to the slowly sinking LWC values towards the fog top and high values at the bottom due to settling of the remaining larger drops.

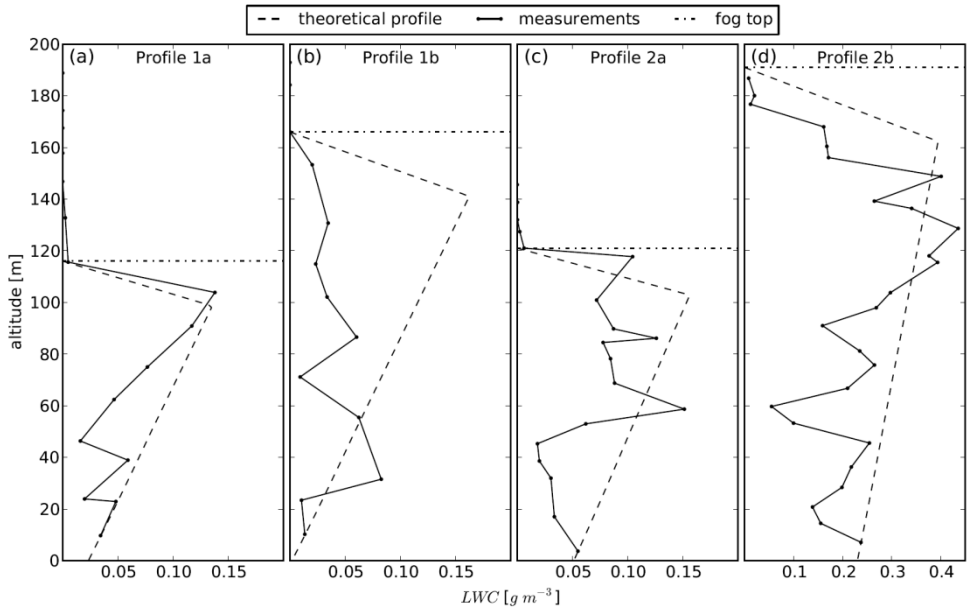

FIGURE 4.10. Comparison between measured and theoretical LWC profiles: (a) and (b) show profiles 1a and 1b of October 29, 2011; (c) and (d) show profiles 2a and 2b of November 20, 2012. Profiles 1a, 2a and 2b were recorded during the mature phase whereas profile 1b was recorded during dissipation. Fog top altitudes are indicated by the thin dashed horizontal line. All profiles are depicted together with their theoretical equivalent.

In profile 2a (Fig. 4.10c) (mature phase) LWC measurements followed the theoretical expectations with increasing values towards higher altitudes. Apart from the similar trend, there was a distinct vertical variance in the data leading to differences between measured and theoretical profile. This resulted in an MAE of 0.042 g m^{-3} and an LWP difference of 32.8 %. While r_{eff} values in profile 1a and 1b played a minor role in profile-internal LWC changes, here drop size changes apparently contributed to the shape of the LWC profile. In short, r_{eff} rose slowly with height and fell rapidly at the

fog top. Together with similarly shaped N_t distributions this resulted in the described LWC profile.

Profile 2b (Fig. 4.10d) (mature phase) showed the highest LWC values during this case study. With an MAE of 0.086 g m^{-3} it also showed the highest absolute difference to its theoretical counterpart. However, the relative LWP difference was only at 25.6% which is the second best value of the four investigated profiles. Again, the measured LWC values showed high variance but generally followed the theoretical distribution. Similarly to profile 2a, drop size changes influenced the LWC distribution to some extent. However, the LWC profile was basically governed by the shape of the corresponding N_t profile.

Referring to the theoretical LWC model of Cermak and Bendix (2011), a good agreement in trend and gradient between measured and theoretical LWC profiles was found for the profiles measured during the mature stage. For the LWC profile measured during the dissipation stage less accordance with the theoretical profile had to be stated. Summarized LWP properties, given in Table 4.2, also point to the conjecture that minimal accordance between theoretical and measured profiles can be found for profiles with minimal LWP values (see profile 1b with 5.829 g m^{-2} and a LWP of 57.3 %). In most profiles, LWC did slowly increase with height and none of the profiles showed a lapse rate higher than the sub-adiabatic postulation. Rapid decreases of LWC values close to the fog top were also found in most of the records. However, profile-internal changes of LWC were mainly governed by changes in N_t whereas r_{eff} was relatively constant at all altitudes. This indicates, that the increase of drop counts due to condensation at remaining nuclei had a greater influence on the fog's density formation than drop growth by coalescence processes. The expected increase in drop size towards greater altitudes as well as constant drop counts in the central fog layer as presented in Brenguier et al. (2000) and Chang and Li (2002) for low stratiform clouds could thus not be affirmed for the observed radiation fog events. Concerning the anticipated shift from adiabatic to sub-adiabatic conditions close to the ground (Cermak and Bendix, 2011), it was not possible to come to a meaningful conclusion.

A comparison with the measurements from the literature showed that both, Okita (1962) and Pinnick et al. (1978), found generally larger LWC values, than one would have expected based on the postulated sub-adiabatic lapse rate (see Table 4.2). On average, the records of Okita (1962) resulted in an MAE of 0.091 g m^{-3} and an LWP difference of -12.7 %. However, LWC distributions showed the same general trend and N_t majorly determined the shape of the LWC profile whereas mean volume radii showed only a slight negative slope towards higher altitudes. The measurements of Pinnick et al. (1978) showed less accordance with the theoretical profile leading to an MAE of 0.097 g m^{-3} and an LWP difference of -27.9%. For a given LWP this would result in an overestimation of the fog's geometrical

thickness. However, a direct comparison between the different data sets is difficult due to the different instrumentations used. All studies, however, are congruent in affirming the general rise of LWC values and none of the studies were able to reinforce the assumption of constant drop counts and growing drop sizes with altitude. On the contrary, r_{eff} was found to be relatively constant within one profile and N_t showed strong variation as well as growing numbers towards the fog top.

TABLE 4.2. Measured and theoretical LWP, mean absolute error (MAE) as well as absolute and relative LWP differences compared to the theoretical profile's LWP of 1a, 1b, 2a, 2b and averages from Okita (1962) and Pinnick et al. (1978)

Profile	LWP_{meas}	LWP_{theo}	MAE	abs. Δ_{LWP}	rel. Δ_{LWP}
1a	7.135	9.053	0.024	1.918	21.2%
1b	5.829	13.659	0.055	7.830	57.3%
2a	8.162	12.140	0.042	3.977	32.8%
2b	42.056	56.520	0.086	14.464	25.6%
Ø	15.796	22.843	0.052	7.047	34.2%
Okita	40.950	36.941	0.091	-3.757	-12.7%
Pinnick	56.038	34.633	0.097	-16.322	-27.9%

4.4 Conclusion

The aim of the present study was to verify the validity of a theoretical fog LWC profile and its applicability for satellite based ground fog detection with a special consideration of the temporal evolution during the fog life cycle. For this purpose LWC profiles were measured during two different fog events by means of a tethered balloon borne composition of meteorological and microphysical measurement instruments including an optical particle counter.

The measurements indicate a good agreement in trend and gradient between measured and theoretical LWC profiles for mature stage observations. The LWC profile measured during the dissipation stage shows less accordance with the theoretical LWC profile. Although the proposed vertical function of Cermak and Bendix (2011) was in general agreement with the LWC measurements during the mature phase, there were some discrepancies due to the vertical variance in the measured profiles. Especially during the onset of dissipation, microphysical conditions were subject to changes on small spatial and temporal scales.

Despite the small dataset it can be concluded that the theoretical considerations concerning the vertical distribution of microphysical fog features should be adapted. The fog evolutionary life cycle should be considered

when formulating and adapting the theoretical LWC profile used in satellite based ground fog detection methods. With respect to the poor accordance between measurement and theory in profiles with small LWP values, these methods could also be adapted by accounting for different theoretical LWC profiles that are assigned to different LWP ranges. LWP derivations from satellite data (e.g. Kawamoto et al. (2001)) could then be used as an adjustment in the vertical LWC function for the calculation of the fog's geometrical thickness. However, for a well-founded adaptation of the theoretical LWC profile under consideration of the fog's evolutionary stages and the observed LWP distributions, more LWC profiles during a great variety of fog events have to be measured.

Accordingly, there is a growing interest for an operational measurement method in addition to the balloon-borne system concerning a comprehensive data set of LWC profiles. Such a measurement method could be realized using the 94 GHz FMCW radar introduced in this study. This radar system is highly suitable for fog detection and monitoring (Bennett et al., 2009; Maier et al., 2013). The measurement system presented in this study can be used to develop a proper relationship between the radar reflectivity (Z) and the liquid water content that could be used to invert measured Z into LWC values.

Acknowledgements

The authors thank the German Research Foundation DFG for funding the project (BE1780/14-1; TH1531/1-1). The work is also part of the COST action EG Climet. The authors are also thankful to Sebastian Achilles for his support during the measurements.

4.5 References

Anasphere. 2012. *SmartTether Operating Manual*. 2 ed., Anasphere Inc., Bozeman, MT, USA, pp. 1-19.

Bendix, J.. 2002. *Working Group I, National Report Germany*. Technical Report. COST 722.

Bendix, J., Eugster, W., Klemm. O., 2011. Fog - boon or bane? *Erdkunde* **65**, 229–232. doi:10.3112/erdkunde.2011.03.01.

Bendix, J., Thies, B., Cermak, J., Nauß, T., 2005. Ground Fog Detection from Space Based on MODIS Daytime Data - A Feasibility Study. *Weather and Forecasting* **20**, 989–1005. doi:10.1175/WAF886.1.

Bendix, J., Thies, B., Nauß, T., Cermak, J. 2006. A feasibility study of daytime fog and low stratus detection with TERRA/AQUA-MODIS over land. *Meteorological Applications* **13**, 111. doi:10.1017/S1350482706002180.

Bennett, A., Gaffard, C., Oakley, T., Huggard, P., Moyna, B., Oldfield, M., Nash, J., Wrench, C. 2009. Observations from the UK Met Office 94 GHz FMCW cloud radar. In: *Proceedings of the 8th International Symposium on Tropospheric Profiling*, Delft. pp. 19–23.

Betts, A.K. 1982. Cloud Thermodynamic Models in Saturation Point Coordinates. *Journal of the Atmospheric Sciences* **39**, 2182–2191. doi:10.1175/1520-0469(1982)039<2182:CTMISP>2.0.CO;2.

Biral 2012. *HSS VPF -730 Combined Visibility & Present Weather Sensor*. Bristol Industrial and Research Associates Limited, Portishead, Bristol, UK.

Boers, R., Mitchell, R.M. 1994. Absorption feedback in stratocumulus clouds Influence on cloud top albedo. *Tellus A* **46**, 229–241. doi:10.1034/j.1600-0870.1994.00001.x.

Bott, A., Trautmann, T. 2002. PAFOG - a new efficient forecast model of radiation fog and low-level stratiform clouds. *Atmospheric Research* **64**, 191–203. doi:10.1016/S0169-8095(02)00091-1.

Brenguier, J.L., Pawlowska, H., Schüller, L., Preusker, R., Fischer, J., Fouquart, Y. 2000. Radiative Properties of Boundary Layer Clouds: Droplet Effective Radius versus Number Concentration. *Journal of the Atmospheric Sciences* **57**, 803–821.

Bruijnzeel, S., Eugster, W., Burkard, R. 2006. Fog as a Hydrologic Input. *Encyclopedia of Hydrological Sciences*, 1–24. doi:10.1002/0470848944.hsa041.

Cermak, J. 2006. *SOFOS - A new Satellite-based Operational Fog Observation Scheme.* Ph.D. thesis. Philipps-University of Marburg, Marburg, pp. 1-147.

Cermak, J., Bendix, J. 2007. Dynamical Nighttime Fog/Low Stratus Detection Based on Meteosat SEVIRI Data: A Feasibility Study. *Pure and Applied Geophysics* **164**, 1179–1192. doi:10.1007/s00024-007-0213-8.

Cermak, J., Bendix, J. 2011. Detecting ground fog from space – a microphysics-based approach. *International Journal of Remote Sensing* **32**, 3345–3371. doi:10.1080/01431161003747505.

Chang, F.l., Li, Z. 2002. Estimating the vertical variation of cloud droplet effective radius using multispectral near-infrared satellite measurements. *Journal of Geophysical Research* **107**, 4257. doi:10.1029/2001JD000766.

Choularton, T.W., Fullarton, G., Latham, J., Mill, C.S., Smith, M.H., Stromberg, I.M. 2007. A field study of radiation fog in meppen, West Germany. *Quarterly Journal of the Royal Meteorological Society* **107**, 381–394. doi:10.1002/qj.49710745209.

Danne, O. 1996. *Messungen physikalischer Eigenschaften stratiformer Bewölkung mit einem 94 GHz - Wolkenradar*. Ph.D. thesis. University of Hannover, Hannover, pp. 1-117.

Deirmendjian, D. 1969. *Electromagnetic Scattering on Spherical Polydispersions.* American Elsevier Publishing Company, New York, USA.

DMT 2009. *Data Analysis User's Guide Chapter I: Single Particle Light Scattering.* Droplet Measurement Technologies, Boulder, CO, USA.

DWD 2013a. Bodenanalysekarten Europa. Online at: URL: http://www.wetter3.de/Archiv/archiv_dwd.html. Last page view: 13/01/2014

DWD 2013b. Die Großwetterlagen Europas. Online at: URL: http://www.dwd.de/GWL. Last page view: 13/01/2014

Ellrod, G.P. 1995. Advances in the Detection and Analysis of Fog at Night Using GOES Multispectral Infrared Imagery. *Weather and Forecasting* **10**, 606–619. doi:10.1175/1520-0434(1995)010<0606:AITDAA>2.0.CO;2.

Eyre, J.R., Brownscombe, J.L., Allam, R.J. 1984. Detection of fog at night using Advanced Very High Resolution Radiometer (AVHRR) imagery. *Meteorological Magazine* **113**, 266–271.

Fuzzi, S., Fachini, M.C., Orsi, G., Lind, J.A., Wobrock, W., Kessel, M., Maser, R., Jaeschke, W., Enderle, K.H., Arends, B.G., Berner, A., Solly, I., Kruisz, C., Reischl, G., Pahl, S., Kaminski, U., Winkler, P., Ogren, J.A., Noone, K.J., Hallenberg, A., Fierlinger-Oberlinger, H., Puxbaum, H., Marzorati, A., Hansson, H.C., Wiedensohler, A., Svenningsson, I.B., Martinsson, B.G., Schell, D., Georgii, H.W. 1992. The Po Valley Fog Experiment 1989. *Tellus B* **44**, 448–468. doi:10.1034/j.1600-0889.1992.t01-4-00002.x.

Fuzzi, S., Laj, P., Ricci, L., Orsi, G., Heintzenberg, J., Wendisch, M., Yuskiewicz, B., Mertes, S., Orsini, D., Schwanz, M., Wiedensohler, A., Stratmann, F., Berg, O.H., Swietlicki, E., Frank, G., Martinsson, B.G., Günther, A., Dierssen, J.P., Schell, D., Jaeschke, W., Berner, A., Dusek, U., Galambos, Z., Kruisz, C., Mesfin, N.S., Wobrock, W., Arends, B., ten Brink, H. 1998. Overview of the Po valley fog experiment 1994 (CHEMDROP). *Contributions to Atmospheric Physics* **71**, 3–19.

Garbow, B.S., Hillstrom, K.E., More, J.J. 1980. MINPACK Subroutine LMDIF.

Glickman, T.S. 2000. *Glossary of Meteorology*. 2 ed., American Meteorological Society, Boston, pp. 1-855.

Gradshteyn, I.S., Ryzhik, I. 2007. *Table of Integrals, Series, and Products*. 7 ed., Academic Press, London, pp. 1-1248.

Gultepe, I., Müller, M.D., Boybeyi, Z. 2006. A New Visibility Parameterization for Warm-Fog Applications in Numerical Weather Prediction Models. *Journal of Applied Meteorology and Climatology* **45**, 1469–1480. doi:10.1175/JAM2423.1.

Gultepe, I., Tardif, R., Michaelides, S.C., Cermak, J., Bott, A., Bendix, J., Müller, M.D., Pagowski, M., Hansen, B., Ellrod, G., Jacobs, W., Toth, G., Cober, S.G. 2007. Fog Research: A Review of Past Achievements and Future Perspectives. *Pure and Applied Geophysics* **164**, 1121–1159. doi:10.1007/s00024-007-0211-x.

Hayasaka, T., Nakajima, T., Fujiyoshi, Y., Ishizaka, Y., Takeda, T., Tanaka, M. 1995. Geometrical Thickness, Liquid Water Content, and Radiative Properties of Stratocumulus Clouds over the Western North Pacific. *Journal of Applied Meteorology* **34**, 460–470. doi:10.1175/1520-0450-34.2.460.

Hess, P. and Brezowsky, H. 1977. Catalog of the general weather situations of Europe (1881-1976). *Reports of the German Weather Service* **113**, 1-54.

Huggard, P. G., Oldfield, M. L., Moyna, B. P., Ellison B. N., Matheson, D. N. and co-authors. 2008. 94 GHz FMCW cloud radar. In: *Proceedings of the SPIE symposium on millimetre wave and terahertz sensors and technology*, 15-18 September, Cardiff, pp. 1-6.

van de Hulst, H.C. 1957. *Light scattering by small particles*. Courier Dover Publications, Mineola N.Y, pp. 1-470.

Hutchison, K.D. 2002. The retrieval of cloud base heights from MODIS and three-dimensional cloud fields from NASA's EOS Aqua mission. *International Journal of Remote Sensing* **23**, 5249–5265. doi:10.1080/01431160110117391.

Iwabuchi, H., Hayasaka, T. 2002. Effects of Cloud Horizontal Inhomogeneity on the Optical Thickness Retrieved from Moderate-Resolution Satellite Data. *Journal of the Atmospheric Sciences* **59**, 2227–2242. doi:10.1175/1520-0469(2002)059<2227:EOCHIO>2.0.CO;2.

Jacobs, W., Nietosvaara, V., Bott, A. Bendix, J., Cermak, J., Michaelides, S., and Gultepe, I. (eds). 2008. *Short range forecasting methods of fog, visibility and low clouds*, COST Action 722 final report, Brussels, Office for official publications of the European Communities, pp. 1-489.

James, P. M. 2007. An objective classification method for Hess and Brezowsky Grosswetterlagen over Europe. *Theor. Appl. Climatol*. **88**, 17-42.

Kawamoto, K., Nakajima, T., Nakajima, T.Y. 2001. A Global Determination of Cloud Microphysics with AVHRR Remote Sensing. *Journal of Climate* **14**, 2054–2068.

Liu, D., Yang, J., Niu, S., Li, Z. 2011. On the evolution and structure of a radiation fog event in Nanjing. *Advances in Atmospheric Sciences* **28**, 223–237. doi:10.1007/s00376-010-0017-0.

Maier, F., Bendix, J., Thies, B. 2011. Simulating Z-LWC Relations in Natural Fogs with Radiative Transfer Calculations for Future Application to a Cloud Radar Profiler. *Pure and Applied Geophysics* **169**, 793–807. doi:10.1007/s00024-011-0332-0.

Maier, F., Bendix, J., Thies, B., 2013. Development and application of a method for the objective differentiation of fog life cycle phases. *Tellus B* **65**, 1–17. doi:10.3402/tellusb.v65i0.19971.

Minnis, P., Young, D.F., Kratz, D.P., Coakley, J.A., King, M.D., Garber, D.P., Heck, P.W., Mayor, S., Arduini, R.F. 1997. Cloud optical property retrieval (subsystem 4.3). Clouds and the Earth's Radiant Energy System (CERES) *Algorithm Theoretical Basis Document*, pp. 1–60.

Nemery, B., Hoet, P.H., Nemmar, A. 2001. The Meuse Valley fog of 1930: an air pollution disaster. *Lancet* **357**, 704–708. doi:10.1016/S0140-6736(00)04135-0.

Okita, T. 1962. Observations of the vertical structure of a stratus cloud and radiation fogs in relation to the mechanism of drizzle formation. *Tellus* **14**, 310–322. doi:10.1111/j.2153-3490.1962.tb01342.x.

Pagowski, M., Gultepe, I., King, P. 2004. Analysis and Modeling of an Extremely Dense Fog Event in Southern Ontario. J*ournal of Applied Meteorology* **43**, 3–16.

Pilié, R., Eddie, W., Mack, E., Rogers, C., Kocmond, W. 1972. PROJECT FOG DROPS Part I: Investigations of Warm Fog Properties. Technical Report August. Cornell Aeronautical Laboratory, Inc.. Buffalo, N.Y.

Pilié, R. J., Mack, E. J., Kocmond, W. C., Rogers, C. W., and Eadie, W.J. 1975a. The life-cycle of valley fog. 1. Micrometeorological characteristics. *Journal of Applied Meteorology* **14**, 347-363.

Pilié, R. J., Mack, E. J., Kocmond, W. C., Eadie, W. J., and Rogers, C. W. 1975b. The life-cycle of valley fog. 2. Fog microphysics. *Journal of Applied Meteorology* **14**, 364-374.

Pinnick, R.G., Hoihjelle, D.L., Fernandez, G., Stenmark, E.B., Lindberg, J.D., Hoidale, G.B., Jennings, S.G. 1978. Vertical Structure in Atmospheric Fog and Haze and Its Effects on Visible and Infrared Extinction. *Journal of the Atmospheric Sciences* **35**, 2020–2032. doi:10.1175/1520-0469(1978)035<2020:VSIAFA>2.0.CO;2.

Pinto, R., Larrain, H., Cereceda, P., Lázaro, P., Osses, P., S., S.R. 2001. Monitoring fog-vegetation communities at a fog-site in Alto Patache, South

of Iquique, Northern Chile, during "El Niño" and "La Niña" events (1997-2000), In: *Second International Conference on Fog and Fog Collection*, International Development Research Center, Ottawa, Canada. pp. 293–296.

Pruppacher, H.R., Klett, J.D. 1997. *Microphysics of clouds and precipitation*. 2 ed., Kluwer Academic Publisher, Doordrecht, Netherlands, pp. 1-954.

Roach, W.T., Brown, R., Caughey, S.J., Crease, B.a., Slingo, A. 1982. A field study of nocturnal stratocumulus: I. Mean structure and budgets. *Quarterly Journal of the Royal Meteorological Society* **108**, 103–123. doi:10.1002/qj.49710845507.

Ronda, R.J., Steeneveld, G.J., Holtslag, A.A.M. 2011. *Can we forecast radiation fog using mesoscale models?* Technical Report, October 2005. Wageningen University. Wageningen.

Schulze-Neuhoff, H. 1976. Detailed analysis of fog based on additional 420 weather stations. *Meteorol. Rundsch*. **29**, 75-84.

Slingo, A., Nicholls, S., Schmetz, J. 1982. Aircraft observations of marine stratocumulus during JASIN. *Quarterly Journal of the Royal Meteorological Society* **108**, 833–856. doi:10.1002/qj.49710845807.

Tardif, R. 2007. The Impact of Vertical Resolution in the Explicit Numerical Forecasting of Radiation Fog: A Case Study. *Pure and Applied Geophysics* **164**, 1221–1240. doi:10.1007/s00024-007-0216-5.

Terradellas, E., Bergot, T. 2007. Comparison between two-single column models designed for short-terms fog and low-clouds forecasting. *Física de la Tierra* **19**, 189–203.

Thoma, C., Schneider, W., Masbou, M., Bott, A. 2012. Integration of Local Observations into the One Dimensional Fog Model PAFOG. *Pure and Applied Geophysics* **169**, 881–893. doi:10.1007/s00024-011-0357-4.

Turner, J., Allam, R.J., Maine, D.R. 1986. A case study of the detection of fog at night using channel 3 and 4 on the Advanced Very High Resolution Radiometer (AVHRR). *Meteorological Magazine* **115**, 285–290.

Wang, J., Daum, P.H., Yum, S.S., Liu, Y., Senum, G.I., Lu, M.L., Seinfeld, J.H., Jonsson, H. 2009. Observations of marine stratocumulus microphysics and implications for processes controlling droplet spectra: Results from the Marine Stratus/Stratocumulus Experiment. *Journal of Geophysical Research* **114**. doi:10.1029/2008JD011035.

Wendisch, M., Mertes, S., Heintzenberg, J., Wiedensohler, A., Schell, D., Wobrock, W., Frank, G., Martinsson, B.G., Fuzzi, S., Orsi, G., Kos, G., Berner, A. 1998. Drop size distribution and LWC in Po Valley fog. *Contributions to Atmospheric Physics* 71, 87–100.

Wieprecht, W., Acker, K., Mertes, S., Collett, J., Jaeschke, W., Brüggemann, E., Möller, D., Herrmann, H. 2005. Cloud physics and cloud water sampler comparison during FEBUKO. *Atmospheric Environment* **39**, 4267–4277. doi:10.1016/j.atmosenv.2005.02.012.

Wobrock, W., Schell, D., Maser, R., Kessel, M., Jaeschke, W., Fuzzi, S., Facchini, M.C., Orsi, G., Marzorati, A., Winkler, P., Arends, B.G., Bendix, J. 1992. Meteorological characteristics of the Po Valley fog. *Tellus B* **44**, 469–488. doi:10.1034/j.1600-0889.1992.t01-4-00003.x.

5. Summary and Outlook

Enlarged knowledge of the spatiotemporal distribution of FLS is of great value in regards to traffic safety and air quality control. Not only the horizontal visibility in fog but also the dissolving power of harmful pollutants in boundary clouds depend on the prevailing small droplets. Since the DSD of both phenomena varies spatially with the vertical extent of these clouds and temporally from formation to dissipation, nowcasting and forecasting of FLS is faced with difficult challenges. Present models have need of theoretical assumptions on vertical microphysical profiles and their evolution during fog life cycle for their computations since real-time data on these cannot be provided contemporaneously so far. For that reason, the IPCC assesses the scientific understanding of FLS still big uncertainties. The investigation of the interaction of aerosol and boundary clouds and therewith their influence on the radiation budget of the earth system has to rely on numerous assumptions instead of substantiated results from measurements. However, no adequate methods for the detection of microphysical properties of FLS have been available so far which could reproduce these differentiated by development stages and over the entire spatial extent.

Existing satellite-based remote sensing instruments such as RADAR or LIDAR feature a relatively high resolution and could therefore provide vertical profiles of microphysical properties. However, the vertical resolution of the CPR on the CloudSat-platform with 30 to 60 m for instance makes it improper for a detailed investigation of the microphysical properties of these cloud phenomena. Besides, there is no direct relationship between recorded signals from RADAR or LIDAR and microphysical properties as LWC. Both quantities depend on the prevailing drop size distribution of FLS. Since the latter can neither be retrieved from reflectivity recordings, assumptions on vertical DSD-profiles have to be made. By this, the usage of existing satellite-retrievals is accompanied with big sources of error particularly if one considers that DSD varies within fog life cycle. In-situ measurements in these boundary clouds do not exhibit this disadvantage of satellite-based approaches because they do not rely on theoretical assumptions. Microphysical properties as DSD or LWC for example can be determined directly by optical instruments. Nevertheless, single field measurements lack in spatial resolution and these investigations often do not encompass the whole fog event. This is caused by the measuring platform that has to be lifted for vertical profiles by stolid balloons. According to COST actions 720 and 722 novel ground-based microwave FMCW cloud RADAR profilers possess the instrumental requirements for deriving microphysical properties such as LWC from Z; but no implemented retrievals have been developed so far. Since for the derivation of vertical LWC-profiles from Z detailed information on prevailing DSD are required, the evolution of the latter as a function of the fog life cycle has to be considered. An accurate classifi-

cation of fog evolutionary stages, accompanied with phase-specific DSD, is a necessary condition for a proper usage of the microwave RADAR profiler. Otherwise, the derivation of vertical LWC-profiles from Z would underlie too big inaccuracies.

Hence, the major **aim** of the thesis was the investigation of the temporal dynamics of fog microphysics with emphasis on DSD over its whole life cycle.

This intention was based on the **hypothesis** that it is possible to separate consecutive evolutionary stages temporally within fog life cycle on the basis of fog microphysics such as DSD at the ground as well as in vertical profiles.

Testing the hypothesis required the development of three novel methodologies composed of an innovative algorithm, a statistical approach and a balloon-borne measuring device. The results of the **three working packages** are in detail:

1. At first, a sensitivity study was conducted which should identify the influencing factors on Z and LWC. Therefore, a literature survey of existing field experiments for fog microphysics was elaborated. It could be shown that it is legitimate to utilize a direct proportionality factor Ω for the derivation of LWC from a given Z. However, Ω strongly depends on the used DSD that can be represented best by the so-called modified gamma distribution. A radiative transfer code was developed that revealed the range of Ω by use of DSD-values from available measurements. Since Ω featured very wide variations, the impact of type and life cycle of fog on Z-LWC-relationship was regarded additionally. A differentiation between advection and radiation fog as well as a separation in evolutionary stages during a fog life cycle resulted in narrower ranges for Ω. Unfortunately, the literature survey also exposed the absence of an objective classification of fog life cycle phases. But this one is essential for accurate phase-specific proportionality factors between Z and LWC.
2. Consequently, a statistical-based method for the classification of fog life cycle phases had to be developed. The three-stage approach is based on a statistical change point analysis of double sum curves of optical and microphysical measured values on the ground. These were recorded during three radiation fog events by an optical particle counter (LWC, N_t, r_{mean}), that was specifically adapted from airborne systems to our needs, and a present weather sensor for horizontal visibility. Each of the three fog occurrences could be divided in three consecutive evolutionary stages from formation to dissipation, regardless which of the microphysical properties or VIS were considered. Moreover, each of the three separated phases of the single fog

events could be aggregated, since they had featured consistent microphysical patterns.

3. In order to enable an exploration of microphysical properties of fog in vertical profiles a tethered balloon-borne device was constructed with the optical particle counter as core. The field study was conducted on two different radiation fog events and the measurements were processed by the previously presented statistical approach again. The derived vertical LWC-profiles were compared to theoretically presumed sub-adiabatic profiles being implemented in satellite-based retrievals. The first two evolutionary stages of fog revealed good accordance with respect to trend and gradient between measured and theoretical LWC-profiles when fog life cycle phases were taken into account; however, the last phase (dissipation stage) featured larger variations.

The **hypothesis** concerning the possibility to find and classify evolutionary stages of fog based on microphysical properties can be verified for measurements by an OPC as well as by a present weather sensor on the ground.

The developed statistical approach for the classification of fog in life cycle phases featured very high significance (see Fig. 5.1). Nevertheless, the exploration of vertical LWC-profiles by use of the balloon-borne system revealed deficits with regard to one out of three evolutionary stages (dissipation stage). This may arise from the relatively small data basis. Hence, the variance within the dissipation stage points out that more LWC-profiles have to be recorded under varying circumstances for a substantiate data basis.

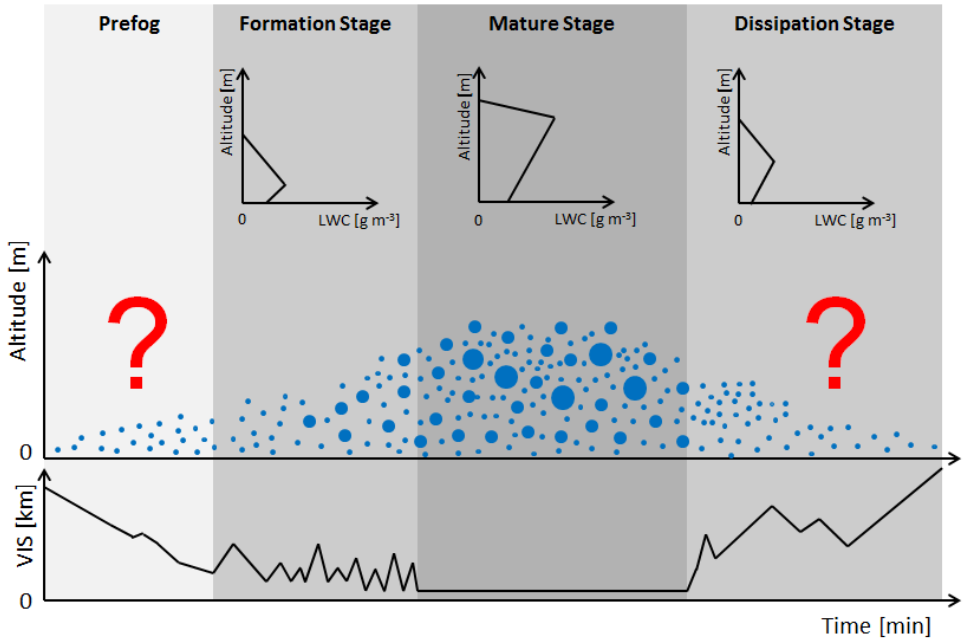

FIG. 5.1. Graphical concept model of the thesis. The three consecutive stages of fog evolution are highlighted in dark grey which can be found by the new statistical approach of this thesis. The corresponding evolution of total number of droplets and their growth as a function of altitude is presented symbolically by blue circles. The horizontal visibility at the ground (VIS) as a result from the prevailing vertical liquid water content-profile (LWC) is added additionally underneath and above, respectively. The red question marks reveal the remaining uncertainties of the progresses involving the evolution and dissipation of fog.

Novel findings of the current thesis are:

1. It is possible to derive vertical LWC-profiles in FLS directly from RADAR reflectivity of a novel 94 GH FMCW cloud RADAR profiler since a direct but non-linear relationship between Z and LWC could be approved whereby further information on the prevailing drop size distribution has to be presumed.
2. Fog occurrences can be separated in three consecutive phases during its life cycle by means of an innovative statistical approach that relies on measured microphysical fog properties or horizontal visibility at the ground.
3. According to balloon-borne measurements of vertical LWC-profiles it is legitimate to interpolate FLS life cycle phases from ground-based measurements of microphysical properties and horizontal visibility in their whole vertical extension.

In future, also the dataset of the statistical approach for the separation of fog life cycle phases at ground level should to be enlarged by further measurements. In fact, the developed approach features high significance. However, narrower ranges of phase-specific DSD could result in more accurate proportionality factors for the derivation of LWC from *Z* by use of microwave cloud RADAR profilers.

The results of the thesis have manifold benefits for climate research and operational FLS applications:

The identification of cloud geometrical thickness and thus the distinction between fog and low stratus by means of **optical satellite retrievals** has to be improved with regards to their reliability. To the present, all satellite-systems rely on theoretical assumptions regarding vertical LWC-profiles, independently from the used measuring instruments. Here, the introduced approach for the classification of evolutionary stages during fog life cycle based on microphysical properties is a valuable step towards the development of a method for the derivation of vertical LWC-profiles from novel FMCW microwave cloud RADAR profilers. These are notably suitable for the exploration of microphysical properties of low clouds and fog with high temporal resolution. The resultant findings about the dynamics of microphysical properties during fog events and low stratus could be used to improve the implemented theoretical assumptions on LWC-profiles in satellite-based approaches for fog detection. This optimization could permit in turn an operational and continuous monitoring of LWC-profiles in low stratus and fog thanks to their high spatiotemporal resolution.

Their relevance becomes obvious regarding the actual Fifth Assessment Report (AR5) from **IPCC**. A great deficit in knowledge with respect to the interactions between low stratus and aerosol is assessed in the report. The influence of low stratus on the radiation heat budget of the earth can be understood better on the basis of more reproducible dynamics of its microphysical properties in global climate prediction models.

Besides, an enhanced understanding of the evolution of DSD during the fog life cycle over the entire extent could help improving now- and forecasting models that are used for **traffic safety** and **air quality** purposes by providing more detailed vertical LWC profiles for the computations.

6. Zusammenfassung und Ausblick

Erweiterte Kenntnisse über die raumzeitliche Verteilung von Nebel und niedrigem Stratus sind von großem Wert für die Verkehrssicherheit und die Luftreinhaltung. Nicht nur die horizontale Sichtweite im Nebel, sondern auch das Lösungsvermögen gefährlicher Schadstoffe in bodennahen Wolken hängen von den vorherrschenden kleinen Tropfen ab. Da das Tropfenspektrum beider Phänomene räumlich in ihrer vertikalen Ausdehnung und zeitlich von der Bildung bis zur Auflösung variiert, stehen Kurzvorhersagen sowie Vorhersagen von Nebel und niedrigem Stratus vor großen Herausforderungen. Die derzeitigen Modelle benötigen theoretische Annahmen über die mikrophysikalischen Vertikalprofile und ihre Entwicklung während des Lebenszyklus für ihre Berechnungen, da bis jetzt Echtzeitdaten über diese nicht simultan zu den Modellen zur Verfügung gestellt werden können. Aus diesem Grund schreibt der IPCC dem wissenschaftlichen Verständnis von Nebel und niedrigem Stratus noch große Unsicherheiten zu. Die Untersuchung der Wechselwirkung zwischen Aerosol und bodennahen Wolken und ihr Einfluss auf den Strahlungshaushalt des Erdsystems basiert auf zahlreichen Annahmen statt auf fundierten Messerergebnissen. Der Grund dafür ist, dass bis jetzt keine adäquaten Methoden zur Erfassung der mikrophysikalischen Eigenschaften von Nebel und niedrigem Stratus verfügbar sind, die diese differenziert nach den Entwicklungsstadien und über ihre gesamte räumliche Ausdehnung reproduzieren können.

Die bestehenden satellitengestützten Fernerkundungsinstrumente wie RADAR und LIDAR besitzen ein relativ großes Auflösungsvermögen und könnten demzufolge Vertikalprofile der mikrophysikalischen Eigenschaften bereitstellen. Jedoch ist zum Beispiel die Auflösung des Cloud Profiling RADARs (CPR) auf der CloudSat-Plattform mit 30 bis 60 m für eine detaillierte Untersuchung der mikrophysikalischen Eigenschaften dieser Wolkenphänomene ungeeignet. Außerdem gibt es nur eine indirekte Beziehung zwischen den aufgezeichneten RADAR- und LIDAR-Signalen und den mikrophysikalischen Eigenschaften wie beispielsweise dem Flüssigwassergehalt (LWC). Sowohl die Radarreflektivität (Z) als auch der LWC hängen von der vorherrschenden Tropfengrößenverteilung des Nebels bzw. des niedrigen Stratus ab. Da das Tropfenspektrum auch nicht aus der aufgezeichneten Radarreflektivität abgeleitet werden kann, müssen Annahmen über sein Vertikalprofil getroffen werden. Dadurch unterliegt die Verwendung der derzeitigen Satellitenretrieval großen Fehlerquellen, besonders wenn man bedenkt, dass die Tropfengrößenverteilung innerhalb des Lebenszyklus des Nebels variiert. In-situ-Messungen in bodennahen Wolken weisen diese Nachteile der satellitengestützten Methoden nicht auf, da sie nicht auf theoretischen Annahmen basieren. Mikrophysikalische Eigenschaften wie z.B. die Tropfengrößenverteilung oder der Flüssigwassergehalt können direkt von optischen Instrumenten gemessen werden. Gleichwohl

mangelt es den einzelnen Messkampagnen am räumlichen Auflösungsvermögen, so dass diese Untersuchungen häufig nicht das ganze Nebelereignis abdecken können. Die unzureichende räumliche Auflösung kann auf die trägen Hubbewegungen der schwerfälligen Fesselballons zurückgeführt werden, an denen die Messplattformen befestigt waren. Laut der COST-Aktionen 720 und 722 besitzen bodengestützte Mikrowellen FMCW Wolken-RADAR-Profiler die messtechnischen Voraussetzungen für die Ableitung der mikrophysikalischen Eigenschaften wie den Flüssigwassergehalt aus der Radarreflektivität. Jedoch sind bisher noch keine implementierten Retrievals für sie entwickelt worden. Da für die Ableitung vertikaler LWC-Profile aus Z detaillierte Informationen über das vorherrschende Tropfenspektrum notwendig sind, muss die Entwicklung des letzteren in Abhängigkeit von den Entwicklungsstadien des Nebels berücksichtigt werden. Eine präzise Klassifikation der Entwicklungsstadien des Nebels mit phasenspezifischen Tropfenspektren ist daher eine notwendige Voraussetzung für die Verwendung von Mikrowellen RADAR-Profilern. Ansonsten würde die Ableitung vertikaler LWC-Profile aus Z zu großen Messungenauigkeiten unterliegen.

Daher war das **Hauptziel** der Dissertation die Untersuchung der zeitlichen Dynamik der Nebelmikrophysik mit Schwerpunkt auf der Tropfengrößenverteilung über den gesamten Lebenszyklus.

Dieses Vorhaben basierte auf der **Hypothese,** dass es möglich ist, die aufeinanderfolgenden Entwicklungsstadien innerhalb des Lebenszyklus, anhand der Mikrophysik wie beispielsweise mittels des Tropfengrößenspektrums am Boden sowie in Vertikalprofilen von Nebel, zeitlich zu differenzieren.

Zur Überprüfung der Hypothese war die Entwicklung eines neuen Methodenverbunds notwendig, der sich aus einem innovativen Algorithmus, einem statistischen Verfahren sowie einer ballongestützten Messvorrichtung zusammensetzte. Die Ergebnisse der drei Arbeitspakete sind im Einzelnen:

1. Zunächst wurde eine Sensitivitätsstudie durchgeführt, die die Einflussfaktoren auf Z und LWC identifizieren sollte. Dazu wurden bei Feldkampagnen gemessene Werte der Nebelmikrophysik aus der Literatur elaboriert. Es konnte gezeigt werden, dass es legitim ist, einen direkten Proportionalitätsfaktor Ω für die Ableitung des LWC aus einem vorgegebenen Z einzuführen. Allerdings hängt Ω von der jeweils angenommenen Tropfengrößenverteilung ab, die am besten von der sogenannten modifizierten Gammaverteilung abgebildet werden kann. Es wurde ein Strahlungstransfercode entwickelt, der die Bandbreite von Ω, unter Berücksichtigung verfügbarer Werte der Tropfengrößenverteilungen von existierenden Messkampagnen, aufzeigte. Da Ω eine große Bandbreite aufwies, wurde zusätzlich der Einfluss des Nebeltyps sowie des Lebenszyklus des Nebels berück-

sichtigt. Sowohl eine Differenzierung zwischen Advektions- und Strahlungsnebel als auch eine Unterteilung in die verschiedenen Entwicklungsstadien während des Lebenszyklus des Nebels führten zu engeren Bandbreiten von Ω. Allerdings ergab die Literaturrecherche, dass es noch keine objektive Klassifizierung der Entwicklungsstadien von Nebel gibt. Aber diese ist eine notwendige Bedingung für eindeutige entwicklungsphasenspezifische Proportionalitätsfaktoren zwischen Z und LWC.

2. Infolgedessen musste eine statistisch basierte Methode zur Klassifizierung des Lebenszyklus von Nebel entwickelt werden. Der dreistufige Ansatz basiert auf einer statistischen Doppelsummenkurvenanalyse der am Boden gemessenen optischen und mikrophysikalischen Eigenschaften. Diese wurden während drei Strahlungsnebelereignissen mit einem optischen Partikelzähler (LWC, N_t, $r_{Durchschnitt}$) aufgezeichnet, der speziell von Flugzeugsystemen an unsere Bedürfnisse angepasst worden war, sowie mit einem Sichtweitesensor für die horizontale Sichtweite. Jedes der drei Nebelereignisse konnte in drei aufeinanderfolgende Entwicklungsstadien, von der Bildung bis zur Auflösung, unterteilt werden, unabhängig davon, welche der mikrophysikalischen Eigenschaften oder die horizontale Sichtweite eingesetzt wurden. Außerdem konnte jedes der drei separierten Entwicklungsstadien der einzelnen Nebelereignisse aggregiert werden, da sie jeweils die gleichen mikrophysikalischen Muster aufwiesen.
3. Um eine genauere Untersuchung der mikrophysikalischen Eigenschaften von Nebel und ihrer vertikalen Verteilung vornehmen zu können, wurde eine angeleinte und ballongestützte Messeinrichtung entwickelt, die mit einem optischen Partikelzähler als Hauptmessinstrument ausgestattet war. Die Feldstudie wurde während zwei Strahlungsnebelereignissen durchgeführt und mittels der weiter oben dargestellten statistischen Methode analysiert. Die so abgeleiteten Vertikalprofile des Flüssigwassergehalts wurden anschließend mit theoretischen subadiabatischen Profilen verglichen, wie sie in den satellitengestützten Retrievals implementiert sind. Die ersten beiden Entwicklungsstadien des Nebels zeigten dabei eine gute Übereinstimmung bezüglich des Trends und des Gradienten zwischen den theoretischen und gemessenen Vertikalprofilen des Flüssigwassergehalts, insofern die einzelnen Entwicklungsstadien des Nebellebenszyklus berücksichtigt worden waren. Allerdings zeigte das letzte Entwicklungsstadium des Nebels, die Auflösungsphase, größere Abweichungen.

Die Hypothese, dass Entwicklungsstadien von Nebel mit Hilfe der mikrophysikalischen Eigenschaften identifiziert und klassifiziert werden

können, kann für Bodenmessungen des optischen Tropfenzählers und des Sichtweitesensors als verifiziert betrachtet werden.

Die entwickelte statistische Methode zur Unterteilung von Nebel in aufeinanderfolgende Entwicklungsstadien wies eine sehr hohe Signifikanz (Abb. 5.1) auf. Allerdings zeigte die Untersuchung der Vertikalprofile des Flüssigwassergehalts mittels eines ballongestützten Messsystems Defizite hinsichtlich einer Entwicklungsphase (Auflösungsphase). Dies ist möglicherweise auf die relativ kleine Datenbasis zurückzuführen. Demzufolge sollten noch mehr Vertikalprofile des Flüssigwassergehalts unter verschiedenen Messbedingungen durchgeführt werden, um eine breitere Datenbasis zu erhalten.

Neue Erkenntnisse der vorliegenden Arbeit sind:

1. Es ist möglich, vertikale Flüssigwassergehaltprofile in Nebel und niedrigem Stratus direkt aus der Radarreflektivität eines neuartigen 94 GHz FMCW Wolkenradarprofilers abzuleiten, da ein direkter, aber nicht-linearer Zusammenhang zwischen Z und dem Flüssigwassergehalt nachgewiesen werden konnte, wobei zusätzliche Informationen über die vorherrschenden Tropfengrößenverteilung vorhanden sein müssen.
2. Nebelereignisse können mit Hilfe einer innovativen statistischen Methode in drei aufeinanderfolgende Entwicklungsstadien innerhalb eines Lebenszyklus unterteilt werden, die auf gemessenen mikrophysikalischen Nebeleigenschaften oder der horizontalen Sichtweite am Boden basiert.
3. In Übereinstimmung mit ballongestützten Messungen von Vertikalprofilen des Flüssigwassergehalts ist es zulässig, die Entwicklungsphasen von Nebel und niedrigem Stratus, die auf Bodenmessungen der mikrophysikalischen Eigenschaften und der horizontalten Sichtweite basieren, über deren komplette vertikale Ausbreitung zu interpolieren.

In naher Zukunft muss auch die Datengrundlage für die statistische Methode zur Unterscheidung der Entwicklungsphasen des Nebels mittels Bodenmessungen vergrößert werden. Auch wenn der entwickelte statistische Ansatz eine hohe Signifikanz besitzt, müssen die Bandbreiten der entwicklungsphasenspezifischen Tropfengrößenverteilungen verkleinert werden, damit genauere Proportionalitätsfaktoren zur Ableitung des Flüssigwassergehalts aus der Radarreflektivität von Mikrowellenwolkenradarprofilern erzielt werden können.

Die Ergebnisse der Dissertation bieten vielfältige Vorteile für die Klimaforschung und der operationellen Erfassung von Nebel und niedrigem Stratus:

Die Bestimmung der optischen Dicken bodennaher Wolken und die damit einhergehende Unterscheidung zwischen Nebel und niedrigem Stratus

mit Hilfe von **optischen Satellitenretrievals** muss hinsichtlich ihrer Verlässlichkeit verbessert werden. Bis jetzt sind alle satellitengestützte Fernerkundungssysteme auf theoretische Annahmen über die Vertikalprofile des Flüssigwassergehalts angewiesen, unabhängig davon, welche Messinstrumente benutzt werden. Der vorgestellte, auf mikrophysikalischen Eigenschaften beruhende, Ansatz zur Klassifizierung der Entwicklungsstadien von Nebel während seines Lebenszyklus, ist ein wertvoller Schritt auf dem Weg zur Entwicklung eines Verfahrens, mit dessen Hilfe Vertikalprofile des Flüssigwassergehalts von neuartigen FMCW Mikrowellenradarprofilern abgeleitet werden können. Diese sind, aufgrund ihrer hohen zeitlichen Auflösung, in besonderem Maße für die Untersuchung der mikrophysikalischen Eigenschaften von niedrigem Stratus und Nebel geeignet. Die daraus resultierenden Erkenntnisse über die Dynamik der mikrophysikalischen Eigenschaften in Nebelereignissen und niedrigem Stratus könnten dazu benutzt werden, die, in satellitengestützten Methoden zur Bestimmung von Nebel, verwendeten theoretischen Annahmen zu verbessern. Diese Optimierung könnte im Umkehrschluss eine operationelle und kontinuierliche Beobachtung der Vertikalprofile des Flüssigwassergehalts in Nebel und niedrigem Stratus, wegen ihres hohen raumzeitlichen Auflösungsvermögens, erleichtern.

Die Relevanz der angesprochenen Monitoringmethoden wird offenkundig, wenn man den aktuellen Fünften Sachstandbericht (AR5) des **IPCC** betrachtet. Dort wird dem wissenschaftlichen Kenntnisstand über die Wechselwirkungen von niedrigem Stratus und Aerosol ein großes Defizit zugeschrieben. Der Einfluss von niedrigem Stratus auf den Strahlungshaushalt der Erde könnte in den globalen Klimavorhersagemodellen mittels einer genauer reproduzierbaren Dynamik seiner mikrophysikalischen Eigenschaften besser abgebildet werden.

Außerdem könnte ein genaueres Verständnis über die Entwicklung der Tropfengrößenverteilung innerhalb des Lebenszyklus über die gesamte Dauer des Nebelereignisses dazu beitragen, die Vorhersagemodelle und Prognosen zu verbessern, die zu Beobachtungszwecken für die **Verkehrssicherheit** und die **Luftreinheit** benutzt werden, indem genauere Vertikalprofile des Flüssigwassergehalts für die Berechnungen zur Verfügung gestellt werden.

7. Appendix

List of Symbols and Acronyms

a	scale parameter of the modified gamma distribution
α	shape parameter of the modified gamma distribution
AGE-2	second aerosol characterization experiment
ASTEX	Atlantic stratocumulus transition experiment
b	shape parameter of the modified gamma distribution
CALIOP	cloud-aerosol LIDAR with orthogonal polarization
CALIPSO	cloud-aerosol LIDAR and infrared pathfinder satellite observations
CDP	cloud droplet probe
CLARE'98	cloud LIDAR and RADAR experiment
COST	European cooperation in Science and technology
CP	change point
CPR	cloud profiling RADAR
CW	continuous wave
D	dissipation stage in fog life cycle
dBz	logarithmical unit of radar reflectivity Z [dBz]
dr	range between minimum and maximum within a drop size spectrum [μm]
DSD	drop size distributions
DWD	Deutscher Wetterdienst/ German weather service
DYCOMS-II	second dynamics and chemistry of the marine stratocumulus field study
EOS	earth observing system
F	formation stage in fog life cycle
f	frequency [Hz]
f(r)	probability density function of the modified gamma distribution
FLS	fog and low stratus
FMCW	frequency modulated continuous wave
γ	shape parameter of the modified gamma distribution
Γ	gamma function
GEO	geostationary orbit
GFM	Gultepe's model for the evolution of radiation fog
H_0	null hypothesis of homogeneity-test of Mann-Whitney
H_A	alternative hypothesis homogeneity-test of Mann-Whitney
IPCC	International Panel on Climate Change
LEO	low earth orbit
LIDAR	light detection and ranging
LOSU	level of scientific understanding

LS	low stratus
LT	local time
LWC	liquid water content [g m^{-3}]
LWP	liquid water path [g m^{-2}]
M	mature fog during in life cycle
m(r)	mass of fog drops per unit volume of air [g cm^{-3}]
MAE	mean absolute error
MGD	modified gamma distribution
m_i	moment of the modified gamma distribution
MODIS	moderate resolution imaging spectroradiometer
n(r)	drop size spectrum per unit volume of air [cm^{-3}]
N_t	total number of drops per unit volume of air [cm^{-3}]
NWP	numerical weather prediction
Ω	proportionality factor for Z-LWC-relation [g mm^{-6}]
OPC	optical particle counter
p	significance level [%]
PDF	probability density function
PFM	Pilié's model for the evolution of radiation fog
Q	extinction efficiency after van de Hulst
r	radius of fog droplet [µm]
ρ	density [g cm^{-3}]
RADAR	radio detecting and ranging
r_c	modal radius of a drop size spectrum [µm]
r_{eff}, r_e	effective radius of the modified gamma distribution [µm]
RF	radiative forcing [W m^{-2}]
RH	relative humidity [%]
r_{max}	maximum radius of a drop size spectrum [µm]
r_{mean}	arithmetic mean droplet radius of a drop size spectrum [µm]
r_{min}	minimum radius of a drop size spectrum [µm]
RTC	radiative transfer code
SEVIRI	spinning enhanced visible and infrared imager
SODAR	sound/sonic detecting and Ranging
T	temperature [°C];[K] or end of a time series [s]
t	time [s]
$\hat{t}$	test statistic of two-sided t-test
$U_{t,T}$	test statistic of homogeneity test of Mann-Whitney
UTC	universal time code
VIS	horizontal visibility [km]
vv	wind speed [m s^{-1}]
WMO	World Meteorological Organization
Z	RADAR reflectivity [mm^6 m^{-3}]
$\hat{z}$	test statistic of Mann-Kendall trend-test

Die Seite 123 (Curriculum Vitae) enthält persönliche Daten.
Sie ist deshalb nicht Bestandteil der Online-Veröffentlichung.

Versicherung

Ich versichere, dass ich meine Dissertation

DIFFERENTIATION OF EVOLUTIONARY STAGES IN FOG LIFE CYCLES BASED ON MICROPHYSICAL PROPERTIES – IMPLICATIONS FOR THE OPERATION OF NOVEL CLOUD RADAR PROFILERS

selbständig ohne unerlaubte Hilfe angefertigt und mich dabei keiner anderen als der von mir ausdrücklich bezeichneten Quellen bedient habe. Alle vollständigen oder sinngemäßen Zitate sind als solche gekennzeichnet.

Die Dissertation wurde in der jetzigen oder einer ähnlichen Form noch bei keiner anderen Hochschule eingereicht und hat noch keinen sonstigen Prüfungszwecken gedient.

Eine frühere Promotion wurde von mir nicht versucht.

Frankfurt am Main, den 16. Februar 2014 _____

(Unterschrift)